CHARACTERIZATION OF FROST GROWTH ON A MEMBRANE

A Thesis Submitted to the College of

Graduate and Postdoctoral Studies

In Partial Fulfillment of the Requirements

For the Degree of Doctor of Philosophy

In the Department of Mechanical Engineering

University of Saskatchewan

Saskatoon

By

Shirin Niroomand

2018

© Copyright Shirin Niroomand, August 2018. All rights reserved.

PERMISSION TO USE

In presenting this thesis in partial fulfillment of the requirements for a Postgraduate degree from the University of Saskatchewan, I agree that the Libraries of this University may make it freely available for inspection. I further agree that permission for copying of this thesis in any manner, in whole or in part, for scholarly purposes may be granted by the professors who supervised my thesis work or, in their absence, by the Head of the Department or the Dean of the College in which my thesis work was done. It is understood that any copying, publication, or use of this thesis or parts thereof for financial gain shall not be allowed without my written permission. It is also understood that due recognition shall be given to me and to the University of Saskatchewan in any scholarly use which may be made of any material in my thesis. Requests for permission to copy or to make other use of material in this thesis in whole or in part should be addressed to:

Head of the Department of Mechanical Engineering
University of Saskatchewan
57 Campus Drive, Saskatoon, Saskatchewan, S7N 5A9
Canada

OR

Dean
College of Graduate and Postdoctoral Studies
University of Saskatchewan
116 Thorvaldson Building, 110 Science Place
Saskatoon, Saskatchewan S7N 5C9
Canada

ABSTRACT

The formation of frost in heat/energy exchangers is inevitable in cold and humid environments, and can cause economic losses and technical problems in frosted exchangers. In recent decades, there has been much interest in developing anti-frosting surfaces to reduce these losses and problems. In HVAC (Heating, Ventilation and Air Conditioning) systems, air-to-air semipermeable membrane energy exchangers have shown to be less susceptible to frosting compared to impermeable plate heat exchangers due to the moisture transfer through the semipermeable membrane. However, there is no data available in the open literature on the initiation and growth of frost on semipermeable membranes.

In this Ph.D. research, frost formation on a membrane is studied quantitatively and qualitatively in order to understand the frost initiation and growth on a membrane. Therefore, frost growth on a semipermeable membrane and an impermeable plate are characterized experimentally, in order to find the effect of moisture transfer through the semipermeable membrane on (1) frosting limit, (2) the process of the frost formation, and (3) the properties of the frost layer. Imaging techniques are used to measure the thickness of the frost layer and delineate the frost formation process.

The results presented in this thesis show that the frost limit on a semipermeable membrane is approximately 5 to 8°C lower than the frost limit for an impermeable plate. Furthermore, it is found that the fundamentals of the process of frost formation on the two surfaces (impermeable plate and semipermeable membrane) are similar: condensation, freezing, and frosting. However, large and distinct water droplets form on the membrane that remain in the liquid phase for a longer time compared to an impermeable plate. Also, the lateral growth of ice crystals that connect frozen droplets is very clear for the semipermeable membrane. The results also show that frost formation is not eliminated on the semipermeable membrane under severe conditions. The frost growth on the semipermeable membrane is very slow for the first 30 min to 60 min of the test, compared to the frost growth on the impermeable plate. Finally, it is shown that the rate of frost growth decreases as the rate of the moisture transfer through the semipermeable membrane increases.

ACKNOWLEDGMENTS

I wish to express sincere gratitude to my advisor, Prof. Carey Simonson, for recruiting me into the graduate program in the Department of Mechanical Engineering at University of the Saskatchewan and for his continues support, patience and motivation through my Ph.D. studies. I'm particularly grateful for the considerable freedom he provided me in all phases of my research. I am particularly grateful to my committee members, Prof. James Bugg, Prof. Scott Noble, and Prof. Lifeng Zhang for their constructive feedback and guidance toward accomplishment of this thesis. I am also extend my appreciation to Prof. Besant for providing advice and inspiration for me and my research.

I would like to convey a special thanks to Dr. Melanie Fauchoux, for her assistance and support in all phases of my research.

A number of other people are due special thanks as well: Dr. E. Walia in Department of Computer Science, Mr. E. Neil in Department of Agriculture, and Mr. Reinink in Department of Mechanical Engineering.

To my fellow graduate students/post-doctorate, Dr. M. Shakouri, Dr. F. Fathieh, Dr. M. Rafati Nasr, Dr. A. Olufade, Mr. D. Storle, Dr. Ge Gaoming, Dr. A. H. Abdel-Salam, Dr. M. R. Abdel-Salam, Mr. A. Hossain, Mr. E. Nampoothiry, and Mr. B. Xing, thank you for the countless hours of assistance. In particular, my special thanks to Mr. P. Navid for our enjoyable discussions about our research.

Last but not the least, I would like to thank my family: my parents and my siblings, and my best friend, Sepehr, for their support and encouragement through my studies.

DEDICATION

This thesis is dedicated to my parents and my siblings for their endless love and support.

TABLE OF CONTENTS

Page

LIST OF FIGURES

Page

LIST OF TABLES

Page

NOMENCLATURE

Acronyms

HVAC	Heating, ventilating and air-conditioning
C/F	Condensation/frosting

Roman Symbols

A	Area of heat/energy transfer [m^2]
B	Systematic uncertainty
C	Concentration [kg_{salt}/kg_{liq}]
C_1, C_2, C_3, C_4, C_5, and C_6	coefficients used to calculate the saturated pressure of water vapour
Cr	Heat capacity ratio of an exchanger
d	Distance from the inlet of the test section [m]
D	Hydraulic diameter [m]
G_c	Gibbs free energy [J]
Gr	Grashof number [-]
h	Convective heat transfer coefficient [$W/(m^2 \cdot K)$]
I_0	Kinetic prefactor
k	Thermal conductivity [W/mK]
k_1	Boltzmann-constant [1.38×10^{-23} J/K]
L	Characteristic length [m];
	Length of the heat/energy transfer surface [m]
m	Mass [kg]
$\dot{m}$	Mass flow rate [kg/s]
m''	Mass per unit area [kg/m^2]
$\Delta mass$	Change in mass of the liquid desiccant inside the test section [kg_{sol}]
NTU_m	Number of mass transfer units of an energy exchanger (-)
Nu	Nusselt number [-]
n	Sampling number
P	Precision uncertainty; Pressure [Pa]
Pr	Prandtl number [-]

q''	Heat transfer per unit area [W/m^2]
$\bar{R}$	Ideal gas constant [J/(kg.K)]
R_a	Arithmetic average roughness [mm]
Ra	Rayleigh number [-]
Re	Reynolds number [-]
RH	Relative humidity [% RH]
R_q	Root mean square roughness [mm]
R_{sk}	Skewness roughness [mm]
t	Time [min]
T	Temperature [°C]
U	Total uncertainty
U_m	Overall mass transfer coefficient [$kg_{air}/(m^2s)$]
V_m	Molar volume of liquid [m^3/mol]
W	Humidity ratio [g/kg]
X	Horizontal axis in Cartesian coordinate
x*	Dimensionless length [-]
XY	Cartesian coordinate plane
y_i	Vertical distance from the mean line [mm]
Y	Vertical axis in Cartesian coordinate

Subscripts

air	Properties of air
avg	Average
conv	Convection
f	Frost
f,s	Frost surface
in	Inlet
latent	Latent moisture transfer
liq	Liquid desiccant
out	Outlet
p	Plate
rad	Radiation

surf	Impermeable plate or permeable membrane surface
w	Water
ws	Saturated water vapour

Greek Symbols

δ	Thickness [mm]
ε	Effectiveness
Δ	Algebraic difference
θ	Direct contact angle [°]
μ	Dynamic viscosity [Pa·s]
ρ	Density [kg/m^3]
σ	The liquid-vapour or the ice-vapour surface energy

CHAPTER 1

INTRODUCTION

1.1 Motivation

Condensation/frosting is a physical phenomenon of deposition of the water vapour on a surface, in the form of water or a porous structure of ice. Condensation/frosting occurs when the temperature of the surface is below the dew point and above/below the freezing point of the surrounding humid air. Condensation/frosting occurs in many industries, such as HVAC (Heating, Ventilating, and Air Conditioning) systems and refrigerators, aviation, electrical transmission, transportation, and wind power [1–3]. Heat/energy exchangers, which are commonly used in different industries to transfer heat and moisture between two fluids, are likely to be used under condensation/frosting conditions in cold climates.

When heat/energy exchangers are operated in cold climates, condensation/frosting can form on the surfaces inside the exchanger, which adds an additional layer of resistance to the surface and results in less heat and moisture transfer through the surface. If the frost continues to build up it can completely cover the surface of the exchanger, and as the frost grows thicker it can block the air flow channel, which further increases the pressure drop across the exchanger and reduces the performance of the exchanger [1,4–7]. Therefore, an understanding of the mechanism of frost formation, investigations of defrosting strategies and frost prevention strategies are very important to help improve the performance of heat/energy exchangers.

Heat/energy exchangers have been used in HVAC systems for different purposes. In a heat exchanger, an impermeable plate[1] (*e.g.* aluminum, copper or impermeable plastic plate) is used to separate two fluids (gas or liquid) in the exchanger, and allows only heat to transfer through the plate. However, an energy exchanger allow both heat and moisture exchange while preventing physical contact between two fluids. Different types of energy exchangers are used in HVAC systems, such as energy wheels, membrane air-to-air or air-to-liquid energy exchangers. In a

[1] In this thesis impermeable plate is denoted by aluminum plate or plastic plate.

membrane energy exchanger, a semipermeable membrane[2] which is capable of transferring both heat and moisture, replaces the plate used in heat exchangers. Membranes allow water vapour to transfer from the humid air to the dry fluid (air or liquid desiccant) on the other side of the membrane. Because of this moisture transfer, the dew point temperature of the humid air decreases as it flows through the exchanger which could result in a lower risk of frosting in the air channel.

Frost formation processes on impermeable surfaces have been studied in many studies. Frost growth is characterized experimentally and numerically in the literature. The effect of operating conditions (surface temperature, air temperature and humidity ratio) and surface properties on frost properties have been investigated. Although, a few studies have shown that air-to-air membrane energy exchangers reduce the risk of frosting [1,8–11]. Yet, there is a lack of studies on frost growth on membranes, specifically the initiation of frost, the mechanism of frost growth and the properties of the frost layer on membranes at different operating conditions. Thus, this thesis provides in-depth research on frost growth on membranes, which is needed for further development of frost-free exchangers.

1.2 Literature review

Condensation/frosting and icing have been interesting topics of research for many years. Figure 1.1 shows the number of studies on frosting, including experimental and numerical investigations, on the process of frost formation, frost layer characterization, and anti-frosting strategies sorting according to the year of publication through the online database: Scopus (www.scopus.com). The results have been collected by searching words "frost formation", "frost layer properties", and "anti-frosting ". The results in Figure 1.1 clearly indicate an increasing trend in the number of studies in recent decades. A review of previous research on frost formation, presented in this section, is divided into four parts. First, research on the process of frost formation on a flat impermeable plate is addressed. Then, in the second part, the methods to measure frost properties are classified. The third part focuses on frost formation in heat/energy exchangers. The fourth section focuses on de-frosting and anti-frosting methods. The literature review presented in this

[2] In this thesis semipermeable membrane is denoted by membrane.

chapter is a general overview. A more detailed review of the literature is provided in the introduction of each chapter.

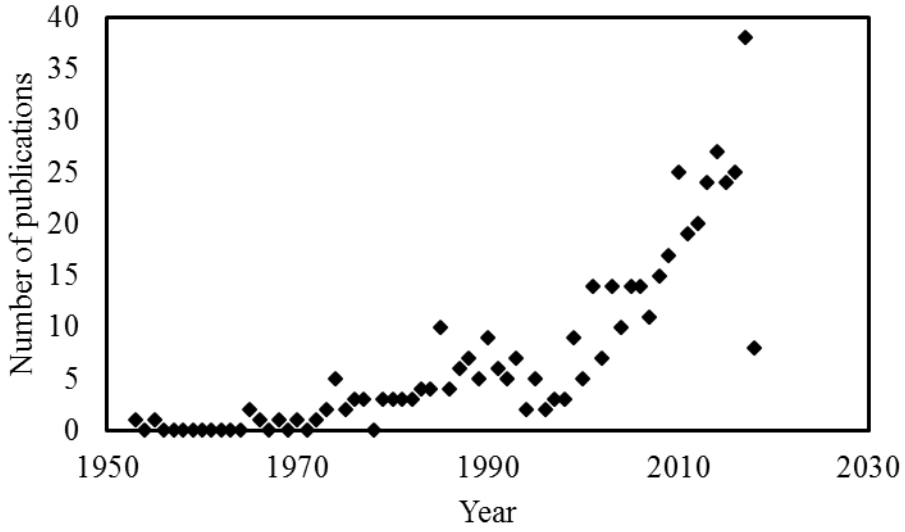

Figure 1.1. Number of publications on frost formation versus year of publication.

1.2.1 Evaluation of frost formation on a flat impermeable plate

When a cold surface is exposed to humid air, frost might form on the surface through two possible processes, depending on the temperature and vapour pressure; condensation frosting or deposition frosting [2,12,13]. When the vapour pressure is above the triple point value, as shown in Figure 1.2, a decrease in the temperature usually causes the nucleation of the water first, and if the temperature reduces below the freezing point temperature, the water will turn into ice, this is termed condensation frosting in the literature [2,12,14–16]. However, at extreme conditions (very low temperature and humidity, conditions below the Triple point value), water vapour transfers into ice directly, which is called deposition frosting [17].

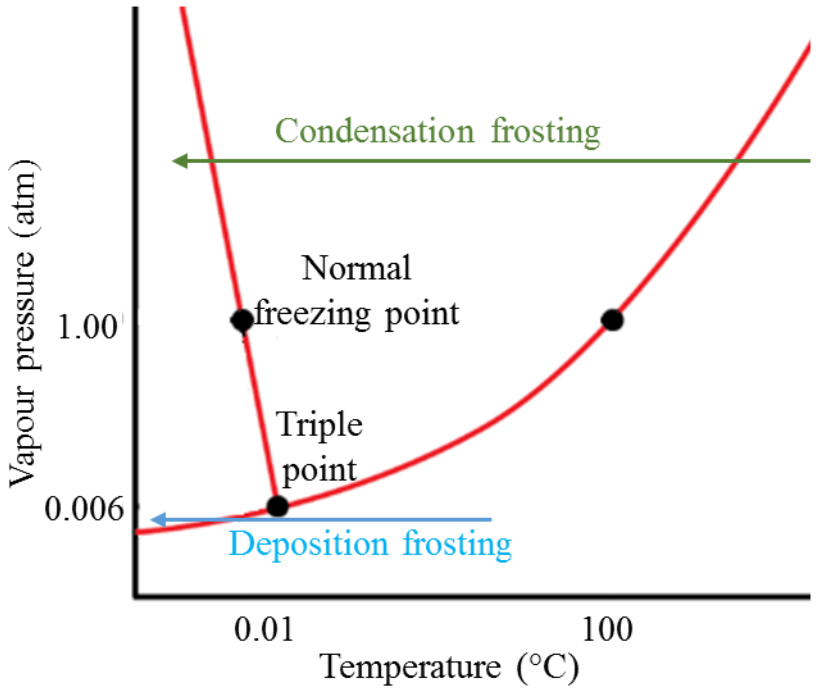

Figure 1.2. Phase diagram of water showing deposition frosting at partial pressure bellow the triple point and condensation frosting above the triple point.

For the operating conditions found in most industrial applications, the common process of frosting is condensation frosting. It has been reported in the literature that the process of the condensation frosting on a surface can be divided into the following stages [2,12,14–16]:

i. Condensation: water vapour forms into liquid water droplets on the surface. (Note that on sufficiently hydrophilic surfaces filmwise condensation occurs which is not in the scope of this study).
ii. Freezing: the water droplets begin to freeze.
iii. Crystal growth: frost halos appear.
iv. Freezing propagation: icing propagates from a frozen droplet toward a neighboring droplet.
v. Frost layer growth: percolation and interaction of ice crystals globally.
vi. Frost layer densification: interbranching between ice crystals forms a 3-dimensional layer of frost on the surface.

Although there are small variations in the names and the definitions of each stage, the principle of the classification is similar. Sometimes, stages v and vi are combined and referred to as the mature growth stage. In general, there are three important phase change processes during the formation of frost on a surface; condensation of the water vapour, the freezing of the condensed water droplets and ablimation of water vapour on frozen droplets. When a droplet freezes in isolation, microscale ice crystals form on the outside of the frozen droplet (*i.e.* frost halos, stage iii). At temperatures above -40°C, all the condensate droplets do not freeze simultaneously but rather freezing is directed from a frozen droplet toward the neighboring droplet though interdroplet interactions due to differences between the water vapour pressure at the surface of a frozen droplet and a liquid droplet and creates ice bridging and dry zone [2,18,19]. At the next stage, freezing percolates globally among all the water droplets on the surface. At the end of stage v, a two-dimensional network of frozen droplets connected by ice branches appears on the surface. Finally, inter-branching between ice crystals produces a three-dimensional network of frost layer on the surface. At this stage, ice crystals may accumulate on the surface of the frost layer and increase the thickness of the frost layer or diffuse into the frost layer and increase the density of the frost layer.

The growth of the frost layer in stage vi (mature growth stage) on an impermeable surface has been studied in the literature both theoretically and experimentally at a variety of conditions (*e.g.* under different operating conditions on vertical and horizontal surfaces, under forced convection and natural convection) to characterize frost properties. In most of these studies, the condensation and freezing stages are ignored, as it was believed that the impact of these stages on the frost layer properties in the mature growth stage are very small. However, more recently [20–27], it has been found that the size and distribution of water droplets at the end of first stage (condensation), the process of freezing of a droplet (stage ii) and freezing propagation (stage iv) and also the duration of these stages have a significant effect on the properties of the frost layer in the mature growth stage.

There are some studies in the literature that have focused on the onset of condensation and freezing, the size and distribution of the condensed water droplets, and examined the factors (*e.g.* operating conditions (air temperature, air humidity ratio, surface temperature) ; and the surface properties (hydrophilicity, hydrophobicity, superhydrophobocity, and roughness)) affecting the condensation, the duration of each stage and the onset and propagating of the freezing

[12,13,18,28–54] Most of the studies in this area used visualization to qualitatively evaluate the initiation and growth of condensation or icing in each stage (stages i, ii, iii, iv and v) [2,16,18,28,29,33,38,42,43,50,52,55–64].

While the process of frost formation on a plate has been well studied, the goal of this Ph.D. research is to determine the process of frost formation on a membrane and to compare it to the process of frosting on a plate, which has not been addressed in the literature.

1.2.2 Methodologies to characterize frost layer properties

The characterization of frost properties has been the focus of many studies in the literature. The important properties are the frost thickness, mass, density and thermal conductivity. Table 1.1 summarizes the studies that measured frost properties, either experimentally or numerically, based on reviewing more than 100 papers published from 1958 to 2018. The number of studies on frost properties by publication year is also provided in Figure 1.3. It can be seen from the literature that frost thickness is the most commonly measured property in the literature.

Table 1.1. A classification of the frost properties in the majority of journal papers published between 1958 and 2018.

Frost layer properties	Experimental	Total number of papers	Theoretical and empirical	Total number of papers
Thickness	[4,7,27,39,40,49,50,58,64–88]	33	[5,17,81,82,89–113]	29
Mass	[17,27,35,40,65–67,69,70,73,76,81–83,86,99,111,114–116]	20	[105,113]	2
Density	[4,14,39,60,65,66,70,73,76,81,83,86,91,92,99,111,114,115,117,118]	20	[5,17,71,75,81,89–91,94,96,100–103,108,111,117–122]	22
Thermal conductivity	[14,27,72,82,111,113]	6	[14,74,89–92,95,96,103,108,111,112,119,121,123]	15
Frost surface roughness	[74]	1	[124]	1

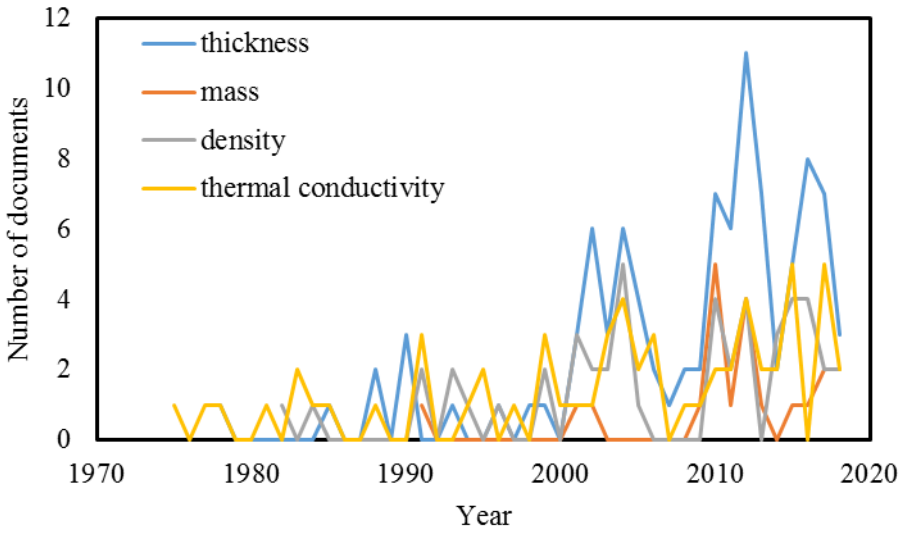

Figure 1.3. Number of published documents on frost property measurement

As the scope of this Ph.D. research is experimental, only the experimental methodologies are discussed here.

Available methods to measure frost thickness are divided into contact and non-contact methods. Non-contact methods (*e.g.* laser, x-ray and optical methods) are promising for measuring frost thickness, since contact measurements (*e.g.* micrometers and thermocouples) require touching the frost layer surface which can damage the frost layer and result in inaccurate measurements. Among the non-contact methods, visualization techniques are often used to determine the thickness of the frost. For example, using laser as a non-contact technique might melt frost crystals. Recently, a review paper [125], summarized the frost thickness measurement techniques that have been used in the literature.

Frost mass is fairly simple to measure directly by weighing or indirectly as the reduction of humidity in the air flowing over a surface. The density of the frost can be determined from the mass and thickness measurements.

The measurement of the frost thermal conductivity requires the surface temperature and thickness of the frost layer, the cold plate temperature and the heat flux so Fourier's law can be used to determine the thermal conductivity of the frost layer. It can be concluded from Table 1.1, that the number of the experimental studies that focused on the frost thermal conductivity measurements are less than the theoretical and empirical studies. This is because the measurement of the frost surface temperature is difficult. In the literature, direct and non-direct measurements have been used to measure the frost surface temperature. Refs. [68,70] used infrared thermometers as a direct method to measure the frost surface temperature, however, the assumed frost emissivity values in those references is uncertain. Fine thermocouples are used as direct contact measurement methods [14,27]. Reliable results from thermocouples requires a good contact between the frost layer surface and thermocouples, however the rough surface of a frost layer makes this impractical.

Another important parameter is surface roughness, especially in modeling frost growth as frost surface roughness will affect the heat and moisture transfer coefficients. In some frosting papers, the frost surface is assumed to be smooth [126], while Ref. [96] shows that frost surface roughness has impact on the convective heat transfer coefficients. Frost surface roughness is measured in only two papers [74,124]. Ref. [74] used a micrometer to measure the roughness of the frost, and

Ref. [124] estimated the roughness of the frost surface inside a tube using methods similar to those used to grade the roughness of a pipe (equivalent sand roughness). Although the frost surface roughness is an important parameter, the measurement techniques in the literature are not well established. In this research, a method to measure frost surface roughness is presented.

Frost properties highly depend on the operating conditions: air temperature, air humidity ratio, air velocity, surface temperature, convection conditions, surface geometry, and surface properties. The effect of operating conditions on frost properties have been experimentally investigated in the literature. However, some unclear and contradictory conclusions still exist, especially concerning the effect of operating conditions on frost mass, which indicates the importance of presenting all details about the experimental conditions and assumptions as small differences in the test conditions might affect frost growth [117].

1.2.3 Frost formation in heat/energy exchangers in HVAC and refrigeration systems

Heat/energy exchangers are widely used in order to transfer heat or energy (heat + moisture) between two fluids. There are different types of heat/energy exchangers in industry: fixed plate heat/energy exchangers, rotary air-to-air heat/energy exchangers (heat/energy wheels), and liquid-to-air heat/energy exchangers.

Some of the studies in the literature are focused on the performance of heat exchangers in frosting conditions [4–7,45,68,76,79,80,104,113,115,118,126–128], whereas, a few studies investigated the performance of energy exchangers in frosting conditions [1,8,10,11,45,120,129–135]. From the literature, it can be concluded that energy exchangers are more frost resistant compared to the heat exchanger at the same conditions, as the moisture transfer depresses the dew point temperature of the humid air. Nevertheless, frost formation is still a problem for energy exchangers.

Among the different energy exchangers, membrane energy exchangers have gained high attention in HVAC applications. A membrane is permeable to water vapour and allows both heat and moisture transfer. Figure 1.4 shows a schematic of heat and energy exchange through a plate and membrane (Figure 1.4(a)) and also compares the process of heat and energy exchange on the psychrometric chart (Figure 1.4(b)). It can be seen that only heat can transfer through the plate, whereas, both heat and moisture (energy) can transfer through the membrane. As shown in the

psychrometric chart (Figure 1.4(b)), in the case of a plate, only the temperature of the air reduces, whereas, in the case of a membrane, both temperature and humidity ratio of the air decreases simultaneously. When the air reaches the saturation conditions (the line showing the process of heat/energy exchange touches the saturation line in the psychrometric chart, Figure 1.4(b)), condensation, which is the requirement for the frost formation, occurs. Based on Figure 1.4(b), it can be seen that the temperature of the air flow over a membrane can go to lower temperatures before saturation occurs compared to a plate.

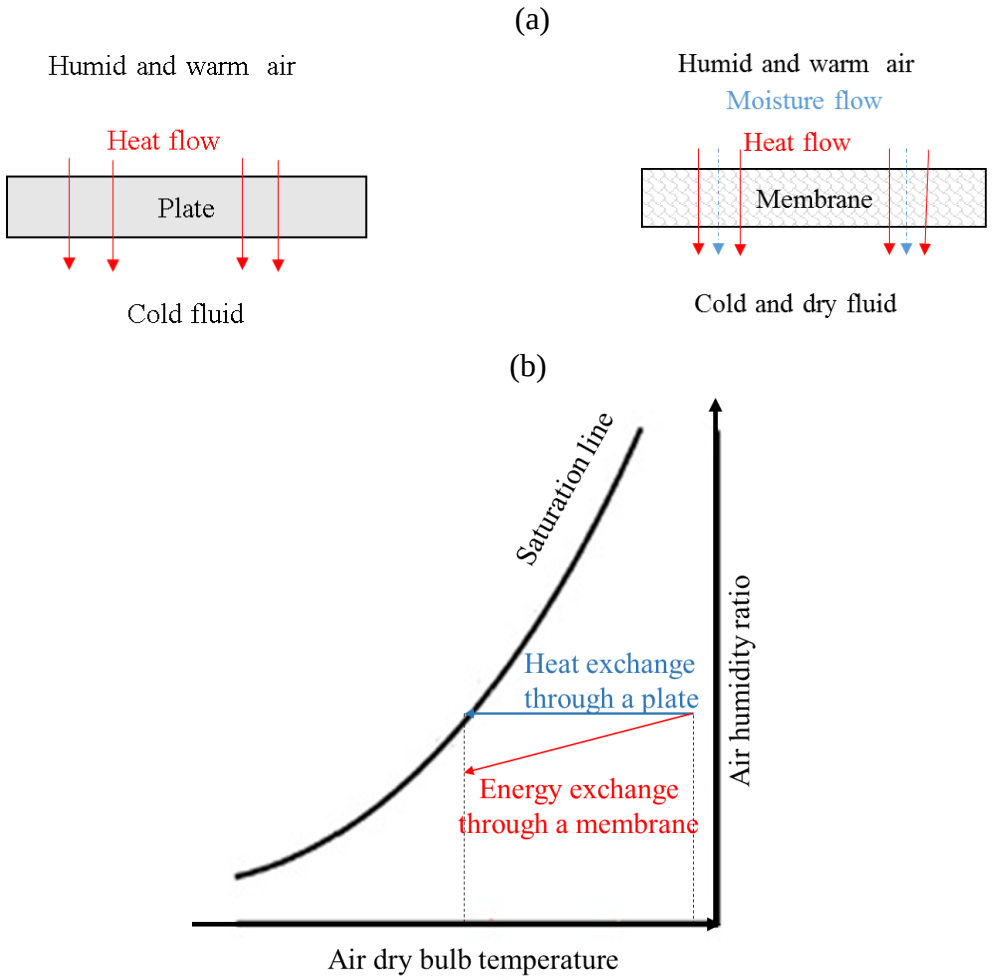

Figure 1.4. (a) Schematic of heat and energy exchange through a plate and membrane, (b) Psychrometric chart showing heat transfer through a plate and heat and moisture transfer through a membrane.

Frost formation in membrane energy exchangers are specifically addressed in the literature in a few studies [8–11,132,133]. Rafati [133] used four methods to detect the occurrence of frosting inside an air-to-air membrane energy exchangers: visual inspection, change in the effectiveness ($\Delta\varepsilon$), change in the pressure drop across the exchanger (Δp), and change in the outlet temperature (ΔT). Further, Rafati [133] defined the frosting limit for an exchanger as the operating conditions at which frost begins to grow in an exchanger. Rafati [133] concluded that the ΔT method detects frosting sooner than the other methods, however, the Δp method is a good indication of the amount of frosting inside the exchanger. However, no information about the process of frost formation, frost properties and the impact of moisture transfer rate through the membrane on frosting is available in the literature.

1.2.4 De-frosting and anti-frosting technologies in refrigeration and air conditioning systems

As mentioned before, frost formation decreases the efficiency of heat/energy exchangers. Therefore, defrosting of the frosted exchanger is crucial. There are several defrosting methodologies that are presented in the literature for both heat and energy exchangers, as follows [44,87,132,136]:

1. Dehumidification of the air inlet humidity
2. Using external sources to remove the frost: External electric, magnetic fields, and ultrasonic vibration
3. Control frosting by design parameters

However, because of the high energy consumption of the defrosting processes, avoiding or preventing frost formation by using anti-frosting materials could be a better solution to the frosting problem. Developing new coatings or surfaces with different roughness [6,27,31,36,38,44,47,51,52,54,56,57,59,60,77,83,114,116,137–141] that are capable of absorbing water, preventing the condensation of water droplet or removing condensed water droplets from the surface; or developing liquid-infused nanostructured surfaces[13,18,28,29,34,36,63,142–144] which are inspired by the anti-frosting properties of human skin, are ongoing research topics in anti-frosting strategies.

The delay in frost formation found in membrane energy exchangers shows membranes are a promising solution to prevent frost formation. Membranes are capable of removing moisture from the humid air continually, and consequently depress the dew point temperature of the humid air. As mentioned in Section 1.2.3, more research is needed to provide a better insight into frost growth on membranes, which is the goal of this Ph.D. research.

1.3 Research objectives

The main purpose of this Ph.D. research is to address the research gaps presented in the previous sections; *i.e.*, to identify the mechanism of frost formation on a membrane, and determine the effect of moisture transfer rate through the membrane on frosting. In this research, the operating conditions that lead to frost growth (frosting limit) and the time that it takes begin frost formation on a membrane is determined. Also, the properties of a frost layer on a membrane and a plastic plate are assessed and compared. Therefore, the objectives are defined as:

1. To apply image processing to characterize frost properties.
2. To identify the effect of moisture transfer on the frosting limit.
3. To determine the mechanisms of frost formation on a membrane.
4. To identify the effect of moisture transfer on frost properties on a membrane.

1.4 List of publications

The outcomes of the current Ph.D. study have been presented in six peer-reviewed journal papers, 1 conference paper, and 1 poster presentation. Chapters 2, 3, and 4 are presented as papers 1, 2, and 3, respectively. Chapter 5, contains the contents of journal paper 4, will be submitted to the International Journal of Heat and Mass Transfer. Papers 5 and 6 are outcomes of a collaboration between this Ph.D. research and a M.Sc. research by Pooya Navid[11]. Papers 5 and 6 are not included in this thesis because they are in Pooya Navid's thesis.

1.4.1 Journal papers

1. S. Niroomand, M. Fauchoux, C. J. Simonson, Experimental characterization of frost growth on a horizontal plate under natural convection, ASME Journal of Thermal Science and Engineering Applications, 2018, accepted.

2. S. Niroomand, M. Fauchoux, C. J. Simonson, Effect of moisture transfer through a semipermeable membrane on condensation/frost limit, ASME Journal of Heat and Mass Transfer, 2018, submitted.
3. S. Niroomand, M. Fauchoux, C. J. Simonson, The mechanism of frost formation on a semipermeable membrane, Langmuir, 2018, submitted.
4. S. Niroomand, M. Fauchoux, C. J. Simonson, Evaluation of the frost properties on a membrane, to be expanded and submitted to International Journal of Heat and Mass Transfer.
5. P. Navid, S. Niroomand, C.J. Simonson, A new approach to delay or prevent frost formation in membranes, ASME Journal of Heat Transfer, 2018, submitted.
6. P. Navid, S. Niroomand, C.J. Simonson, Theoretical model for predicting frosting limit in membranes, International Journal of Refrigeration, 2018, submitted.

1.4.2 Conference paper

1. N. Niroomand, M. Fauchoux, E. Walia, C. J. Simonson, Characterization of frost formation on a cold surface, CANCAM conference, Victoria, Canada, May 2017. Presented by S. Niroomand.

1.4.3 Conference poster

1. N. Niroomand, M. Fauchoux, P. Navid, E. Walia, C.J. Simonson, Frost formation in membranes for HVAC applications, ASHRAE Chapter Regional Conference, May 12, 2016, Saskatoon. Presented by S. Niroomand.

1.5 Thesis overview

This thesis is written in manuscript-style, and consists of six chapters. Chapter 1 presents an overview of the research motivation, background and research objectives. Chapters 2, 3 and 4 each include a research paper that address as one of the objectives. Chapter 5 is written as a regular chapter. The results of Chapter 5 will be the basis of a paper that will be submitted to the International Journal of Heat and Mass Transfer. At the end, Chapter 6 contains the summary and conclusions of the thesis. It should be noted that the manuscripts are slightly modified to present the material in a logical sequence and to follow the thesis formatting. Figure 1.5 shows the outline of the thesis with the objectives addressed in each chapter. A brief overview of each chapter and the authors' contributions to each paper are also given at the beginning of each chapter.

CHAPTER 1: Introduction

CHAPTER 2: Characterization of frost layer on a surface

Manuscript: Experimental characterization of frost growth on a horizontal plate under natural convection

Objective #1: To apply image processing to characterize frost properties

CHAPTER 3: Frosting limit for a plastic plate and membrane

Manuscript: Effect of moisture transfer through a membrane on condensation/frosting limit

Objective #2: To identify the effect of moisture transfer on frosting limit

CHAPTER 4: **The mechanisms of frost formation on a membrane**

Manuscript: The mechanisms of frost formation on a membrane

Objective #3: To determine the mechanism of frost formation on a membrane

CHAPTER 5: **Comparison of frost properties on a plastic plate and a membrane**

Manuscript: Evaluation of the frost properties on a membrane

Objective #1: To apply image processing to characterize frost properties

Objective #4: To identify the effect of moisture transfer on frost properties on a membrane

CHAPTER 6: Summary, conclusions and recommendations for future work

Figure 1.5. Thesis outline with objectives and manuscript titles for each chapter.

CHAPTER 2

CHARACTERIZATION OF FROST LAYER ON A SURFACE

2.1 Overview

This chapter mainly addresses the first objective of this Ph.D. research (*i.e.* to apply image processing to characterize frost properties), especially frost surface roughness, on a surface. To meet the objective, a test facility was designed and built to study frost growth on a flat aluminum plate under natural convection conditions. Natural convection conditions are selected because the temperature and air humidity over the surface are uniform, which results in an approximately uniform frost layer over the surface. The description of the test facility and uncertainty analysis are presented in this chapter. Afterward, the imaging techniques used to measure the thickness and surface roughness of the frost layer are presented. Frost mass is measured by using a measurement in order to find frost density. Also, the frosting process is explained with the help of visualization.

This chapter has been accepted for publication in Journal of Thermal Science and Engineering Applications. The development of the test facility, experimental testing and image analyses and manuscript writing were performed by the Ph.D student, Ms. Shirin Niroomand. Dr. Melanie Fauchoux, contributed to this manuscript by proofreading the manuscript, and providing guidance to clarify the discussions in this manuscript. Prof. Carey J. Simonson (supervisor) critically reviewed the manuscript.

Experimental characterization of frost growth on a horizontal plate under natural convection

S. Niroomand, M.T. Fauchoux, C. J. Simonson

Department of Mechanical Engineering, University of Saskatchewan, 57 Campus Drive, Saskatoon, SK, Canada S7N 5A9

2.2 Abstract

This chapter presents an experimental study of frost formation on a plate under natural convection conditions. Frost thickness, mass, density and surface roughness are measured during each test. Frost thickness and roughness are measured using an image processing technique. The effect of operating conditions (temperature of the plate, and temperature and relative humidity of the air) on the properties of frost are investigated. Frost surface roughness is quantified using two parameters; the average roughness and the skewness of the roughness, which can describe the frost layer shape. The surface roughness of the frost layer is considerably higher than the roughness of the aluminum plate, which should be considered in frosting studies. In this chapter, it is shown that frost surface roughness is related to the frost layer shape, porosity and density. It is also found that the aluminum plate temperature affects the frost surface roughness significantly; as the aluminum plate temperature decreases, the frost layer has a high average roughness and negative skewness, which correspond to a highly porous, low density frost layer. Increasing the air humidity and air temperature affects the average surface roughness slightly but not the skewness of the frost surface.

2.3 Introduction

As was discussed in Chapter 1, a full understanding of the frost growth process is needed to develop methods to delay or eliminate frost in heat exchangers. Thus, in this chapter, test methods to characterize frost layer properties are established, which is the first step of this Ph.D. research on using membranes that could prevent frost formation in exchangers.

Frost forms on a surface when the temperature of the surface is less than the dew point temperature and freezing point temperature of the surrounding air. Frost is a porous media, composed of air voids and ice crystals. Frost growth begins with the formation of ice crystals, as moisture from the air condenses or sublimates onto the surface [145]. The ice crystals continue to grow as water

vapour is transferred from the air to the frost layer. The result is an intricate, porous matrix of frost [145]. The water vapour transferred to the frost layer may either change phase at the surface of the frost layer and increase the thickness of the frost layer; or it may diffuse into the frost layer, change phase within the frost layer and increase the density of the frost layer [145]. Eq. (2.1) shows the division of the mass flux to the frost layer into two terms resulting in an increase in density ($\dot{m}_{\rho}^{"}$) and thickness ($\dot{m}_{\delta}^{"}$), which has been used in the literature to model the frost formation process [91,104,110,121].

$$\dot{m}_{f}^{"} = \frac{\partial(\rho_f \delta_f)}{\partial t} = \dot{m}_{\delta}^{"} + \dot{m}_{\rho}^{"} \tag{2.1}$$

Frost research has shown that the shape of the ice crystals that form on a surface depend on the operating conditions. The main parameters that affect the shape of frost crystals are aluminum plate temperature and air humidity ratio. Several laboratory studies have been done to study the shape of ice crystals at different environmental conditions. Figure 2.1 shows different types of ice crystals grown on a rabbit hair, at different air temperatures and humidity ratios [146]. It can be seen that ice crystals with a needle shape formed at warmer temperatures (Figure 2.1(a), (b) and (c)) and with a flat shape at colder temperatures (Figure 2.1(d), (e) and (f)). The formation of different crystal shapes results in frost layers with different surface characteristics (e.g. different porosity, surface roughness and thermal properties).

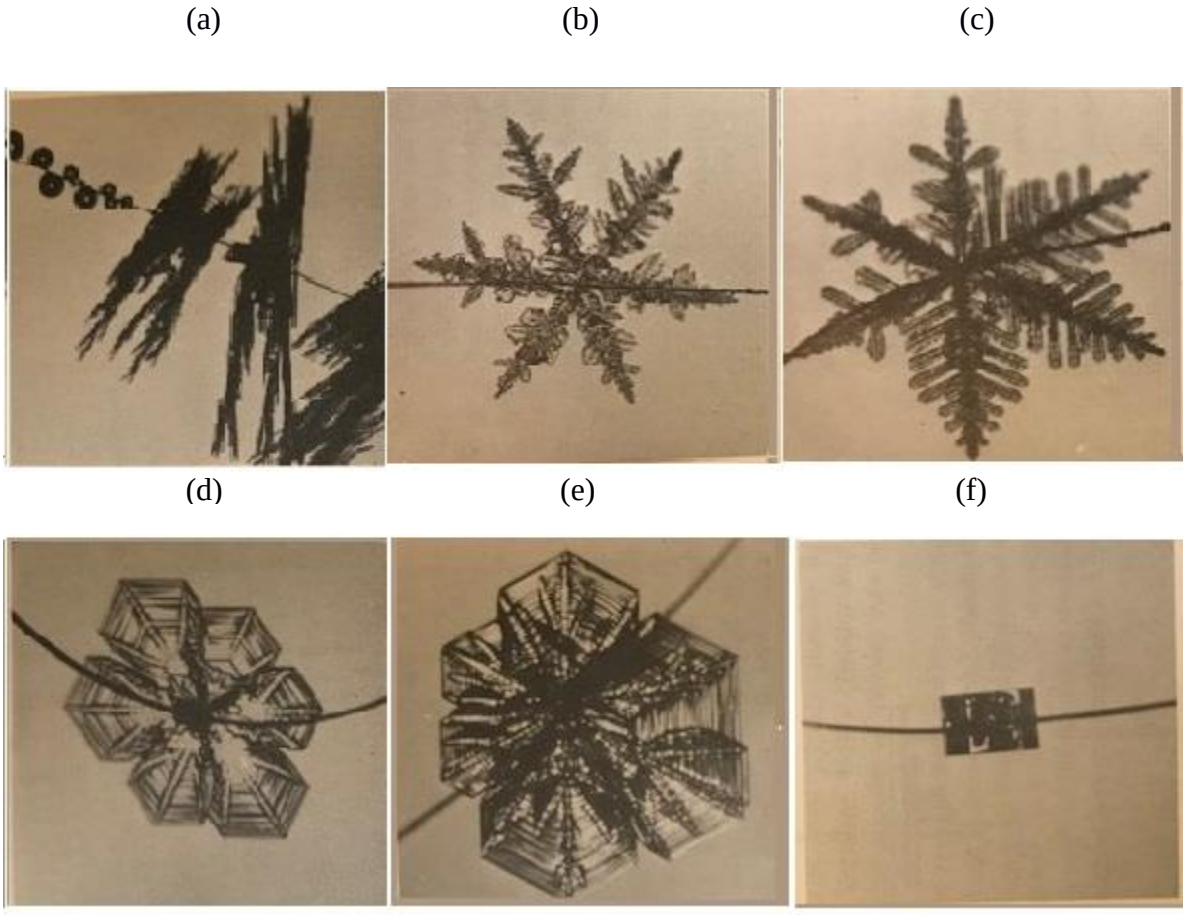

Figure 2.1. The shape of ice crystals grown at different air temperatures, (a) Needles, -6°C (b) Dendrite, -13°C (c) Dendrite, -13°C (d) Sector plate, -17 °C (e) Double sector plate, -15°C (f) Column, -18°C [10].

Many researchers have divided frost formation into different time periods to help characterize the complex nature of frost growth [12,14,48]. Hayashi et al. [14] were the first to characterize frost formation into three distinct periods; "crystal growth", "frost layer growth", and "frost layer full growth". In the "crystal growth" period, small frost crystals cover the cold surface. The frost crystals continue to grow in the vertical direction until a thin layer of frost covers the surface (i.e. $\dot{m}_{\delta}^{"}$ dominates). In the "frost layer growth" period, new frost branches form on the crystals at the frost layer surface ($\dot{m}_{\delta}^{"}$), or frost is deposited within the frost layer ($\dot{m}_{\rho}^{"}$) until a thick and porous layer of frost forms on the surface. In the "frost layer full growth" period, the shape of frost layer does not change, but the frost layer become a dense and tight layer. Hayashi[14] compared the

shape of the frost crystals and the roughness of the frost surface visually during each period and under different operating conditions. They concluded that the shape of the frost crystals is affected by surface temperature and air humidity ratio, but not by air velocity.

Frost formation has been modeled and predicted numerically, however, many assumptions were needed to simplify the numerical models [82], [85], [94], [99], [102], [107], [110], [116]. Breque et al. [96] investigated the effect of different assumptions that have been used to simplify frost growth models, on the prediction of frost growth. They concluded that one way to improve the modeling of frost is to use more accurate correlations for the convective heat and mass transfer coefficients. The heat and mass transfer coefficients are affected by several parameters of the frost, such as thickness, density and the surface characteristics. O'Neal [22] modeled frost growth by using results from other researchers for the frost thermal conductivity and tortuosity. However, because of a lack of information about the frost surface roughness, the surface of the frost layer was assumed as a smooth wall.

Many experimental studies has been conducted to measure frost properties, such as frost thickness, mass, density, and thermal conductivity, at different conditions [27,58,70,73,75,82,90,108]. Brian et al. [73] measured and correlated frost density and thermal conductivity on a cold surface under forced convection conditions. They concluded that the density gradient in the frost layer is negligible, which was later used as an assumption to model frost growth [90]. Leoni et al. [117] presented a comparative study of available data in the literature, including both theoretical models and experimental measurements, for frost thickness and density measurements for different operating conditions and different plate geometries. They found that frost thickness increases with decreasing plate temperature and increasing air relative humidity, and that frost density increases with increasing plate temperature. However, they found some contradictory information about the relation between frost density and air relative humidity. There are also contradictory conclusions for the effect of operating conditions on the mass of frost. Comparing frost property results from the literature shows some contradictory conclusions, which shows that frost properties are strongly a function of experiment of conditions [26, 27].

When studying the effects of operating conditions on frost properties, most of the studies have considered only forced convection conditions [12]–[15]. The goal of the present research is to

study frost growth in heat exchangers, which will also be under forced convection conditions. However, as the velocity of the air is one of the operating conditions that may affect frost growth, the study will first focus on frost growth under natural convection conditions, to study the effects of surface temperature and air humidity ratio on frost growth, independent of air velocity. Under forced convection conditions, frost properties change along the length of the plate. It is expected that under natural convection conditions the frost properties will be uniform over the plate. Natural convection conditions are often used in fundamental studies of frost formation, for example, studies to find the effect of a surface with new properties (i.e. hydrophobicity or hydrophilicity) on frost growth [31,58,59,77,147], and in the refrigeration industry, to study frost growth on a fin or a vertical surface [80,82,88].

In summary, the shape of the frost crystals, which is believed affects frost density and porosity, is primarily dependent on the air humidity ratio and plate temperature, as well as the air temperature, surface properties and time. This chapter presents experimental measurements of characterization of frost layer on an aluminum plate, during the frost layer growth period, under natural convection with different operating conditions. Characterization of the frost layer includes measurements of the frost surface roughness, about which no detailed information has been found in the literature. Frost roughness is measured using well-established image processing methods, as a parameter to quantify the shape of the frost layer and to describe frost growth under different temperature and humidity conditions and furthermore, the relation between frost roughness and density is shown by using experimental results.

2.4 Frost growth experiments

2.4.1 Test facility

A schematic of the test facility used to measure the properties of frost (mass, thickness, density and surface roughness) on an aluminum plate is shown in Figure 2.2. Experiments were conducted in an environmental chamber under natural convection conditions, where the air temperature and relative humidity could be maintained within ±0.2°C and ±2% RH, respectively. Unpolished aluminum plates with dimensions of 4.5 cm × 4.5 cm × 0.06 cm were used as the surfaces for frost growth. The roughness of the aluminum plates were measured using an Optical Profilometer, and the average roughness was found to be between 0.6 μm and 1.5 μm. Six of these aluminum plates

were placed on an isothermal block. The isothermal block consisted of two main parts; the bottom part which housed a cooling coil, and the top part, which was a thick aluminum plate. The two parts of the isothermal block which are covered with thermal paste, are shown in Figure 2.2(b). Flowing cold refrigerant in the cooling coil, provided by a thermal bath, cooled the isothermal block to a constant temperature. The flow rate of the refrigerant was the same in all experiments. One plate was used to measure the plate surface temperature, one plate to measure the frost thickness, and the other four to measure the mass of frost growth on the plates at different times during the test. The surface temperature measurement was made using a T-type thermocouple, affixed to the surface of the aluminum plate using a thermal paste. The thermocouples were calibrated with a Hart scientific 9107 Dry Well Calibrator and found to have an uncertainty equal to ±0.2°C [41]. The mass and thickness measurements will be discussed in more detail in Sections 2.4.2.2 and 2.4.2.1.

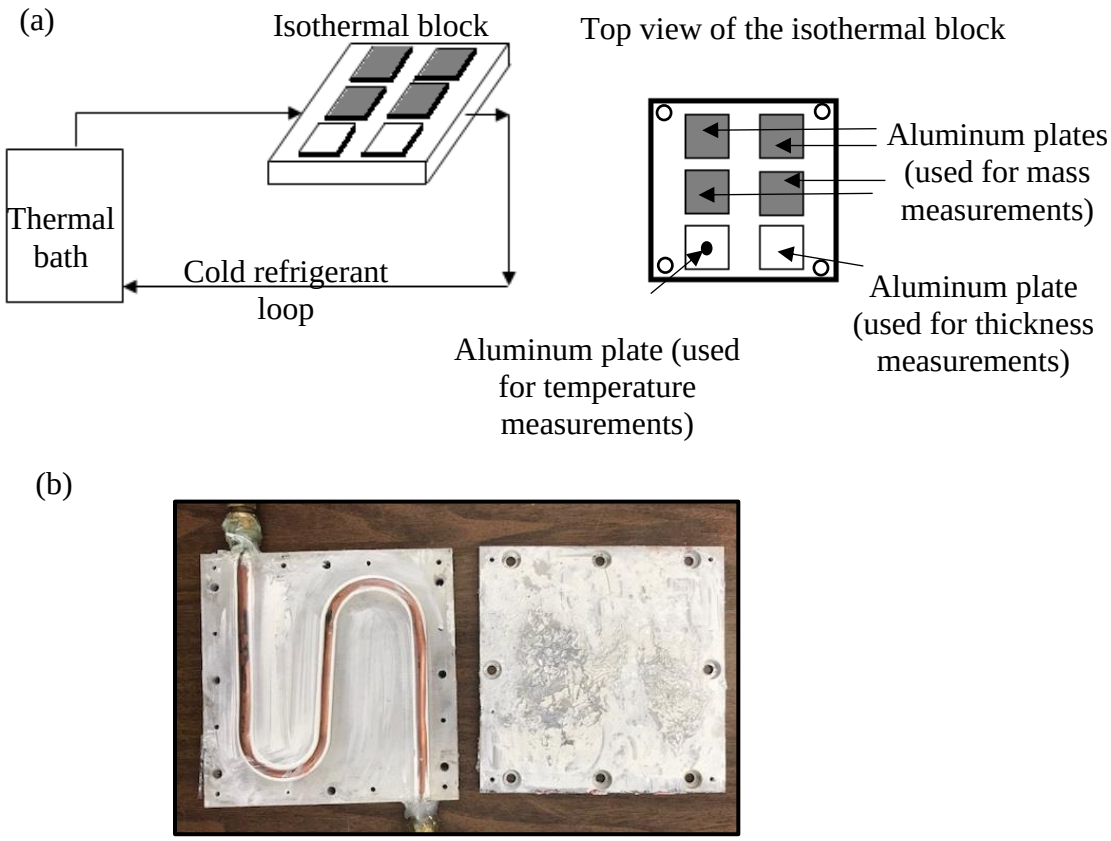

Figure 2.2. Schematic of (a) the experimental setup showing the isothermal block test section containing six aluminum plates to measure frost mass, thickness and surface temperature and (b) the two parts of the isothermal block.

To verify the isothermal condition of the block, the surface temperature of the block was measured at four locations (marked with open circles on the top view of the isothermal block in Figure 2.2). It was found that the maximum temperature differences along the surface of the isothermal block are at the four extreme corners. The temperatures measured at each location are shown in Figure 2.3, for four different tests. The legend for the graph is the temperature of the aluminum plate (T_p) measured during each test. The difference in temperature across the isothermal block is less than 0.5°C during all tests, so the block is considered to be at a constant surface temperature.

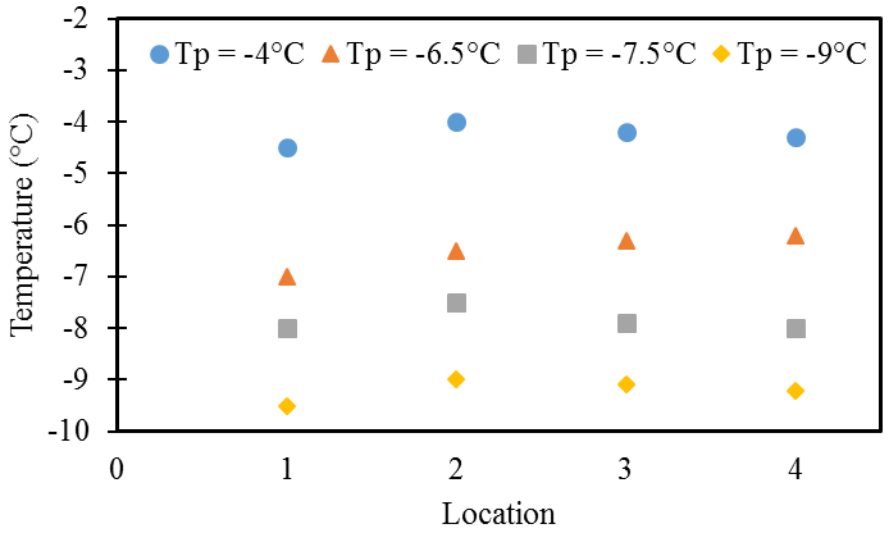

Figure 2.3. Temperature of the isothermal block during tests conducted at four different conditions (Locations 1, 2, 3 and 4 are marked with open circles on the top view of the isothermal block in Figure 2.2).

During testing, the isothermal block was located on a table and covered with a large acrylic box, with one open side. The sides of the acrylic box were in contact with the table, therefore, the isothermal block was fully enclosed by the table and the box on three sides. The purpose of the box was to shield the test section (isothermal block) from any air currents caused by the fans inside the environmental chamber. The box (60 cm × 50 cm × 30 cm) was large compared to the size of the isothermal block (10 cm × 10 cm× 2 cm), to allow natural convection to occur above the block, without interference from the walls or roof of the box. The box was open on one side to allow removal of the plates for mass measurements. The temperature and velocity of the air inside the box were measured to calculate the ratio Gr/Re^2 which indicates whether natural or forced convection forces are dominant. To calculate Gr and Re, the length of the isothermal block is considered as the characteristic length. The results confirmed that natural convection conditions were dominant ($Gr/Re^2 = 30 \sim 50$).

2.4.2 Measurements, data analysis and uncertainty

Before each experiment, the surface of each plate was wiped clean with a dry cotton towel and attached to the isothermal block with thermal paste, to ensure good contact. The plates and

isothermal block were covered with a thin aluminum sheet to avoid direct contact with the humid air prior to the start of the test. The flow of the coolant was then started to cool the isothermal block and aluminum plates to the desired temperature. When the plate temperature, air temperature and air relative humidity reached the desired conditions, the aluminum sheet was removed and the experiment started. The mass and thickness of the frost deposited on the aluminum plates were measured every 30 min, and each experiment was run for 120 min.

2.4.2.1 Mass of frost

The mass of the frost was measured by removing one of the four aluminum plates designated for mass measurement (the shaded plates in Figure 2.2) from the test surface every 30 min. The plate was removed using tweezers and placed in a sealed plastic plate container. Tweezers were used to reduce physical damage to the frost and prevent melting of the frost during this process. The sealed container prevented the loss of mass during the measurement procedure. The mass of the container including the frosted plate was measured using a mass balance (±0.0001 g precision). The container was then opened and left at room temperature to allow the frost to melt and the water to evaporate completely. The mass of the container with the dry plate inside was then measured. The difference in these two measurements is the mass of the frost on the plate (m_f). The mass per unit area (m''_f) was calculated by dividing the mass of the frost by the area of the plate.

To calculate the total uncertainty in the mass measurements, which also included the calibration procedure, the systematic (B) and random (P) uncertainties were determined based on ASME Standard 19 [148] using 95% confidence intervals. The systematic uncertainties in the mass measurement and mass per unit area were found to be ±0.07 g and ±0.03 kg/m^2 by calibrating the mass balance using calibration weights. To determine the random uncertainty, the mass of frost deposited on all four plates was measured at the same time (30 min after the beginning of the test). The random uncertainties in the mass and mass per unit area were found to be ±0.03 g and ±0.013 kg/m^2, respectively, assuming a negligible uncertainty in the area measurement. In calculating the random uncertainty in this way, it includes the uncertainty due to the temperature difference along the isothermal block. The total uncertainties in the mass and mass per unit area were calculated to be ±0.08 g and ±0.03 kg/m^2. For the tests in this chapter, these absolute uncertainty values

correspond to ±30% of the measured mass per area after 30 min of testing, which it will reduce to 9% of the measured mass per area after 120 min.

2.4.2.2 Frost thickness

The thickness of the frost layer on one aluminum plate was measured by taking photographs of the side of the plate, and analyzing these images using computer software. It is assumed that the average thickness of the frost layer viewed from the side of the test section, represents the average thickness of the frost layer across the whole plate surface. A digital camera (Kodak z990) was set on a tripod facing the side of the test section. The camera was focused on the edge of the plate closest to the camera. Images with an average resolution of 110 pixel/mm were taken. Two software programs, ImageJ (National Institutes of Health) and MATLAB (MathWorks), were used to process and analyze the images and to determine the frost layer thickness. This method assumes the frost surface is two-dimensional, neglecting the differences across the width of the plate, which is reasonable for natural convection.

A photograph of the side view of the aluminum plate at the beginning of the test is shown in Figure 2.4(a), and the same plate, after 30 min of testing, is shown in Figure 2.4(b). The thickness of the frost layer (δ_f) was calculated as:

$$\delta_f = \left(\delta_P + \delta_f\right) - (\delta_P) \tag{2.2}$$

where δ_p is the thickness of the plate and (δ_p+ δ_f) is the average distance between the top surface of the frost layer and the top of the isothermal block. The side of the isothermal block is shaded red in the photographs to increase the contrast between the aluminum plate and the isothermal block.

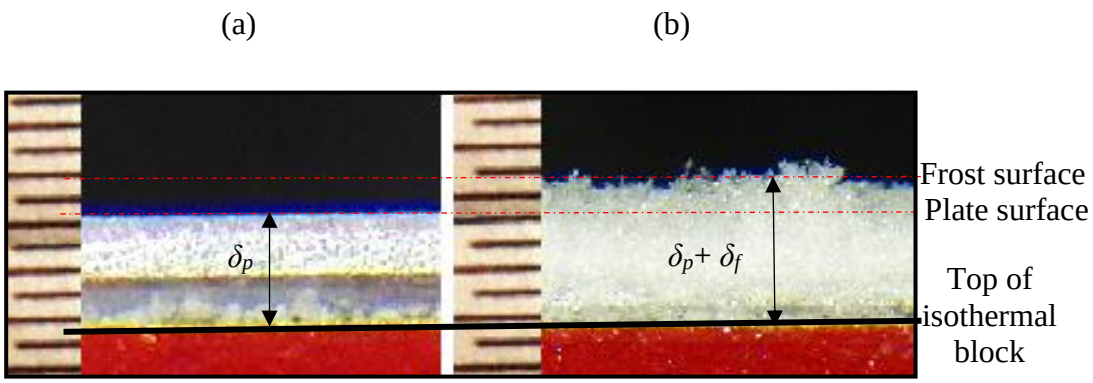

Figure 2.4. Photographs of the side view of the aluminum plate on top of the isothermal block with (a) no frost at the beginning of a test and (b) frost accumulation after 30 min of testing.

Because the frost surface is not smooth, ($\delta_p+ \delta_f$) will vary along the length of the plate. To calculate ($\delta_p+ \delta_f$) for the whole plate, the frost surface and the top of isothermal block were detected and mapped at all pixel points along the plate length. Figure 2.5 shows the steps used in the thickness measurement process. The light part of the image is the frost layer and the aluminum plate, the rest of the image is the background. Each pixel in the image has a value (between 0 and 255) that represents its intensity. To distinguish between frost and background, the image was converted to a black and white, binary image, using ImageJ, as seen in Figure 2.5(b). In binary images, there are only two possible values for each pixel, 0 for black and 1 for white. To make the binary image, each pixel in the original image with a value greater than a threshold value was replaced with a white pixel and each pixel with a value lower than the threshold was replaced with a black pixel. The default threshold value used by ImageJ is 125. Since the contrast between the frost layer and the background was high in this experiment, changing the threshold value between 100 and 150 had a very minor effect on the results. Therefore, the default threshold value of 125 was used for all images.

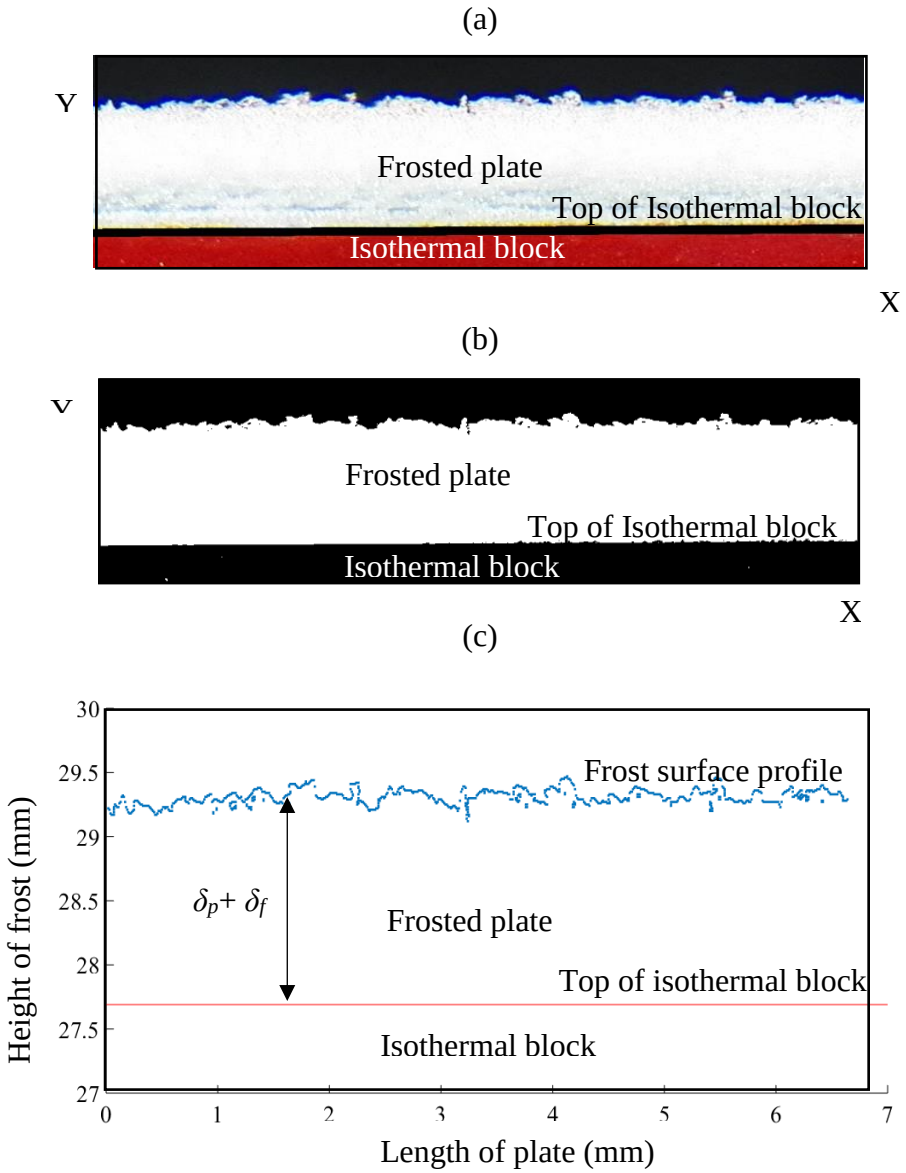

Figure 2.5. The process used to determine the thickness of the frosted plate ($\delta_p + \delta_f$) at each point along the plate, starting with (a) an image from the side view of the frosted plate, (b) the converted binary image of (a), and then (c) the height of the frost surface and the base line (in mm).

The frost surface and the top of the isothermal block are the points where the pixel values abruptly change between 1 (white) and 0 (black). The two surfaces were detected using a program written in Matlab. The program started from the top of the image and scanned down to find the position of the last black pixel, the frost surface, and the last white pixel, the top of the isothermal block. In order to convert the position of the pixels in the XY coordinate system to physical units, a scale was set that converts pixel size to mm. A ruler was fixed beside the test section and was used to determine the conversion scale for each image. Based on this scale, the frost surface and the base line were plotted, as shown in Figure 2.5 (c). The thickness of the frost was then determined from these values.

The systematic uncertainty in the thickness measurement was calculated by measuring the thickness of a standard plate with known thickness (2.542 mm), which was placed on the aluminum plate, and analyzed in the same manner as the frost thickness. The analysis was performed three times to determine the thickness of the standard plate and the average was found to be 2.528 mm. The combination of the difference between these two measurements (0.014 mm) and the resolution of the photos (0.009 mm based on 110 pixel/mm) is used as an estimation of the systematic uncertainty in the average thickness measurement which determined to be ±0.016 mm.

To calculate the random uncertainty of the thickness measurement, the frost thickness was calculated using three images of frost taken at one time. The random uncertainty was found to be ±0.017 mm and the total uncertainty to be ±0.02 mm. The uncertainty in the thickness measurement includes the error in scaling and image analysis. For the range of tested operating conditions, the relative uncertainty in the thickness is equal to ±7% for the thinnest frost layer and ±2% for the thickest frost layer.

It should be noted that when calculating the thickness and surface roughness, any re-entered features, where the frost layer overhangs another part of the frost surface, were ignored. While these are evident in the photographs, the techniques used to determine surface roughness are not able to account for these features. This problem has been noted in other research found in the literature and is something that requires further investigation to solve. These features may have a significant effect on the properties of the frost layer, as they could produce air pockets, which would increase the thermal resistance of the frost layer, but are not considered here.

2.4.2.3 Frost surface roughness

The surface roughness of the frost layer is calculated from the surface profile generated during the thickness measurement discussed previously. The roughness represents the shape of the frost surface that has formed on the plate, which changes with operating conditions and time. Two variables were used to quantify the surface roughness: the arithmetic average of the absolute values of the profile height deviations from the mean (R_a) and the skewness of the surface profile (R_{sk}), based on ASME Standard B46.1[149]. Several other variables, taken from the literature, were considered for the surface roughness, however, the results showed that R_a and R_{sk} describe the frost layer shape more clearly. R_a describes the average height of the peaks and valleys of the surface compared to the mean line, as

$$R_a = \frac{1}{n}\sum_{i=1}^{n}|y_i| \tag{2.3}$$

where n is the number of samples, equal to the number of pixels along the X-axis of the plate, and y_i is the distance from the frost surface to the mean line, at each pixel location along the plate.

As there are 110 pixel/mm and the plate is 4.5 cm long, n = 4950 pixels. This value will change if the number of pixels per mm changes, due to using a different camera or changing the field of view. This is an important number, as the accuracy of the surface roughness values will decrease as n decreases. It is felt that the chosen number of pixels per mm is acceptable to obtain accurate results, as the measured roughness values (0.03 mm to 0.2 mm) are much higher than the resolution of the pictures (9 µm). Another factor that will affect the uncertainty of the measurements is the length of the plate considered. If only a fraction of the plate were considered, rather than the full length, the uncertainty would increase. Testing various observation widths, it was found that the length considered should be at least greater than 1 cm to ensure accurate results.

The skewness of the roughness (R_{sk}) indicates whether the frost surface has more peaks or valley, and is calculated from

$$R_{sk} = \frac{1}{n\,{R_q}^3}\left[\frac{1}{n}\sum_{i=1}^{n}(y_i)^3\right] \tag{2.4}$$

$$\text{where } R_q = \left(\frac{1}{n}\sum_{i=1}^{n}|y_i|^2\right)^{0.5} \tag{2.5}$$

The R_a value itself does not provide information about shape of frost surface, it presents the mean deviation in height of surface profile; surface with high R_a value, has very deep valleys or long peaks, and surface with low R_a value, has very shallow valleys or short peaks. It should be noted that existence of a few non-typical peaks or valleys does not affect R_a. However, R_{sk} represents the distribution of the surface profile about the mean line. An example sketch of two frost surfaces are shown in Figure 2.6. In the top sketch, there is a small number of fairly large valleys. This results in a negative value for R_{sk}. In the second sketch, a small number of fairly large peaks results in a positive value for R_{sk}. In other words, when a frost layer has a relatively uniform surface, but deep valleys, the surface will have a negative R_{sk} value. Alternatively, if the frost layer consists of a few peaks on a nearly uniform surface, R_{sk} will have a positive value.

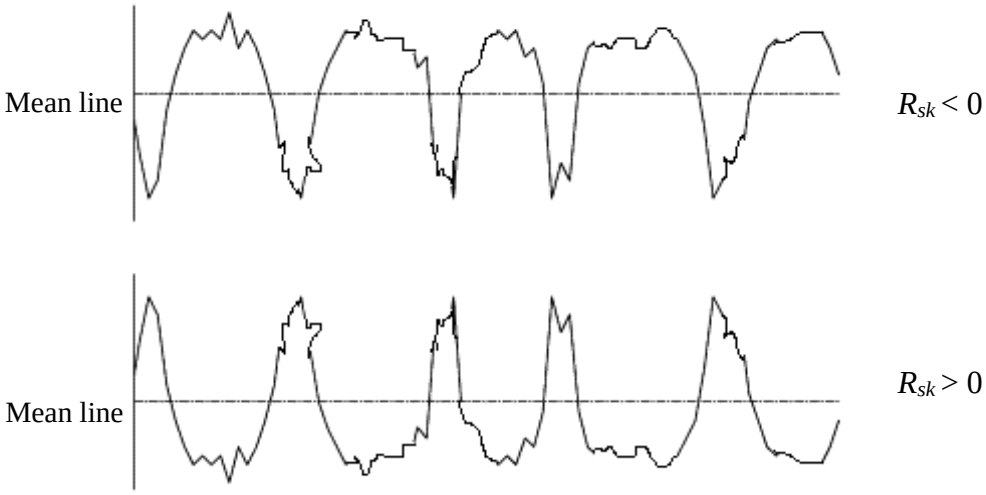

Figure 2.6. Examples of frost surfaces with negative and positive R_{sk} values, for the same R_a value.

2.4.2.4 Frost density

The density of the frost (ρ_f) was calculated by dividing the frost mass per unit area ($m_f^{"}$) by the frost thickness (δ_f), as follows;

$$\rho_f = \frac{m_f^{"}}{\delta_f} \tag{2.6}$$

Propagation of uncertainty was used to calculate the uncertainty in the density from the uncertainties in the thickness and mass of the frost [40].

2.4.3 Repeatability of the experiment

To determine the repeatability of the experiments, the experiment was repeated three times when T_p = -10°C and the results for mass measurements are shown in Figure 2.7(a). Also, all experiments at other conditions were repeated twice. Figure 2.7(a) also shows results from two experiments when T_p = -21°C, where air temperature and humidity ratio were the same as the experiment with T_p = -10°C. Figure 2.7(b) shows the repeatability of the thickness measurement at a plate temperature of -10°C. It can be seen that there is good repeatability of the entire experiment within the experimental uncertainties for both the thickness and mass measurements.

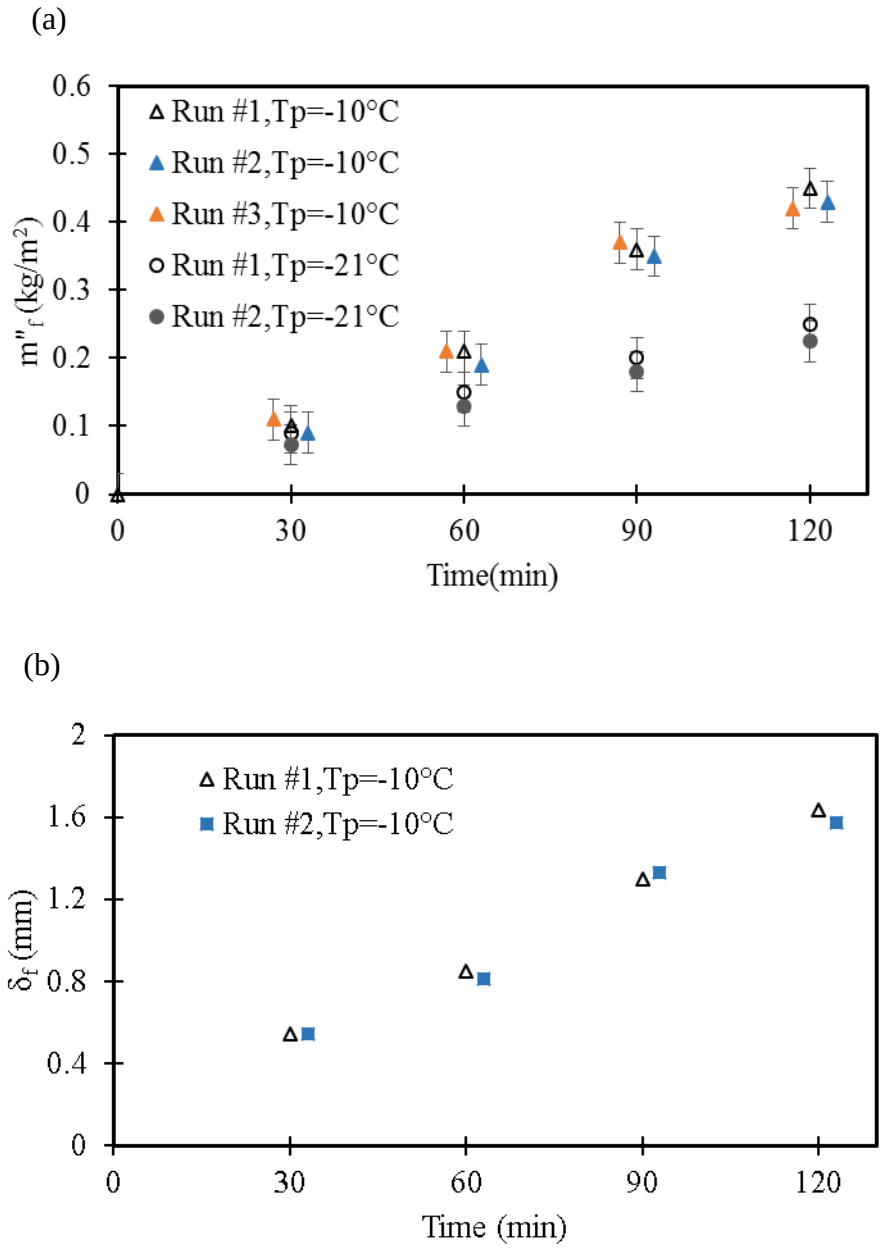

Figure 2.7. Repeatability of (a) the mass measurement and (b) the thickness measurement for tests at the same operating conditions for air (T_{air} = 20°C, RH_{air} = 50% RH) and different plate temperature (T_p = -10, -21°C). Each set of measurements were taken at the same time during the two experiments but are shown slightly offset to avoid the symbols from overlapping each other. The error bars represent the 95% uncertainty bounds in the measured variables. Error bars are not shown for the frost thickness because the uncertainty (±0.02 mm) is smaller than the symbols.

2.5 Verification with results from the literature

The thickness measurements are compared with results from the literature in Figure 2.8, as most of the research on frost growth on a horizontal plate under natural convection conditions have focused on the frost thickness measurement. Results from the present work at two different plate temperatures (T_P = -10°C & -21°C), but at the same air temperature and humidity ratio (T_{air} = 20°C, RH_{air} = 50% RH), are compared with two results from the literature. Hao et al. [58] measured frost thickness at T_{air} = 23°C, RH_{air} = 61 % RH, and T_P = -19°C on an aluminum plate under natural convection conditions. Liu [23] measured frost thickness at lower air temperature and humidity ratio and higher plate temperature (T_{air} = 17.5°C, RH_{air} = 42 %, T_P = -10.4°C) on a copper plate under natural convection conditions. Results from the present work were done at the air temperature and humidity ratio between the two test conditions from the literature, and at two plate temperature; one at T_P = -21°C, which is close to the result from Hao et al. [58], and the other at T_P = - 10°C, which is close to the result from Liu et al. [23]. The measurements of thickness over time, show similar trends to those found in the literature, but the absolute values are different. As expected, higher air relative humidity and air temperature results in a larger frost thickness. This gives confidence that the methods used in this study are acceptable for measuring the frost thickness.

It can be seen that the uncertainty in thickness measurement is low in this chapter, which is the result of using image processing to find the thickness. By using photography and image processing, the minimum resolution of 9 µ is possible, which is low compared to the other thickness measurements methods.

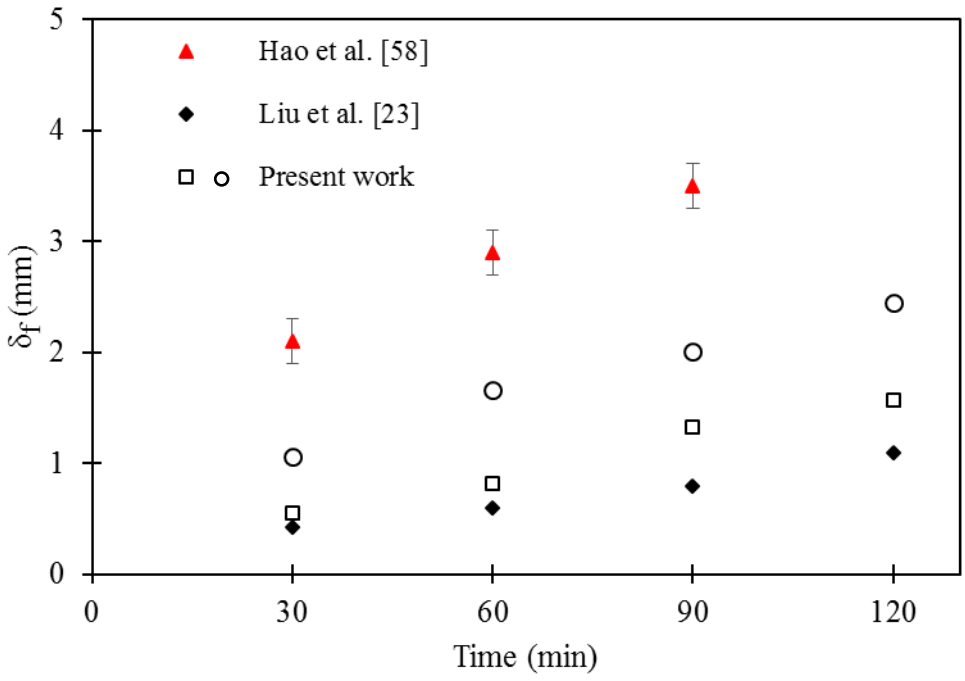

Figure 2.8. Comparison of frost thickness and the current work (T_{air} = 20°C, RH_{air} = 50% RH, T_p = -10°C and -21°C, and with results from the literature [23]&[58], where

- □ T_{air}=20°C, RH_{air}=50 %, T_P= -10°C
- ○ T_{air}=20°C, RH_{air}=50 %, T_P= -21°C
- ▲ T_{air}=23°C, RH_{air}=61 %, T_P= -19°C
- ◆ T_{air}=17.5°C, RH_{air}=42 %, T_P= -10.4°C

2.6 Experimental results and discussion

2.6.1 Plate temperature (T_P)

To determine the effect of the plate temperature on frost growth, tests were performed at two different plate surface temperatures, T_p = -21°C and T_p = -10°C. Photographs were taken at the start of the test (Time = 0 min), at Time = 2 min, Time = 30 min, and every 30 min after that. The photographs for these two tests can be seen in Figure 2.9.

During the early stage of frost formation (Time = 2 min) at T_p = -21°C (Figure 2.9(a)), frost grew as needle shaped crystals in the vertical direction, far apart from each other. After 30 min, a thick layer of dendritic and big feather-like crystals with high porosity appeared on the plate. The ice crystals are long with a plate shape on the top. As the test went on, the ice crystal growth continued until a thick, uniform and porous layer of frost formed. At the end of the test, the frost layer at T_p = -21°C had a fragile, weak structure and was easily removed with small vibrations of the plate.

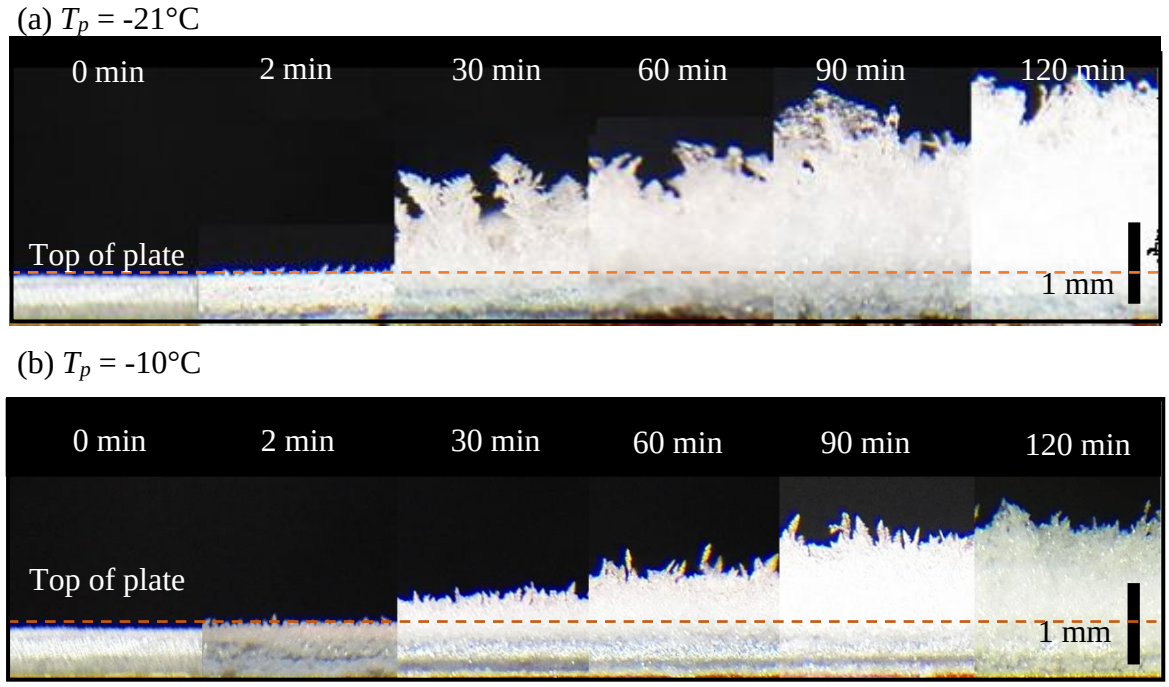

Figure 2.9. Frost growth on the plate at (a) T_p = -21°C and (b) T_p = -10°C with T_{air} = 20°C and RH_{air} = 50% RH.

Frost growth on the plate at T_p = -10°C is shown in Figure 2.9(b). At the very beginning of the test (Time = 2 min), a very thin layer of frost with short crystals close to each other formed on the plate. As the frost grew, needle shaped ice crystals formed over the whole surface of the plate. As time progressed, the frost layer continued to grow, but still with the needle-shaped crystals protruding from the frost surface. The resulting frost layer was thin and dense.

These results show that the behaviour of frost growth on a surface is dependent on the temperature of the surface. Comparing the photographs taken at the two plate temperatures at each time step, the frost on the colder plate (T_p = -21°C) is thicker, more porous and has a feather-like structure with high amount of air pocket (because of the re-entered feather of the frost surface at T_p = -21°C), which decreases the thermal conductivity and increases the thermal resistance of the frost layer. The frost on the warmer plate (T_p = -10°C) is thinner, denser and has a needle like structure on the top. Formation of different frost crystals results in a higher porosity of the frost layer on the plate at the lower temperature, which agrees well with the literature [2], [14].

The measurements of thickness, mass per unit area, density and surface roughness for the frost on the two plates at different temperatures are shown in Figure 2.10. The thicknesses of the two frost layers are shown at four time steps, in Figure 2.10(a). The frost layer is thicker when T_p = -21°C compared to when T_p = -10°C, as seen in the photographs, which agrees with the literature [58,70,117]. The rate of frost growth can be seen in this graph by looking at the slope between points. It can be seen that the initial rate of frost growth (between 0 min and 30 min) for the colder plate is 0.03 mm/min, which is higher than that for T_p = -10°C (which is 0.015 mm/min). After 30 min, the rate of frost growth is approximately constant for both plate temperatures (about 0.01 mm/min for both conditions).

The mass per unit area and the density of the frost on the plate are given in Figure 2.10(b) and 10(c), respectively. For both plate temperatures, the mass accumulation increases throughout the tests. During the first 60 min of the test, the difference between frost mass at two plate temperatures are less than the uncertainty in measurements, and then frost mass increases slightly at T_p = -10°C compared to the frost mass at T_p = -21°C. For the frost mass, the number of data points available in the literature is limited (especially on a horizontal plate under natural convection conditions), and sometimes results are even contradictory. For example, Lee et al. [70] showed higher frost mass accumulation on a vertical plate with lower temperature under natural convection conditions. Fossa et al. [82] showed that frost mass is not affected by plate temperature. Therefore, a more detail investigation is presented in APPENDIX A to justify the results. It can be concluded that the lower mass of the frost at T_p = -21°C could be because of the formation of a thick, porous and rough layer of frost on the surface that reduces the potential driving force for frost formation compared to the test when T_p = -10°C. It can be seen in Figure 2.10 (c) that the density is considerably higher for the test with T_p = -10°C, compared to the test with T_p = -21°C. The formation of frost layer with low density and high thickness at lower plate temperatures has been reported in the literature [14,103,117]. In each case the tests were repeated to ensure the results are accurate.

Based on the these results, it can be concluded that at higher surface temperatures (-10°C), the moisture transfer from the air to the frost layer is predominantly in the form of $\dot{m}''_{\rho}$, which results in thin, dense frost; while at lower surface temperatures (-21°C), the moisture transfer is

predominantly in the form of $\dot{m}''_{\delta}$, resulting in thick, light, porous frost. It should be noted that $\dot{m}''_{\rho}$ and $\dot{m}''_{\delta}$ are defined in Eq. 2.1.

The surface average roughness and skewness are shown in Figure 2.10(d) and (e). Initially the average roughness is much higher when T_p = -21°C then when T_p = -10°C, which is confirmed in the photographs from Figure 2.9. It can be seen that within the first 60 min of the test, average roughness at T_p = -21°C, is about 0.2 mm which is large compared to the average roughness of the Aluminum sheet (0.6 ~ 1.5 μm). As frost continues to grow, the surface roughness gradually decreases for the case when T_p = -21°C, which indicates inter-branching between frost crystals on the top surface. These branches tend to fill the valleys and result in more uniform frost surface (i.e., lower value of R_a). The R_a gradually increases for the case when T_p = -10°C, because of the growth of needle shaped crystals. It can be seen that after 120 min, R_a is the same for the two plate temperatures, however, at T_p = -21°C the frost layer is more porous than at T_p = - 10°C (i.e., lower density in Figure 2.10(c)).

Conversely, the skewness of the roughness distribution is higher and consistently positive when T_p = -10°C, and lower and negative when T_p = -21°C. This indicates that when T_p = -10°C the frost surface is made up of more peaks than valleys, which agrees with the photographs that show needle like structures rising out of the frost layer. When T_p = -21°C the frost surface has a negative R_{sk} which shows more valleys exists. This agrees with the photographs which show feather like crystal structures. The results from these two tests show that the surface temperature has a significant impact on the frost layer shape, which is quantified with R_{sk}.

The results suggest that there is a connection between the surface roughness and the density of the frost. A positive R_{sk} and low R_a corresponds to a frost layer with relatively less porosity and high density and a negative R_{sk} and high R_a corresponds to frost layer with relatively high porosity and low density. A relationship between surface roughness and frost density would be very useful in practical applications. It may not be easy to measure the density of frost inside an energy exchanger, or duct, but it may be possible to visually inspect the frost, estimate the surface roughness from photos and then determine the density of the frost from these relationship. However, more research is needed to determine the exact relationship.

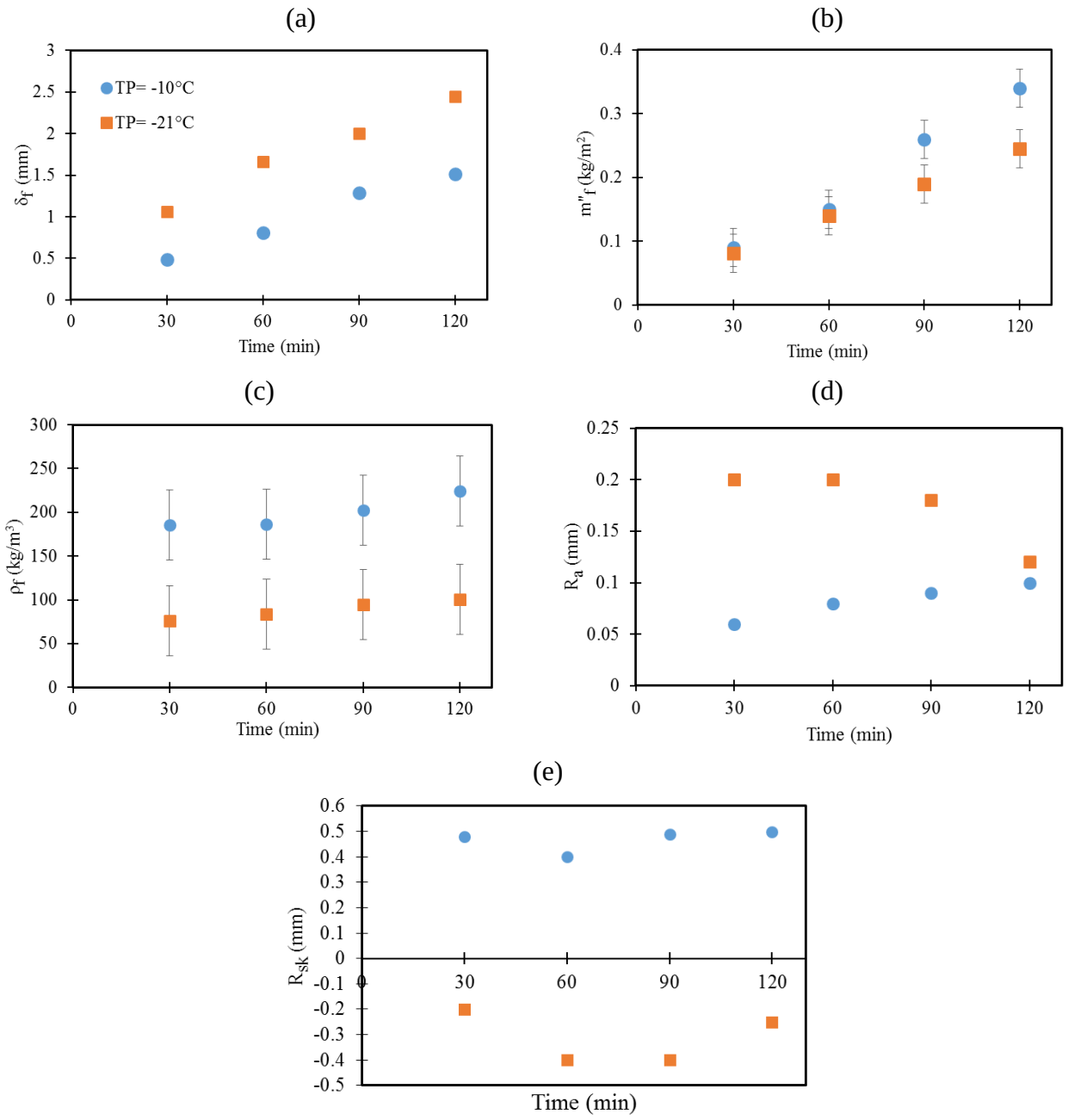

Figure 2.10. The effect of plate temperature on (a) frost thickness, (b) mass, (c) density, (d) average frost roughness, and (e) skewness roughness with T_{air} = 20°C and RH_{air} = 50% RH. (error bars are not shown for the frost thickness because the uncertainty (±0.02 mm) is smaller than the symbols)

2.6.2 Air relative humidity (RH_{air})

To determine the effect of the air relative humidity on frost growth, tests were performed at two different air relative humidity levels, RH_{air} = 50% RH and RH_{air} = 30% RH, at a plate temperature of T_p = -10°C. Photographs for the two tests can be seen in Figure 2.11, at intervals of 30 min (the test with T_p = -10°C and RH_{air} = 50% RH was repeated in Figure 2.10 but is repeated in Figure 2.11 for comparison). The structure of the frost appears to be the same in both cases, however the needle-like crystals are smaller when RH_{air} = 30% RH. The thickness of the frost is also smaller when RH_{air} = 30% RH, at each time step. This is expected, as there will be less overall moisture transfer from the air to the frost layer at the lower RH_{air} level.

(a) RH_{air} = 50% RH

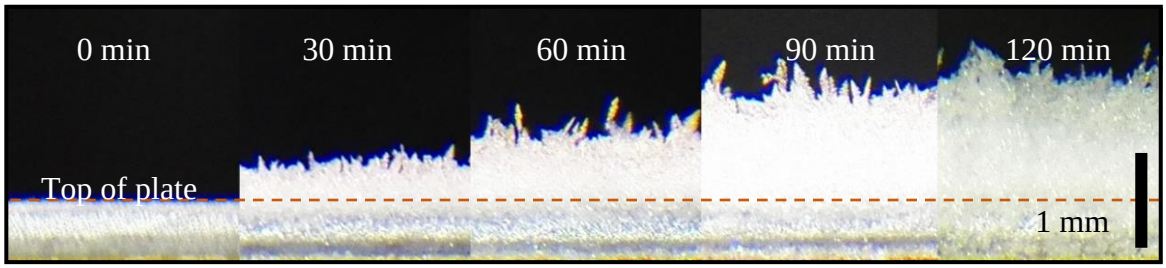

(b) RH_{air} = 30% RH

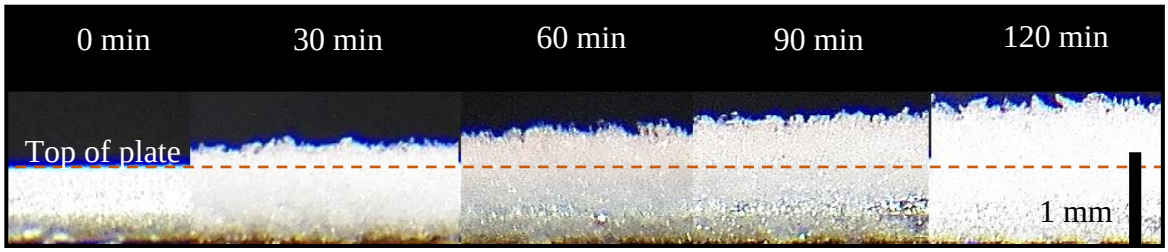

Figure 2.11. Photographs showing the frost growth process with time for (a) RH_{air} = 50% RH and (b) RH_{air} = 30% RH, with T_p = -10°C and T_{air} = 20°C.

The influence of the air relative humidity on the frost thickness, mass per unit area, density and surface roughness is shown in Figure 2.12. The thickness of the frost when RH_{air} = 30% RH is significantly lower than when RH_{air} = 50% RH, as was seen in the photographs. At the first 30 min of the test the rate of growth when RH_{air} = 50% RH is equal to 0.015 mm/min which is higher than that when RH_{air} = 30% RH, which is equal to 0.009 mm/min. After 30 min the rate of frost growth is almost constant for both conditions (0.01 mm/min when RH_{air} = 50% RH and 0.002 mm/min

when RH_{air} = 30% RH). The mass of the frost is lower when RH_{air} = 30% RH, due to the lower driving potential for moisture transfer from the air, as seen in Figure 2.12(b). However, the difference between frost mass at two air relative humidities is smaller than the uncertainty in mass measurement at the first 60 min. The density of the frost at RH_{air} = 30% RH is higher that the frost density at RH_{air} = 50% RH, as shown in Figure 2.12(c). The formation of the frost layer with higher mass and thickness, but lower density at higher air humidity were found in the literature[117][82]. The R_a and R_{sk} of the frost surface are shown in Figure 2.12(d) and Figure 2.12(e). Figure 2.12(d) shows that R_a is lower at RH_{air} = 30% RH, than R_a at RH_{air} = 50% RH, while R_{sk} is positive for both air RH values. This means that the frost layers at RH_{air} = 30% RH and 50% RH have a similar shape, but with a slightly higher roughness when the air is more humid, which result in the frost layers with the slightly lower density, but the same shape.

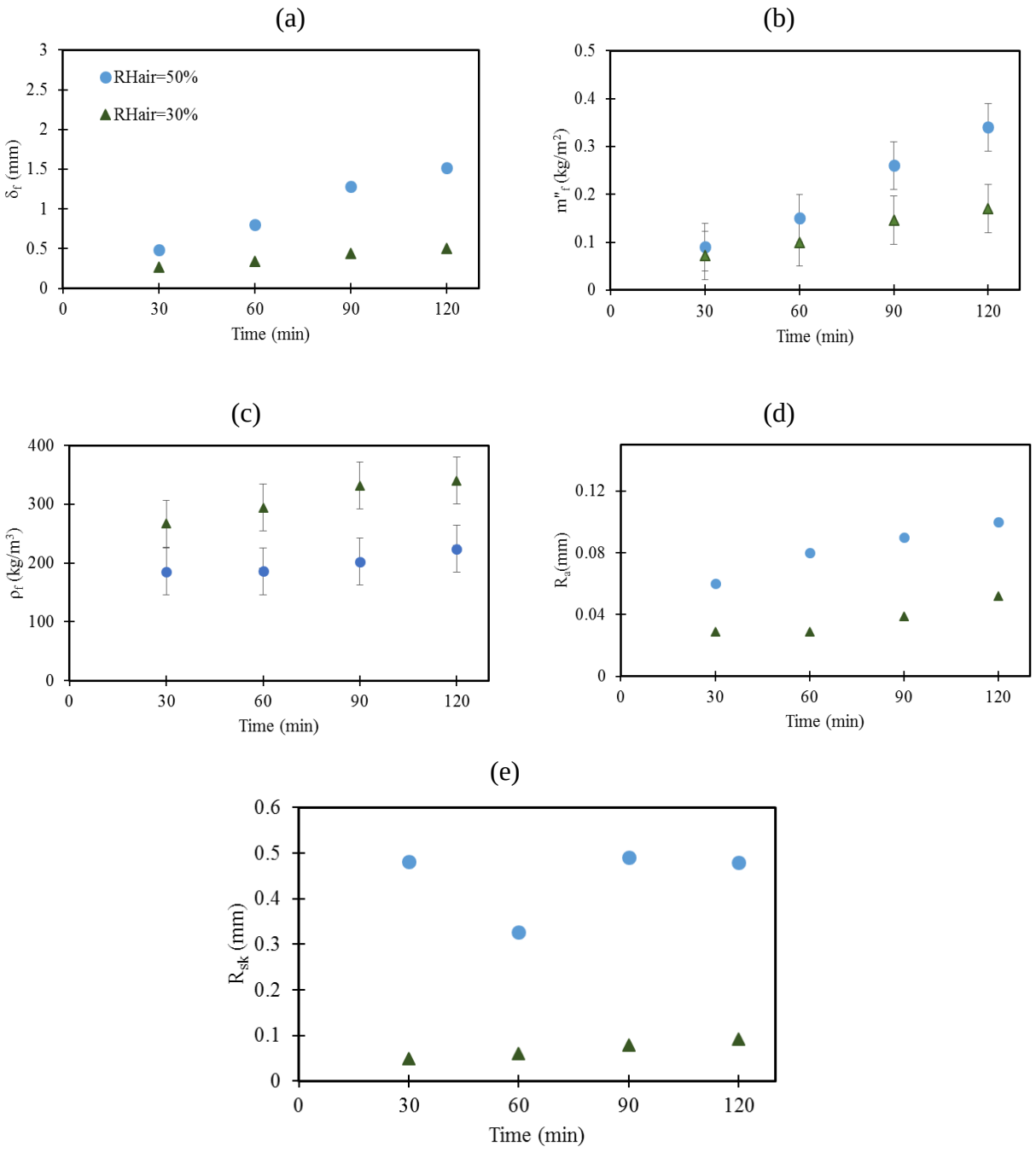

Figure 2.12. The effect of air relative humidity on frost properties (a) frost thickness, (b) mass, (c) density, (d) average frost roughness, and (e) skewness roughness with T_{air} = 20°C and T_p = -10°C. (Error bars are not shown for the frost thickness because the uncertainty (0.02 mm) is smaller than the symbols).

2.6.3 Air temperature (T_{air})

The previous tests for surface temperature and air relative humidity have been performed at an air temperature of T_{air} = 20°C. To see the effect of the air temperature on the frost growth, a test is performed at T_a = 15°C, with T_p = -10°C and RH_{air} = 50% RH. Photographs of the tests at T_{air} = 20°C and T_{air} = 15°C are shown in Figure 2.13. The frost layer that formed at T_{air} = 15°C is thinner than the frost layer at T_{air} = 20°C. The frost crystals at the two different air temperatures are similar, however, the frost layer at T_{air} = 15°C looks more uniform than the frost layer at T_{air} = 20°C.

(a) T_{air} = 20°C

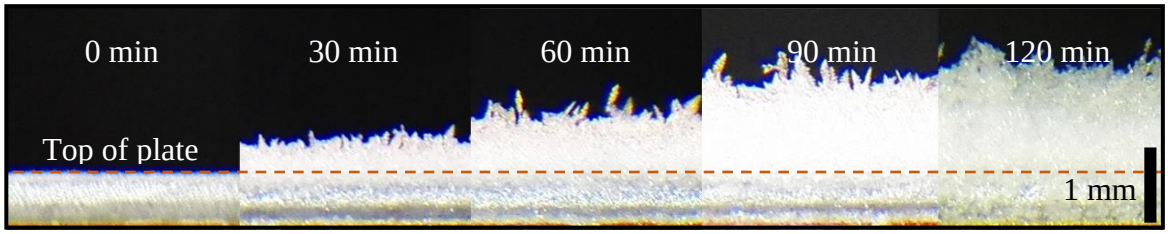

(b) T_{air} = 15°C

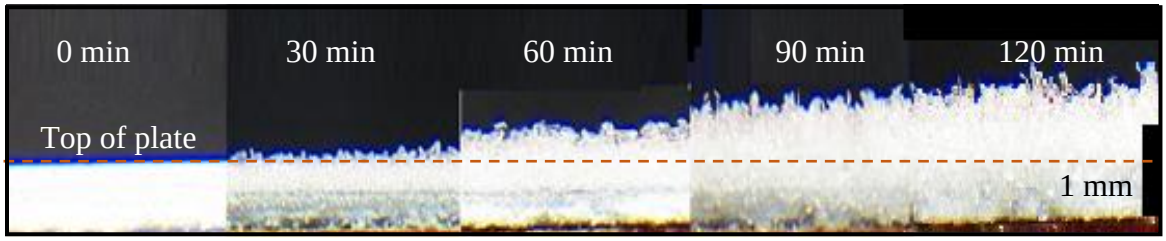

Figure 2.13. Photographs showing the frost growth process when (a) T_{air} = 20°C and (b) T_{air} = 15°C with T_p = -10°C and RH_{air} = 50% RH.

Figure 2.14 presents the effect of air temperature on the frost properties. As seen in the photographs of Figure 2.13, decreasing the air temperature decreases the frost thickness (Figure 2.14(a)) and mass (Figure 2.14(b)). At the first 30 min of the test the rate of growth when T_{air} = 20°C is equal to 0.015 mm/min which is higher than that when T_{air} = 15°C, which is equal to 0.01 mm/min. After 30 min the rate of frost growth is almost constant for both conditions (0.01 mm/min when T_{air} = 20°C and 0.005 mm/min when T_{air} = 15°C).When the air temperature decreases, at constant RH_{air}, the amount of moisture in the air, W_{air}, also decreases, which reduces the driving potential for moisture transfer, and therefore less frost forms on the plate at the lower air temperature. The

frost density is slightly higher at T_{air} = 15°C compared to those at T_{air} = 20°C, as seen in Figure 2.14(c) and (d). Figure 2.14(e) shows that R_{sk} for the two frost layers are positive, which means that the frost structures are mainly similar at T_{air} = 15°C and T_{air} = 20°C.

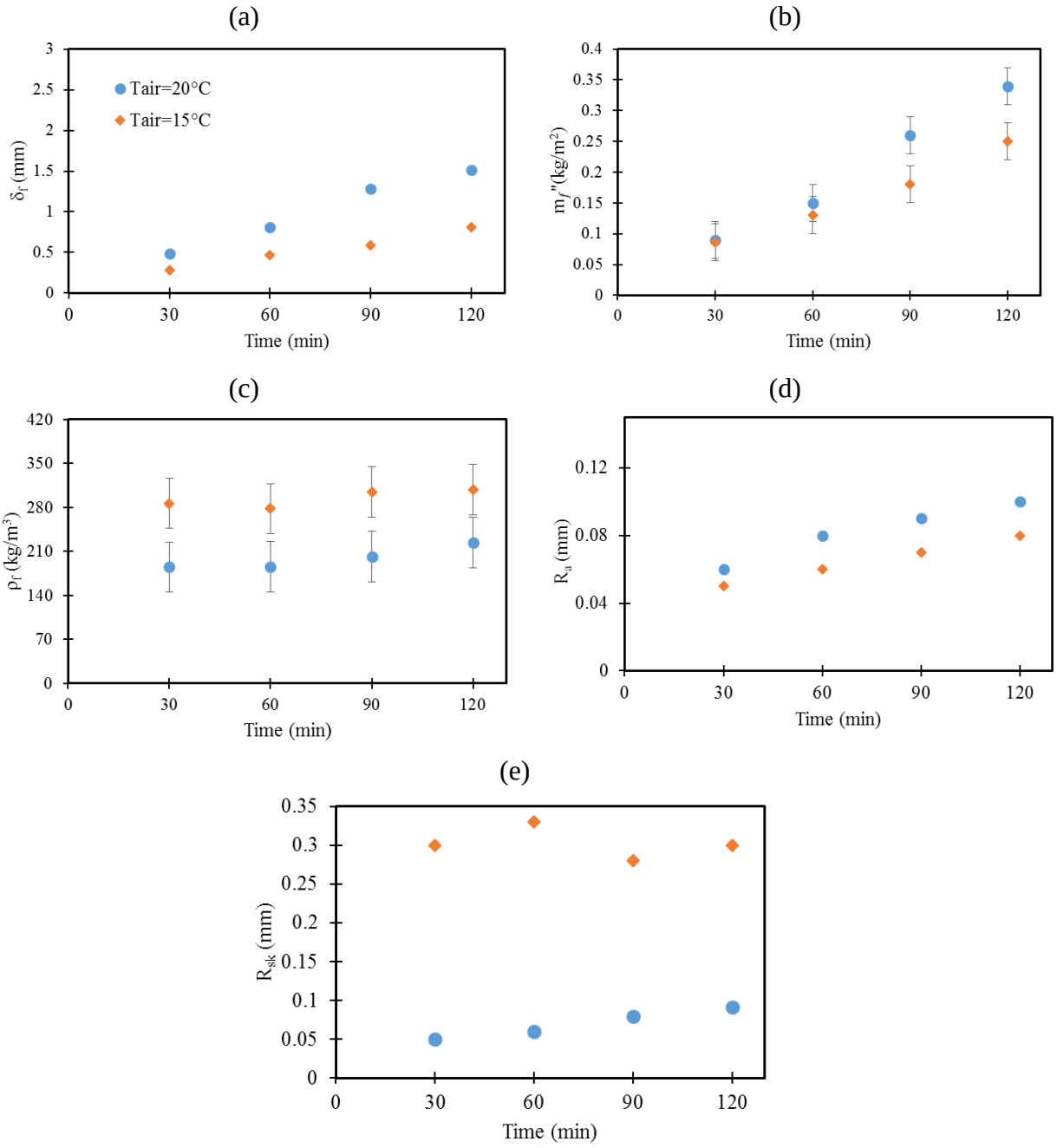

Figure 2.14. Effect of air temperature on frost properties (a) frost thickness, (b) mass, (c) density, (d) average frost roughness, and (e) skewness roughness with T_p = -10°C, RH_{air} = 50% RH. (Error bars are not shown for the frost thickness because the uncertainty (±0.02 mm) is smaller than the symbols).

2.7 Summary

Using photographs and measurements, the effects of surface temperature, air relative humidity and air temperature on the surface, thickness, mass and density of frost on a flat plate under natural convection conditions has been studied in this chapter. The most significant effect on the frost properties is due to a change in the surface temperature of the plate. At a higher surface temperature, the moisture transfer from the air to the frost layer was predominantly by diffusion into the frost layer, creating a thin, but dense frost layer. At a lower surface temperature, the moisture transfer was predominantly by deposition onto the frost layer surface, creating a thick, but porous frost layer. A change in the air relative humidity or the air temperature had an effect on the thickness, mass and density of the frost, but a negligible effect on the shape of the frost. The overall frost shape was similar in these cases.

Frost properties are believed to be a function of both surface properties (surface, hydrophobicity and hydrophilicity) and operating conditions (plate temperature, air temperature and humidity ratio). However, comparing the frost thickness and the frost mass at Time = 30 min, from Figure 2.9, Figure 2.12 and Figure 2.14, shows that changing the operating conditions has an effect on the thickness, but not on the mass. After Time = 30 min, changing the operating conditions has an effect on both the thickness and the mass. This suggests that frost mass may be a function of surface properties only at the early stages of frost growth, which should be further studied.

The frost roughness is quantified as the average roughness and skewness of the roughness. It has been shown that by using R_a and R_{sk}, the shape of the frost layer can be described well. Lower surface temperatures result in high R_a and negative R_{sk}, which correspond to a thick, porous and low density frost layer, while higher surface temperatures result in low R_a and positive R_{sk}, which corresponds to a thin, dense frost layer. Air humidity ratio does not affect R_{sk} but it affects R_a slightly; higher R_a results in lower density while the frost structure is the same. Frost roughness especially at lower plate temperatures is considerably high compared to the surface roughness of the plate, which can affect the deposition process and also heat and mass transfer process. However, there can find a relation between the frost density and the roughness of the frost independent to the operating conditions, as shown in Figure 2.15. As it can be seen, as the frost roughness increases the density of the frost layer decreases as explained before. Also, the very low

frost density corresponds to the frost layer with negative skewness. The relationship between the surface roughness values and the density of the frost layer could be very useful for practical applications of measuring frost inside of an energy exchanger, so should be further studied.

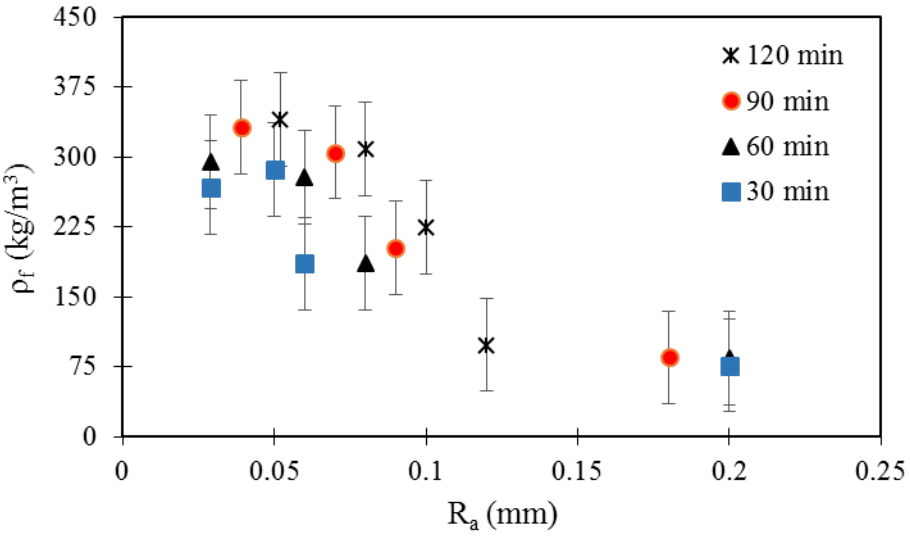

Figure 2.15. Density of frost vs. frost surface roughness.

2.8 Conclusion

Frost formation is a complicated process that occurs in devices that operate under low temperature conditions. In this chapter, the methods to characterize frost layer properties are developed and, the effect of operating conditions on frost thickness, mass, density and roughness under natural convection conditions is studied. The key findings are summarized as follows:

- The shape of frost layer is quantified with frost surface roughness.
- When needle shaped frost crystals (result in positive skewness) form on the surface, average roughness increases with time (with the high rate of the growth at the first 30 min, and then the slower rate of growth after 30 min). However, in case of the formation of the plate shape crystals (results in negative skewness), average roughness decreases with time.
- The average roughness is related to the frost density regardless of the operating conditions; as frost surface roughness increases, the density of the frost layer decreases.
- The thickness and mass of the frost layer increase with time, however, the rate of growth depends on the operating conditions.
- The surface temperature has the greatest effect on the properties of frost, particularly on the surface roughness and density of the frost.
- Lower plate temperatures result in higher frost thermal resistances, but higher frost porosity, which may make it easier to remove frost with external forces.

CHAPTER 3

FROSTING LIMIT FOR A PLATE AND MEMBRANE

3.1 Overview

This chapter mainly addresses the second objective of this Ph.D. research (*i.e.* to identify the effect of moisture transfer on frosting limit). Since the effect of moisture transfer through membranes on frosting limit under natural convection is smaller than the effect of moisture transfer through membranes on frosting limit under forced convection[11], a forced convection test facility is used in this chapter, rather than the natural convection test facility in Chapter 2. In order to find the effect of moisture transfer, two different surfaces: a membrane and plastic plate, are tested in the new test facility. In this chapter, the test facility, measurement uncertainty, experimental procedure and surface properties are introduced. Afterward, the frosting limits for both surfaces are presented and compared. Furthermore, the effect of the moisture transfer rate on frost initiation is investigated.

The manuscript presented in this chapter has been submitted to the ASME Journal of Heat Transfer. The development of the test facility, experimental testing and data analyses and manuscript writing were performed by the Ph.D student, Ms. Shirin Niroomand. Dr. Melanie Fauchoux, contributed to this manuscript by proofreading the manuscript, and providing guidance to clarify the discussions in this manuscript. Prof. Carey J. Simonson (supervisor) critically reviewed the manuscript.

Effect of moisture transfer through a semipermeable membrane on condensation/frosting limit

S. Niroomand, M.T. Fauchoux, C. J. Simonson

3.2 Abstract

This chapter investigates frost formation on a flat horizontal surface with humid air flowing over the surface and a cold liquid desiccant flowing below the surface. Two different surfaces: a membrane and a plastic plate are tested. The condensation/frosting limit, that is, the lowest air humidity ratio ($W_{air,in}$) at a constant liquid temperature, (T_{liq}), or the highest T_{liq} at a constant $W_{air,in}$ that leads to condensation/frosting, is determined for each surface. The main aim of this chapter is to find the effect of moisture transfer through the membrane on the condensation/frosting limit. It is found that the membrane has a lower condensation/frosting limit, due the moisture transfer through the membrane, which dehumidifies the air flow. For a given $W_{air,in}$, the surface temperature can be approximately 5 to 8°C lower when using a membrane, compared to a plastic plate, before condensation/frosting occurs. Furthermore, it is shown that at some operating conditions, frost appears on the membrane only at the air flow entrance of the test section, while the plastic plate was fully covered with frost at the same operating conditions. Moreover, it is shown that increasing the moisture transfer rate through the membrane, decreases the frosting limit and delays frost formation.

3.3 Introduction

The importance of developing anti-frosting surfaces has been already discussed in Chapter 1. As mentioned in Section 1.2, the onset and the process of the frost growth on a membrane has not been addressed in the literature. The main goal of this chapter is to address the effect of moisture transfer on the onset of the frost formation on a membrane.

Frost can occur under two scenarios; condensation frosting and deposition frosting, depending on the environmental conditions (temperature and vapour pressure) [2,12], as mentioned in Section 1.2.1. In condensation frosting, liquid droplets form on the surface, then these droplets grow to form bigger droplets, and then eventually freeze if the surface temperature is below the freezing point. When the first layer of frozen droplets forms on the surface, ice growth continues on the surface and around the ice crystal tips, until a layer of frost appears. In general, the size of

the first water droplets formed on a plastic plate, is very small (in order of μm), also the freezing period is very short, thus, it is very difficult to visualize the condensation period. When the temperature of the surface is not below the freezing temperature, however, water droplets continue to grow until very large water droplets cover the surface. In the present research, condensation frosting occurs, however, in most experiments the formation of water droplets are not distinguished.

Numerical modeling of frost formation on a cold plastic plate has been studied by many researchers [3-6]. A lack of knowledge about frost properties makes this difficult and has resulted in numerus studies to experimentally quantify frost properties (such as frost density, thickness, and thermal conductivity) at different conditions. Many researchers have developed test facilities to measure frost properties on a plastic plate at different operating conditions [65,111]. Biguria et al. [111] used their findings from experimental measurements to develop correlations to predict frost growth and also to explain the observed behavior of the frost growth. Other researchers have studied the effect of surface properties (hydrophilicity and hydrophobicity) on frost formation. Shin et al. [27] studied the effect of surface hydrophilicity on frost thermal conductivity and density. They showed that a thick, low density frost layer formed on a surface with high degree of hydrophobicity (which has a high dynamic contact angle, DCA). Furthermore, it has been shown by some researchers that frost properties (e.g.: thickness, density) are different at various locations from the leading edge of the surface [27,48,65].

Avoiding or delaying frost formation on cold surfaces has been addressed by some researchers [43,44,59,83,135,150]. Okoroafor et al. [83] developed a new hydrophilic coating that minimizes frost growth on a cold surface. They measured frost thickness by using a video measurement system, to study the rate of frost growth on the surface. They showed that their coating could minimize frost growth due to the absorption of the water vapour. Liu et al. [59] investigated the structure of frost on a coated surface with an anti-frosting paint, and concluded that the frost formed on the coated surface had a fragile structure that could easily be removed by external forces. Holmberg [135] studied the conditions (cold surface temperature and air relative humidity) at which frost growth begins on a desiccant coated surface used in energy wheels. He found that frosting begins at a lower temperature in a coated energy wheel compared to a non-coated one. Wang et al. [44] reviewed some anti-frosting technologies in refrigeration and air

conditioning fields, including avoiding frosting by dehumidification of the air by solid/liquid desiccant which could be an effective way to avoid frosting if an efficient regeneration method were developed.

As mentioned in Section 1.2.3, membranes have drawn considerable interest in heating, ventilation, and air conditioning (HVAC) systems recently. It has been shown that heat exchangers constructed with permeable membranes, which allow both heat and moisture transfer, are less susceptible to frost formation than exchangers constructed with impermeable materials [8,45]. Rafatinasr et al. [1,133] and Liu et al. [8] developed a test facility to detect the initiation of frosting and to measure the mass of the frost formed in small-scale, membrane cross-flow air-to-air energy exchangers. They found that less frost formed inside a permeable membrane energy exchanger compared to a plate based heat exchanger. However, they were not able to directly evaluate the formation of the frost on the permeable membrane inside the exchanger, which was the motivation for this research.

In this chapter, the formation of condensation/frost on a membrane and a plastic plate is observed directly, under forced convection conditions. Multiple operating conditions are tested, to determine at which conditions condensation/frost forms on the plastic plate and the membrane. Furthermore, the initiation time for frost formation on both surfaces is evaluated. Finally, the effect of increasing the moisture transfer rate through a membrane on frosting limit is measured and discussed.

3.4 Experiments

3.4.1 Test Facility and operating conditions

The test facility designed to study the effect of moisture transfer on frosting under forced convention conditions is shown in Figure 3.1(a). The test facility was designed to create a cold surface, with warm humid air passing over the top of the surface. A cold liquid desiccant passed underneath the surface to maintain a constant surface temperature and create a driving potential for moisture transfer through the membrane. The major parts of the test facility are the test section, the cold liquid loop and the air supply section. The cold liquid loop consists of a pump, a thermal bath, which cools the liquid desiccant to the desired temperature, and a storage container. The air supply section includes an air compressor, air humidifier and two mass flow controllers.

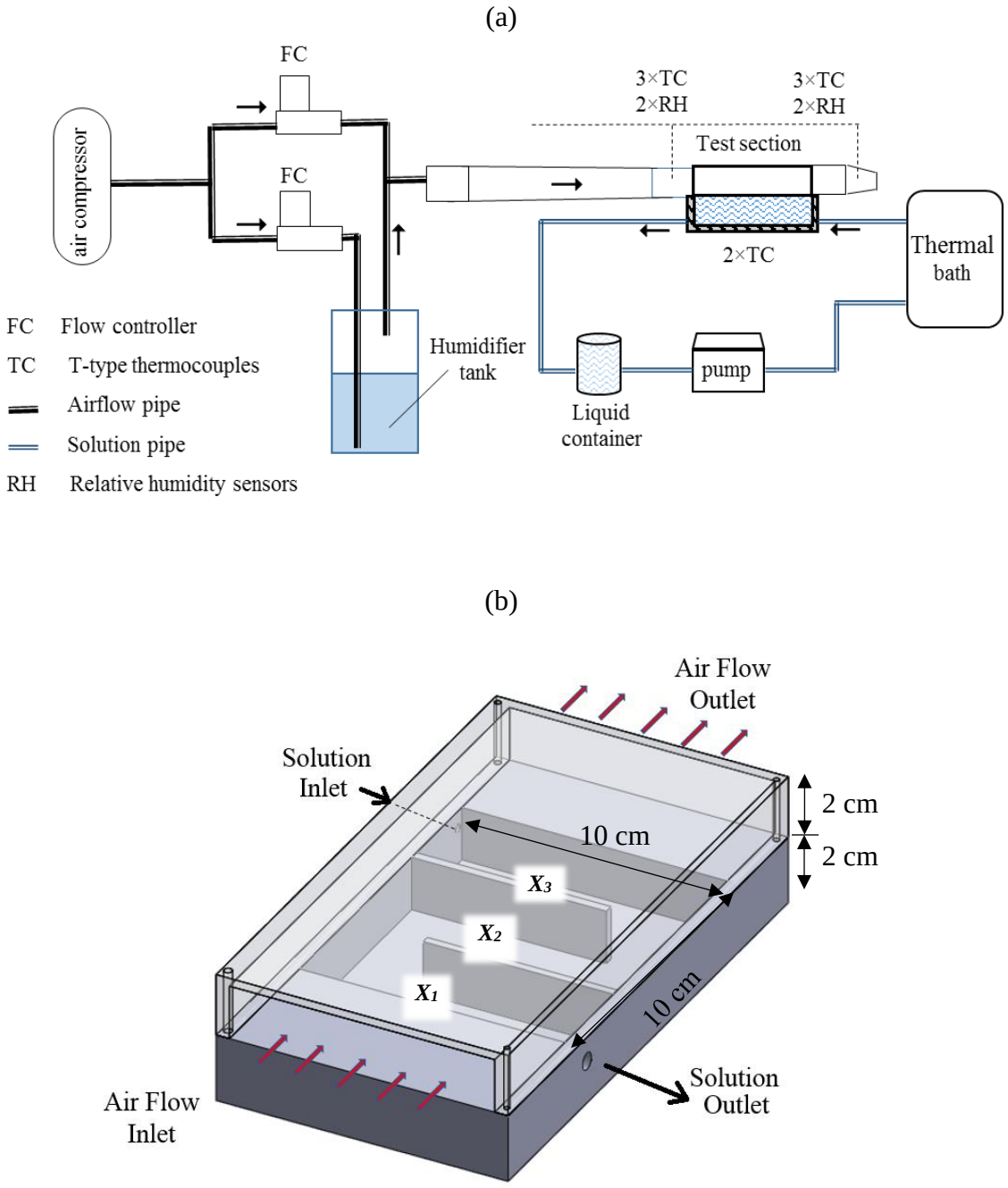

Figure 3.1. Schematic of (a) the test facility and (b) the test section.

On the air side, dry air at room temperature is supplied to the test facility from a compressor. Prior to the test section, the air stream is divided into two; one air stream passes through a well-sealed tank of water (humidifier tank) to create humid air, and the other air stream bypasses the tank to maintain dry air. The two air streams are then mixed to create one air flow at the desired air

humidity ratio. The volume flow rate of the two air streams are set and controlled using two mass flow controllers with a maximum flow rate of 200 L/min each. The air channel was designed so that the air flow would be fully developed prior to entering the test section.

The temperature of the air is measured at three points across the width of the air channel both upstream and downstream of the test section, using T-type thermocouples. The relative humidity (RH) of the air is measured at two points across the width of the air channel at the same locations as the temperature. The RH is measured using Honeywell HIH humidity sensors. The temperature and RH measurements reported as the inlet and outlet conditions are the average of the measurements at each location. An uncertainty analysis is provided in Section 3.4.3

A schematic of the test section, with dimensions, is shown in Figure 3.1(b). The bottom of the test section, which contains the cold liquid desiccant is made of PVC, which is resistant to corrosion from the liquid desiccant. As shown in Figure 3.1(b), the test section is divided into three channels, which allows liquid desiccant to flow evenly through the test section. The top of the test section is made of clear acrylic, to allow for visualization of the cold surface during testing. The test section is insulated, to reduce the heat gains from the environment. The insulation covering the top of the test section can be removed to allow photographs of the test section to be taken. The air and the cold liquid desiccant flow through the test section in a cross-flow pattern.

The cold liquid desiccant is an aqueous solution of Lithium Chloride (LiCl). The concentration of a salt solution, C_{liq}, is defined as

$$C_{\mathrm{liq}} = \frac{m_{\mathrm{salt}}}{m_{\mathrm{salt}} + m_{\mathrm{w}}} * 100 \tag{3.1}$$

where m is mass [kg], and the subscripts "salt" and "w" refer to the salt and water, respectively. An equivalent air humidity ratio (W) can be defined for a salt solution, based on the temperature, the concentration of the solution and the type of salt used. To avoid crystallization or icing in the mixed solution, the concentration of the solution should be kept within the solubility boundary for that salt solution, as defined by [151]. The temperature of the liquid desiccant was measured using two thermocouples placed in the liquid desiccant side of the test section. The reported liquid temperature is the average of the reading from the two thermocouples.

To directly observe the frost formation on the surface, a camera with a super macro lens (Canon EOS M3, Canon macro 28 mm), with a resolution of ~5 µm, was set up to capture photographs of the top of the test section. Photographs of the surface were taken every 5 min for the first 15 min of the test, and then every 15 min for the remainder of the test. The photographs were taken at three locations along the length of the test section, indicated in Figure 3.1(b); one near the air inlet (X_1), one in the middle of the surface (X_2) and one near the air outlet (X_3). Photographs were taken at multiple locations because the literature shows that the distance from the leading edge affects frost growth.

3.4.2 Surface materials

Frosting tests were performed on two different surfaces, a membrane and a plastic plate, which were glued to the test section. Both surfaces were stretched carefully before gluing to remove any wrinkling and bulging. The membrane used was Propore^{TM,} which is a micro-permeable polypropylene membrane affixed to a non-woven polypropylene fabric. The non-woven fabric provides support to the membrane as it is highly elastic. The non-woven fabric side was in contact with the air and the membrane side was in contact with the liquid desiccant. Figure 3.2 shows the membrane with the non-woven fabric separated from the membrane itself. The properties of the membrane are presented in Table 3.1.

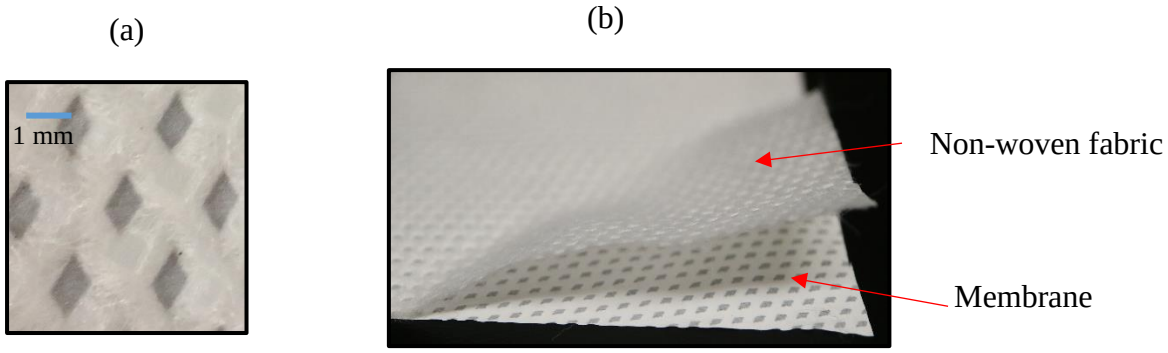

Figure 3.2. Photograph of (a) the top view of the Propore^{TM} membrane, and (b) the membrane and the supporting non-woven fabric.

The plastic plate is a vapour barrier sheet with thermal properties as presented in Table 3.1. As moisture cannot transfer through the plastic plate, comparison of the condensation/frosting limits for the plastic plate and for the membrane will show the effect of moisture transfer on frost growth.

Since the wettability of a surface affects frost formation, the direct contact angle (DCA), which is an indication of the degree of wettability, was measured for both surfaces. A small DCA ($\theta < 90$) corresponds to a high wettability (hydrophilic surface), whereas a large DCA corresponds to a low wettability (hydrophobic surface)[152]. The DCA was measured using a Portable Contact Angle Measurement Meter. The direct contact angle of the membrane and plastic plate are compared in Figure 3.3. It can be seen both surfaces could be considered as hydrophobic surfaces.

Table 3.1. Properties of Propore^{TM} [153] and the plastic plate [154].

Property	Propore ^{TM}	plastic plate
Thickness	0.22 mm	0.16 mm
Thermal conductivity	0.334 W/(m·K)	0.35 W/(m·K)
Resistance to moisture	125 s/m	10^5 s/m

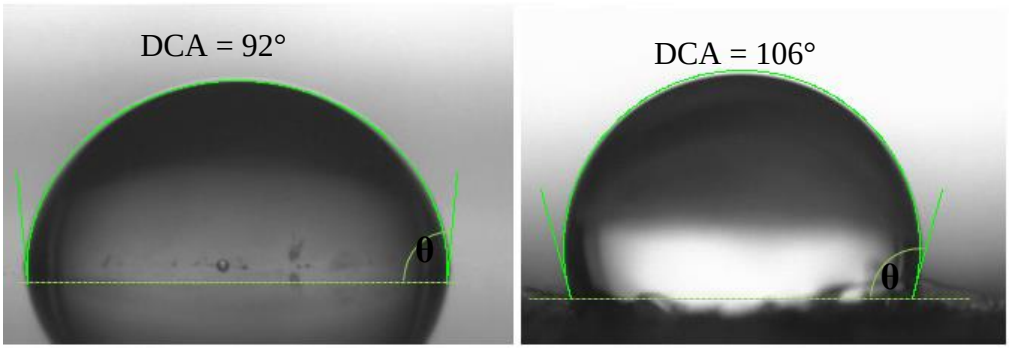

Figure 3.3. DCA measurements for (a) the plastic plate and (b) the membrane.

3.4.3 Measurement uncertainty

The uncertainty of each measurement is determined based on ASME Standard 19.1 [154]. The thermocouples are calibrated with a Hart Scientific 9107 Dry Well Calibrator and found to have a systematic uncertainty (B) of ±0.1°C and random uncertainties (P) between ±0.02°C and ±0.06°C. Total uncertainties for inlet and outlet air temperatures and liquid temperatures are equal to ±0.2°C, ±0.2°C and ±0.1°C, respectively. The relative humidity sensors were calibrated with a Thunder

Scientific Model 1200 Mini Humidity Generator. The sensors have a systematic uncertainty of ±0.7% RH, and random uncertainties between ±0.3% RH and ±0.4% RH, which results in total inlet and outlet uncertainties equal to ±1.0 % RH and ±1.1 % RH.

The humidity ratio of the air at the inlet and outlet is calculated from the air temperature and relative humidity, based on the following equation:

$$W = 0.6219 \frac{RH * P_{ws}}{P - RH * P_{ws}} \tag{3.2}$$

Where RH, P_{ws} and P are relative humidity, saturated pressure of water vapour and atmospheric pressure of the lab (95.9 kPa), respectively. P_{ws} is calculated from temperature, based on Eq.(3.3). The uncertainty in W is calculated using propagation of uncertainty and the uncertainties in the temperature and relative humidity measurements.

$$P_{ws} = \exp[\frac{C_1}{T} + C_2 + C_3 T + C_4 T^2 + C_5 T^3 + C_6 (lnT)] \tag{3.3}$$

where $C_1 = -5.8002206 \times 10^3$ $C_3 = -4.8640239 \times 10^{-2}$ $C_5 = -1.4452093 \times 10^{-8}$

$C_2 = 1.3914993$ $C_4 = 4.1764768 \times 10^{-5}$ $C_6 = 6.5459673$

The systematic uncertainty of each mass flow controller is about 1% of the maximum flow rate and the maximum random uncertainty in the volume flow rates is 0.007 L/min.

3.4.4 Surface temperature

The temperature at the air-surface interface ($T_{surf,air}$) changes along the length of the test section, due to changes in the air temperature and the developing thermal boundary layer. A schematic of the test section is shown in Figure 3.4. The air enters at a certain temperature and is cooled, as heat is transferred to the cold liquid below the surface. The air leaves the test section at a lower temperature, as indicated in the schematic. At each location along the length of the test section, it is assumed that the heat transfer is one-dimensional and can be represented with the thermal

resistance circuit shown. The heat transfer consists of convection from the air to the surface, conduction through the surface and convection into the liquid. The liquid mass flow rate in the experiment is large, to provide almost constant liquid temperature in the test section. Therefore, it is assumed that the temperature of the liquid (T_{liq}) is constant along the length of the test section and is equal to the average temperatures from the two thermocouples at the inlet and outlet of the test section.

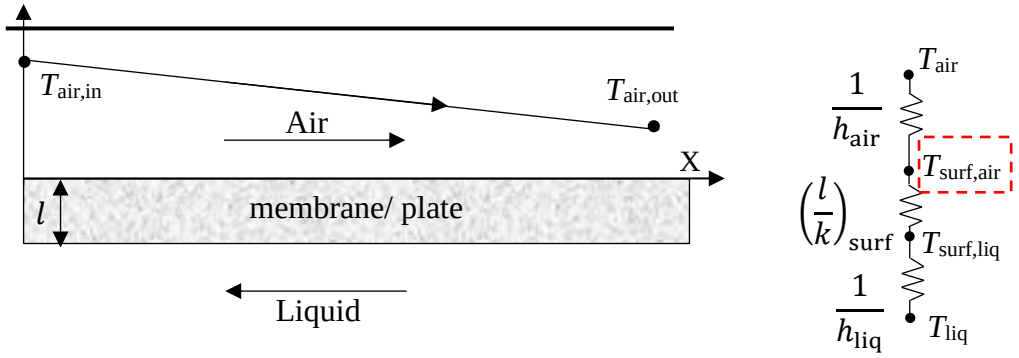

Figure 3.4. Schematic of the surface with air flow on the top and liquid flow under the surface, and the equivalent thermal resistance circuit.

Based on the thermal resistance circuit in Figure 3.4 and the assumptions listed previously, $T_{surf,air}$ can be calculated from Eq. (3.4), for various positions along the test section. It is assumed that the change in air temperature is linear along the test section, with the measured values used for the inlet and outlet temperatures.

$$q'' = \frac{T_{air} - T_{liq}}{\frac{1}{h_{air}} + (\frac{l}{k})_{surf} + \frac{1}{h_{liq}}} = \frac{T_{air} - T_{surf,air}}{\frac{1}{h_{air}}} \tag{3.4}$$

The convective heat transfer coefficient of thermally developing laminar flow through a rectangular duct under forced convection conditions, with a constant temperature on the bottom wall, is calculated based on Eq. (3.5)[155].

$$Nu = \frac{hD}{k} = 1.66\, Re^{1/3} Pr^{1/3} \left(\frac{\mu_{avg}}{\mu_{bulk}}\right)^{0.14} \left(\frac{L}{D}\right)^{-1/3} \tag{3.5}$$

where μ_{avg} is the dynamic viscosity at the average air temperature [Pa·s], μ_{bulk} is the dynamic viscosity at the bulk air temperature [Pa·s] and L is the length of the heat transfer surface [m]. The convective heat transfer coefficient in the liquid desiccant for a rectangular channel with forced convention is found using Eq. (3.6) [155].

$$Nu = 1.6\, Re^{1/3} Pr^{1/3} \left(\frac{L}{D}\right)^{-1/3} \tag{3.6}$$

The calculations show that the thermal resistances of the membrane and plastic plate are very small when compared to the resistance of the air and liquid desiccant thermal boundary layers. Therefore, the calculated surface temperatures for the membrane and plastic plate are very close to each other.

In addition to the calculation, $T_{surf,air}$ is also measured at one location during each test. One T-type thermocouple was attached to the surface in the centre of the test section, using thermal paste. It is seen that for a fixed liquid temperature, the surface temperature for both the membrane and plastic plate are very close to each other, within the limits of uncertainty, which was expected based on the results of the calculations of $T_{surf,air}$.

The value of $T_{surf,air}$ for three different liquid temperatures is shown in Figure 3.5. The calculations are performed in intervals of 1 cm along the length of the plastic plate. The measured surface temperatures are shown at the 5 cm mark, with the dashed circle around the data point. It can be seen that the calculated values agree well with the measurements.

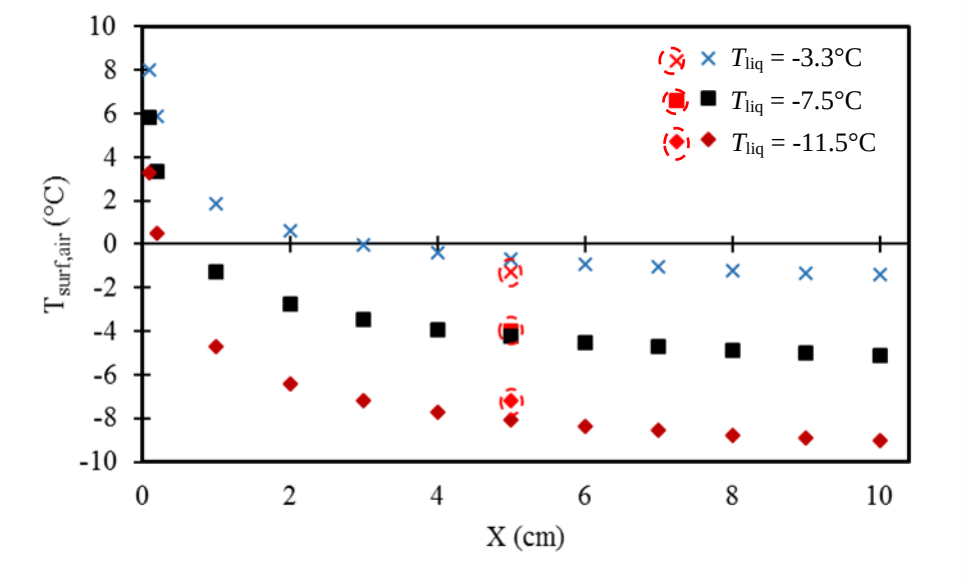

Figure 3.5. Change in $T_{surf,air}$ along the test section. The measured values are indicated by a red circle around the symbol.

3.5 Experimental procedure

Before each experiment, the surface of the test section is covered with an aluminum sheet to prevent frost growth during the experiment start up. After that, the inlet air conditions (temperature, humidity ratio and mass flow rate) and liquid temperature are set to the desired values. Once the inlet air and liquid conditions have reached their set points, within experimental uncertainty, the surface is uncovered and exposed to the humid air. This is considered the start of the test. At this point, the outlet air temperature, air humidity ratio and surface temperature begin to change gradually, due to the heat and moisture transfer through the surface. After 1~1.5 h, the outlet air temperature reaches steady state conditions (the changes in $T_{air,out}$ are less than the corresponding uncertainty). The time for frost growth to begin on the surface varied, due to the different operating conditions.

The frosting limit is defined as the lowest $W_{air,in}$ at constant T_{liq}, or highest T_{liq} at constant $W_{air,in}$ that leads to condensation/frost forming on the surface. To measure the frosting limit for each surface, one condition ($W_{air,in}$ or T_{liq}) was changed while all other conditions were kept constant. Table 3.2 shows the operating conditions tested in this chapter. The air flow in the test section was selected so that it is in the laminar flow regime. The images are analyzed using ImageJ [156] to

detect the initiation of the frosting/condensation on both surfaces at the beginning of the test when water droplets or ice particles are very small.

Table 3.2. Experimental operating conditions.

Parameter	Value
Air Reynolds number (*Re*)	190 (-)
Air mass flow rate ($\dot{m}_{air}$)	0.18 g/s
Air temperature ($T_{air,in}$)	23 ~ 24°C
Air humidity ratio ($W_{air,in}$)	1.5 ~ 7 g_w/kg_{air}
Liquid flow rate ($\dot{m}_{liq}$)	0.01 kg/s
Liquid concentration (C_{liq})	22%
Liquid Temperature (T_{liq})	-3 ~ -14°C

3.6 Results and discussion

Experiments were conducted to find the condensation/frosting limit for a membrane and a plastic plate. Multiple tests were conducted under different operating conditions, to find the conditions (T_{liq} and $W_{air,in}$) where frost will form. The first tests were performed at the highest liquid temperature, T_{liq} = -3.1°C and an air humidity ratio of $W_{air,in}$ = 2.3 ~ 2.6 g_w/kg_{air}. There was no sign of frost or condensation on either the membrane or the plastic plate under these conditions. Tests were then conducted at the same liquid temperature, with step increases in the air humidity ratio, until frost or condensation appeared on the surface. The test procedure was then repeated for lower liquid temperatures. The test results will be presented in two sections; first tests where only condensation formed will be discussed, and then tests where frost formed will be discussed. Following that, the results of the condensation/frosting limit are presented. Finally, the effect of increasing moisture transfer through the membrane on the time to frost initiation on a membrane is discussed.

3.6.1 Condensation

Following the tests where no frost or condensation formed on the surfaces, tests were performed at the same liquid temperature, T_{liq} = -3.1°C, but higher air humidity to find the conditions at which

condensation/frost formed on the surfaces. Very small water droplets were first seen on the plastic plate when $W_{air,in}$ = 3.9 g_w/kg_{air}. Water droplets first appeared on the membrane at a higher humidity ratio, $W_{air,in}$ = 4.6 g_w/kg_{air}, only at the air inlet (X_1). In both cases the water droplets are small, and hard to see in the photographs, so the images are not shown here.

The formation of condensation on the plastic plate when T_{liq} = -3.1°C and $W_{air,in}$ = 5.8 g_w/kg_{air} is shown in Figure 3.6. As described previously, three photographs were taken at each time step, one near the airflow inlet (X_1), one in the middle of the test section (X_2) and one near the airflow outlet (X_3). It can be seen from the first row of pictures, that at Time = 0 min, there is no condensation on the plastic plate. The next row shows that after 10 min, small water droplets form, fairly close to each other, on the surface. It can also be seen that more water droplets form at X_1 then at X_2 and X_3. At Time = 45 min, it can be seen that droplets continue to form and near the airflow inlet they begin to coalesce to form bigger droplets. This process continues, until the water droplets reach approximately 1 mm in diameter, at Time = 110 min. It can be seen that after 90 min, the distribution of droplets is less uniform, with small droplets existing between the larger droplets.

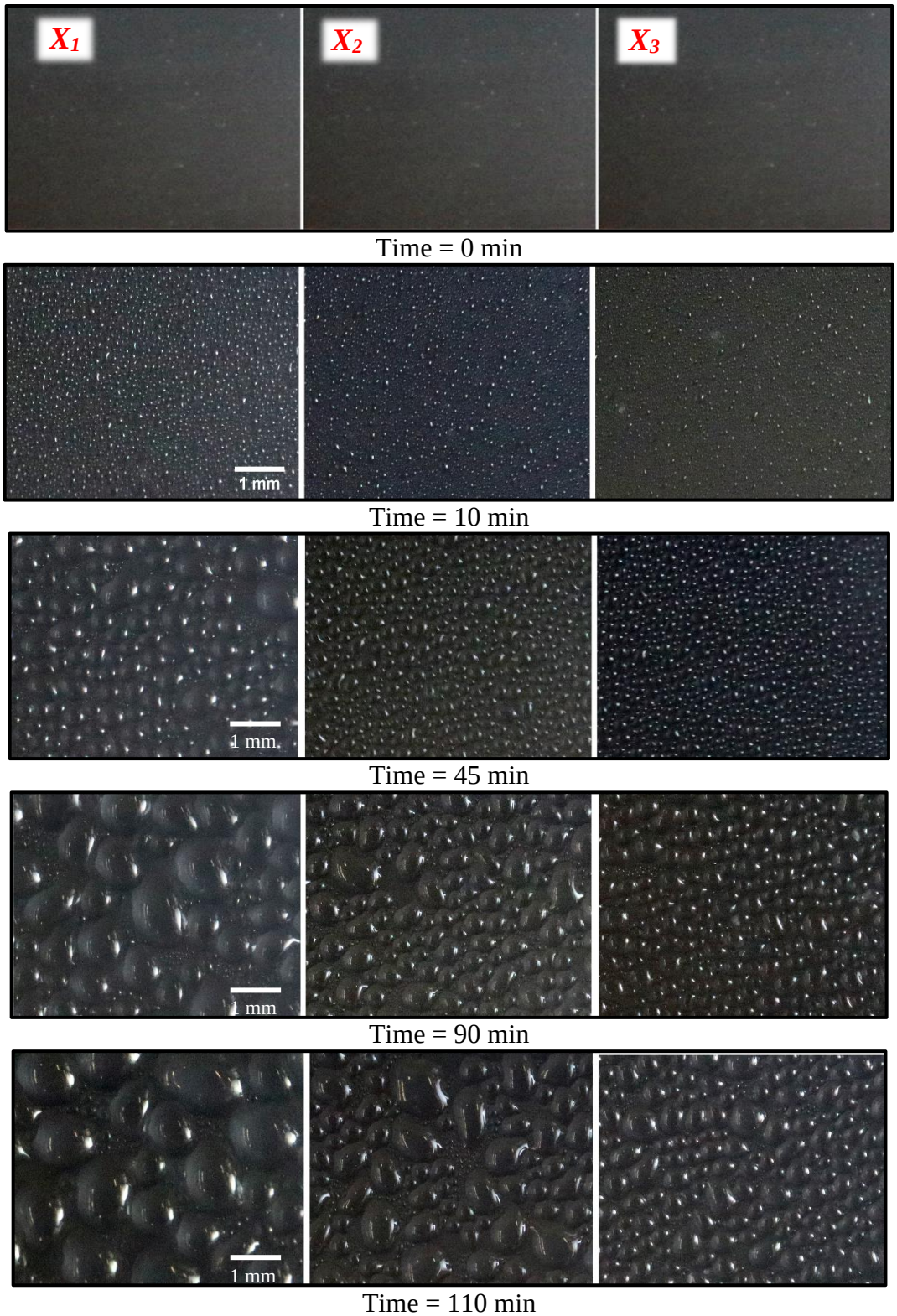

Figure 3.6. Condensation on a plastic plate, when $W_{air,in}$ = 5.8 g_w/kg_{air}, and T_{liq} = -3.1°C, at the airflow inlet (X_1), middle (X_2), and outlet (X_3) of the test section.

The membrane is shown, for the test conditions of T_{liq} = -3.1°C and $W_{air,in}$ = 6.3 g_w/kg_{air} in Figure 3.7. Again, the membrane is fresh, with no condensation/frost at Time = 0 min. Water droplets begin to form near the airflow inlet (X_1) after 10 min. At Time = 110 min water droplets have formed at the inlet and middle of the test section, but not at the outlet. The water droplets are large, covering the openings in the non-woven fabric. Comparing Figure 3.6 and Figure 3.7 reveals that the water droplets are larger and more numerous on the plastic plate than the membrane, despite $W_{air,in}$ being higher in the membrane test.

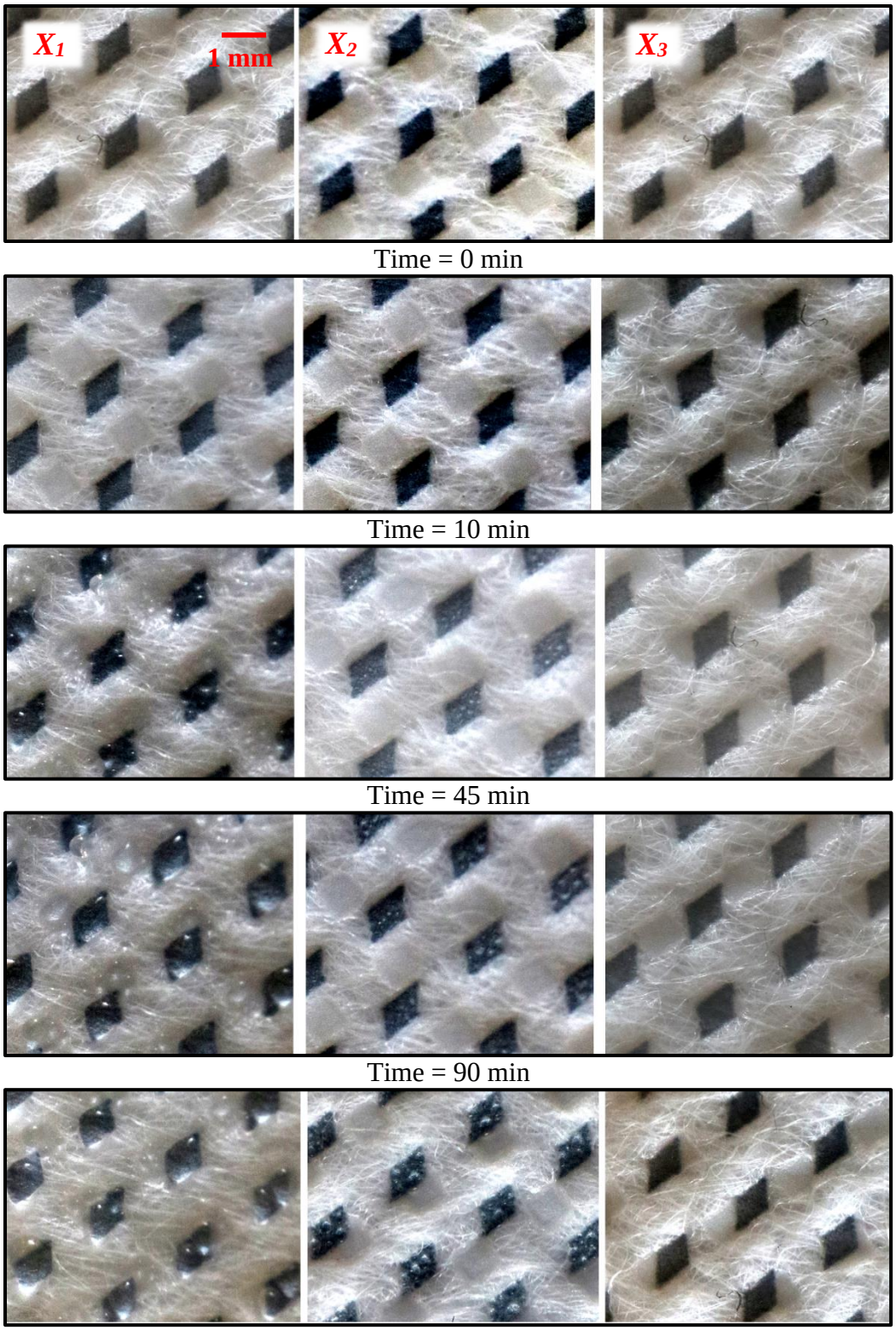

Figure 3.7. Condensation on a membrane, when $W_{air,in}$ = 6.3 g_w/kg_{air}, and T_{liq} = 3.1°C, at the airflow inlet (X_1), middle (X_2), and outlet (X_3) of the test section.

3.6.2 Frosting

When $T_{liq} \leq$ -7°C, frost was observed on both the plastic plate and the membrane. During some tests there was only frost growth on a portion of the surface, and in some cases the surface was fully covered with frost. To show the difference in the behaviour of the frost under these conditions, this section is split into partial frosting and full frosting.

3.6.3 Partial frosting

Frost growth on the plastic plate and the membrane, at Time = 150 min, when T_{liq} = -7.5°C and $W_{air,in} \approx 3.6\ g_w/kg_{air}$, is shown in Figure 3.8 and Figure 3.9, respectively. It can be seen in Figure 3.8 that the plastic plate is covered with frost, when compared with the fresh plastic plate shown in Figure 3.6(a). As with the water droplets, more frost is formed at the inlet of the test section (X_1). Figure 3.9 shows that frost only covers about 20% of the membrane area at the inlet, compared to the fresh membrane shown in Figure 3.7(a). There is no frost formed at the other two locations on the membrane. The reason for partial condensation/frosting on a membrane, is the developing thermal and concentration boundary layer and enhanced heat and mass transfer coefficients near the entrance. From a practical point of view, covering 20% of the area with frost might not affect the performance of a full-scale membrane energy exchanger.

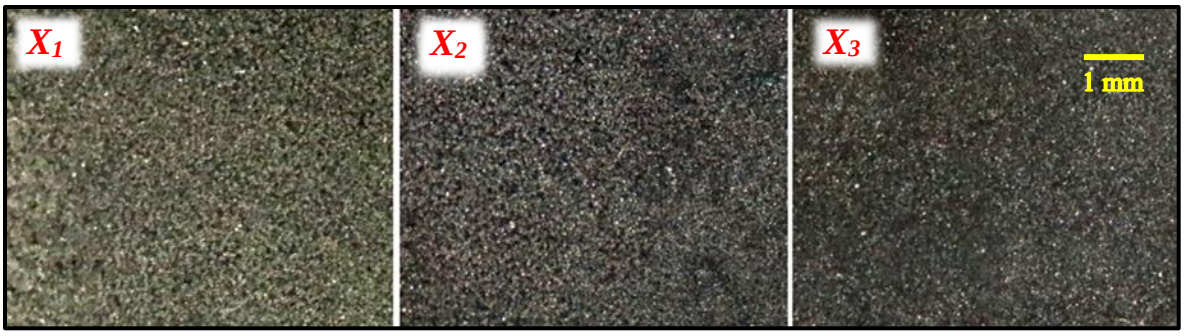

Time =150 min

Figure 3.8. Partial frost growth on a plastic plate, with $W_{air,in}$ = 3.7 g_w/kg_{air} and T_{liq} = - 0.5°C.

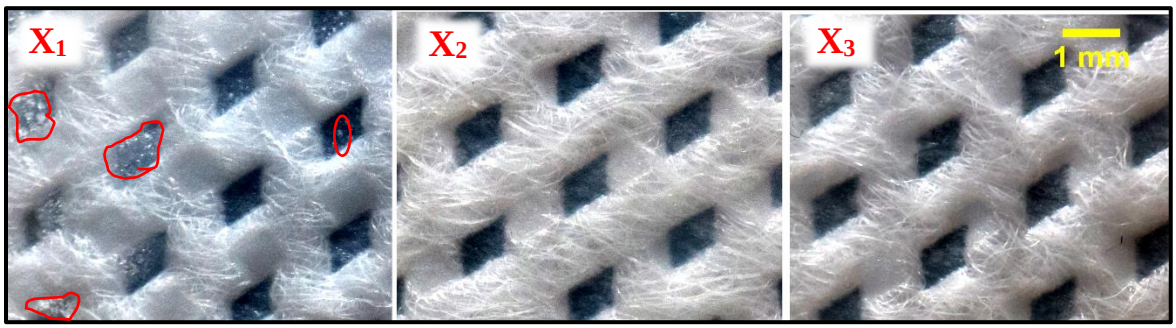

Time= 150 min

Figure 3.9. Partial frost growth on a membrane, with $W_{air,in}$ =3.5 g_w/kg_{air}, and T_{liq} = -7.5°C.

3.6.4 Full frosting

For T_{liq} = -11.8°C and $W_{air,in}$ = 7.5 g_w/kg_{air}, frost formation on the plastic plate, at three distances from the inlet (X_1, X_2 and X_3), is shown in Figure 3.10. It can be seen that after 2 min, small ice particles appear on the plastic plate, mostly near the inlet (X_1). The remainder of the plastic plate remains mostly frost free. After 10 min, a thicker layer of frost covers the whole plastic plate, with more frost accumulating at X_1. Finally, after 120 min a thick frost layer, which is thicker at the inlet and thinner at the outlet, forms on the whole plastic plate.

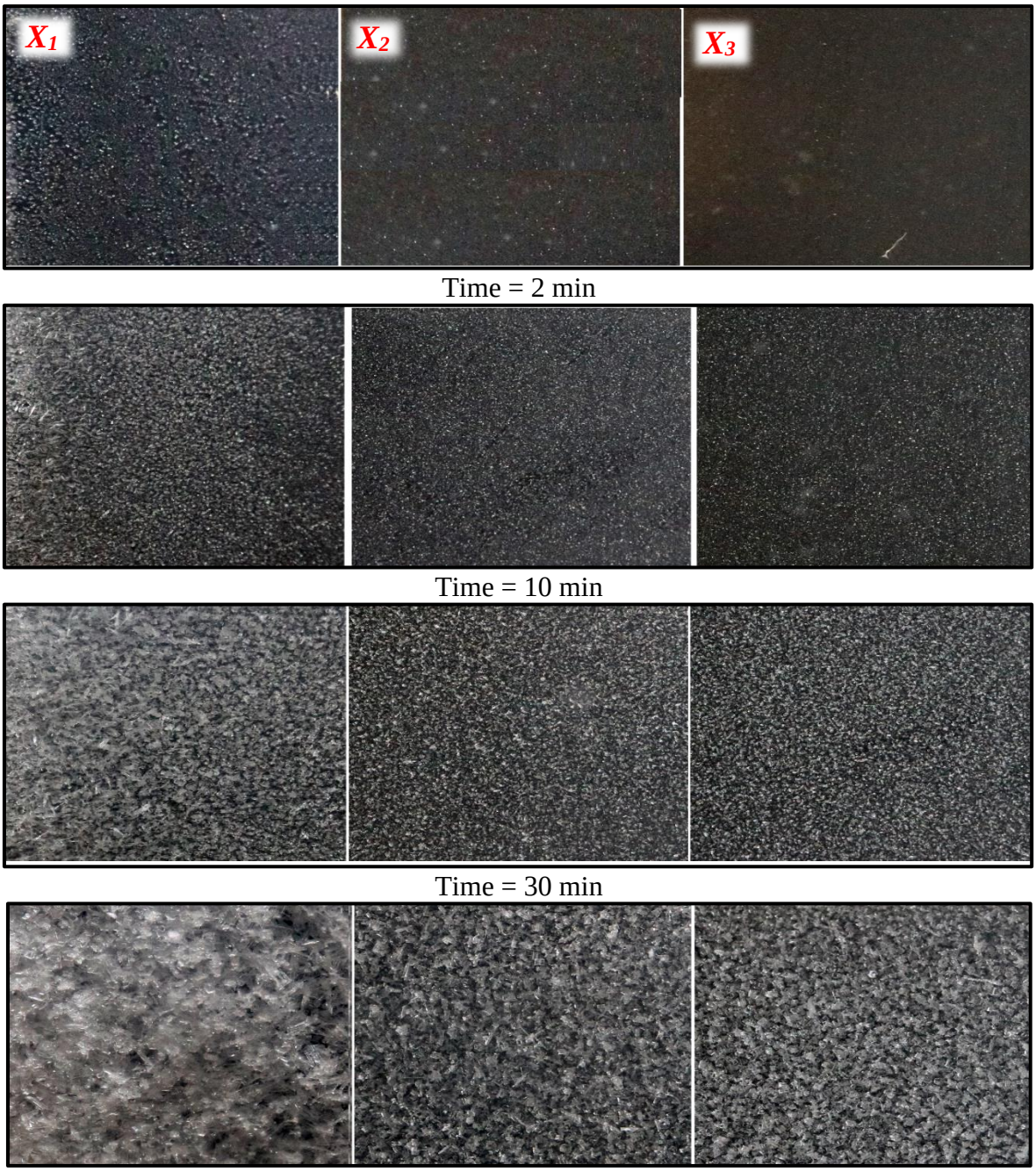

Figure 3.10. Frost growth on a plastic plate, with $W_{air,in}$ = 7.5 g_w/kg_{air}, and T_{liq} = -11.8°C.

Frost formation on the membrane is shown in Figure 3.11, for the same operating conditions as the test on the plastic plate shown in Figure 3.10. After 10 min a few small ice particles formed on the membrane, close to the inlet. In this case, it took 30 min for frost to cover the membrane

completely, as compared to the plastic plate, which was covered with frost throughout the test section after only 10 min. After 120 min a thicker layer of frost covered the whole membrane, and was thicker at the inlet of the test section. It can be seen that most of the pores in the membrane have been completely covered at the X_1 position.

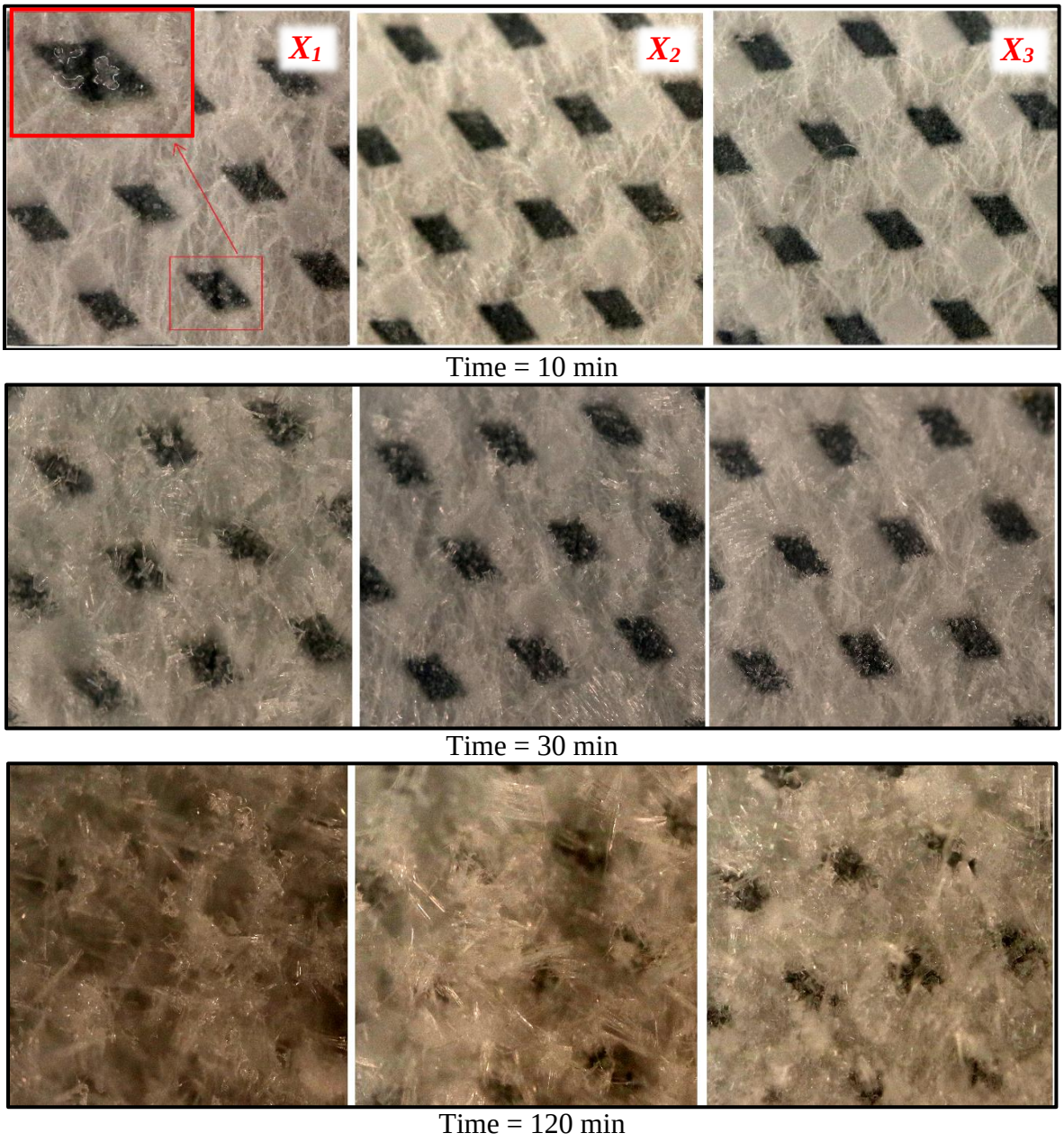

Figure 3.11. Frost growth on a membrane, with $W_{air,in}$ = 7.5 g_w/kg_{air}, and T_{liq} = -11.8°C.

3.6.5 Condensation/frosting limit

A total of 16 tests were performed on the plastic plate and 20 tests on the membrane. The operating conditions for each test are plotted in Figure 3.12 for the plastic plate, and Figure 3.13 for the membrane. As shown in the legend of each figure, a solid circle is used to indicate a test where no frost or condensation was seen, an open square to indicate partial condensation or frosting, and a solid square to indicate full frosting. The dashed vertical line indicates the tests where condensation formed (to the right of the line) and the tests where frost formed (to the left of the line). Note that the temperature presented is the liquid temperature, not the corresponding surface temperature, as the surface temperature changes through the test section. As shown previously in Figure 3.5, the average surface temperature is approximately 3°C higher than the liquid temperature.

For the plastic plate there were six tests where no condensation/frost formed, and nine tests where condensation or frost formed, as shown in Figure 3.12. Based on these results, the condensation/frosting limit is shown with a dashed line (labeled C/F limit). When T_{liq} = -3.1°C, the humidity ratio of the air can be increased to $W_{air,in}$ = 3.9 g_w/kg_{air} before condensation forms. At this temperature no frosting occurred. As T_{liq} decreases to -7.5°C, the humidity ratio of the air can only get up to $W_{air,in}$ = 2.8 g_w/kg_{air} before frost forms. As T_{liq} goes even lower, to -13°C, the humidity ratio of the air can only get up to $W_{air,in}$ = 1.5 g_w/kg_{air} before frost forms. This chart can be used to determine when an energy exchanger made with plastic plates will experience condensation and frosting. If this plastic plate was used in an exchanger, the surface temperature should be maintained about -4°C (liquid temperature of -7°C) in order to completely avoid frost growth in the exchanger, and potential blockage of air channels. However, in cold climates, the liquid temperature will drop below -4°C, in which case, the acceptable temperature to avoid frosting can be determined based on the humidity ratio of the air through the exchanger.

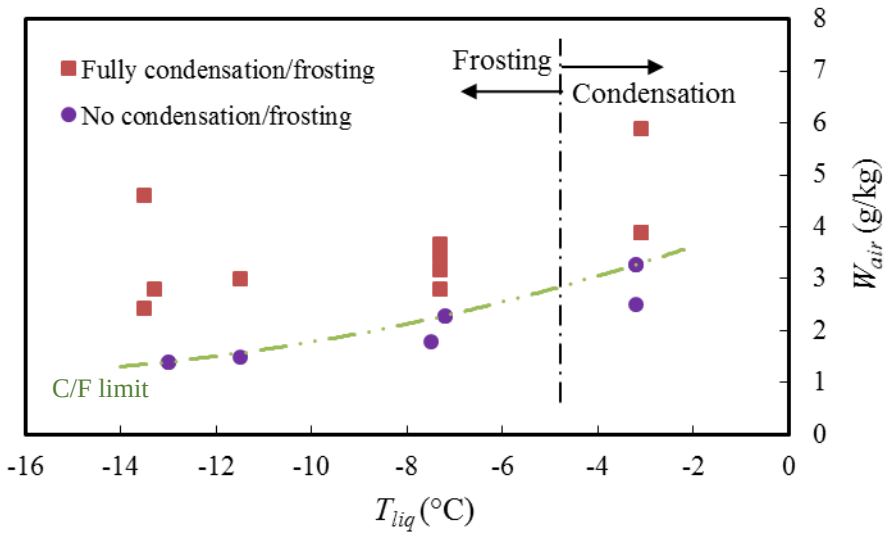

Figure 3.12. Test points showing operating condition with condensation/frosting and without condensation/frosting on a plastic plate (dashed lines are plotted to help visualization, and shows the condensation/frosting (C/F) limits).

For the membrane there were seven tests where no condensation/frost formed, nine tests with partial frost formation (conditions were condensation/frost formed only at the entrance), and four tests with full frost formation. In this case, two separate condensation/frosting limits are identified, C/F limit I and C/F limit II. C/F limit I indicates the limit where no condensation/frost exists. Above this line, partial condensation/frost occurs. C/F limit II indicates the limit where full condensation/frosting occurs. When T_{liq} = -3.1°C, the air humidity ratio can be 4.0 g_w/kg_{air} before condensation begins to form on the membrane, and 6.5 g_w/kg_{air} before condensation fully covers the membrane. As T_{liq} = -7.5°C, the humidity ratio of the air can get up to $W_{air,in}$ = 3.1 g_w/kg_{air} before frost begins to form, and $W_{air,in}$ = 4.6 g_w/kg_{air} before frost fully covers the membrane. As T_{liq} goes even lower, to -13.5°C, the humidity ratio of the air can only get up to $W_{air,in}$ = 2.0 g_w/kg_{air} before frost begins to form, and $W_{air,in}$ = 3.8 g_w/kg_{air} before frost fully covers the membrane. Again, this chart can be used to determine when an energy exchanger made with membranes, will experience condensation and frosting.

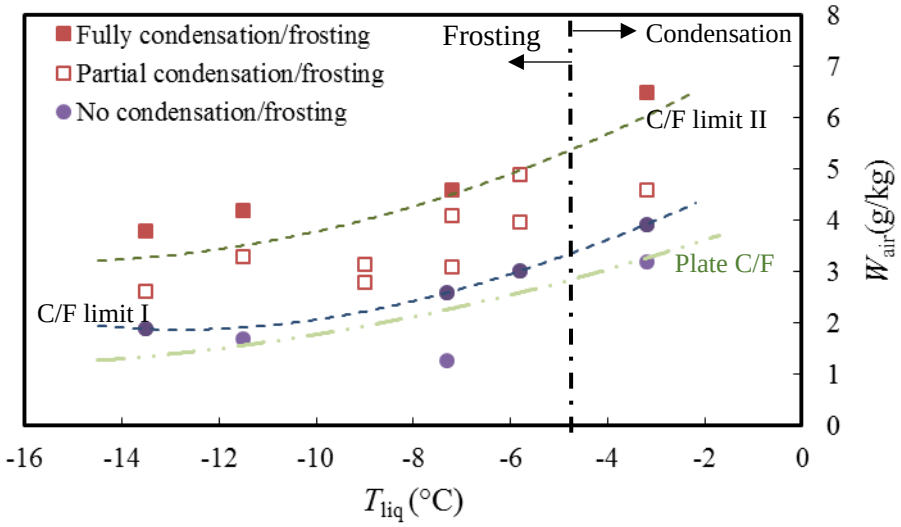

Figure 3.13. Test points showing operating condition with condensation/frosting and without condensation/frosting on a membrane (dashed lines are plotted to help visualization, and shows the condensation/frosting (C/F) limits). C/F limit I indicates the limit where no condensation/frost exists. C/F limit II indicates the limit where full condensation/frosting occurs.

The C/F limit for the plastic plate is also shown in Figure 3.13, to show the comparison between the plastic plate and the membrane. It can be seen that the C/F limit is slightly lower for the plastic plate than the C/F limit I for the membrane. This shows that the onset of condensation/frost occurs at a slightly higher $W_{air,in}$ for the membrane, due to the moisture transfer through the membrane. The difference between the plastic plate C/F limit and the membrane C/F limit II is comparatively large. This shows that $W_{air,in}$ can be considerably larger, for the same surface temperature, before the membrane will be fully covered with condensation/frost. For a given $W_{air,in}$ value, the surface temperature can be approximately 5 to 8°C lower when using a membrane, compared to a plastic plate, before condensation/frosting occurs. Again, this is due to the moisture transfer through the membrane, which lowers the air dew point temperature, and reduces the risk of frost. The effect of the moisture transfer through the membrane is largest at higher T_{liq} values (-3.1°C), and decreases as T_{liq} decreases, as the frosting limits get closer together.

3.6.6 Initiation time for frosting

The results presented for the condensation/frosting limit were for the final amount of frost that formed on the plastic plate and the membrane at different operating conditions. However, it was found that the membrane also effected the time at which condensation/frost first formed as well. For the plastic plate, the initiation time for condensation/frosting was very short, and was not detectable with the test methods used in this research. With the membrane, the initiation time was delayed, and was observable. The initiation time, defined as the time for the first water droplets or ice particles to be observed on the membrane is presented in Figure 3.14. As T_{liq} decreases or $W_{air,in}$ increases, the initiation time decreases. From this it can be concluded that membranes can delay frosting, however at extreme operating conditions (high air humidity ratio and low liquid temperatures), the effect of the moisture transfer through the membrane decreases.

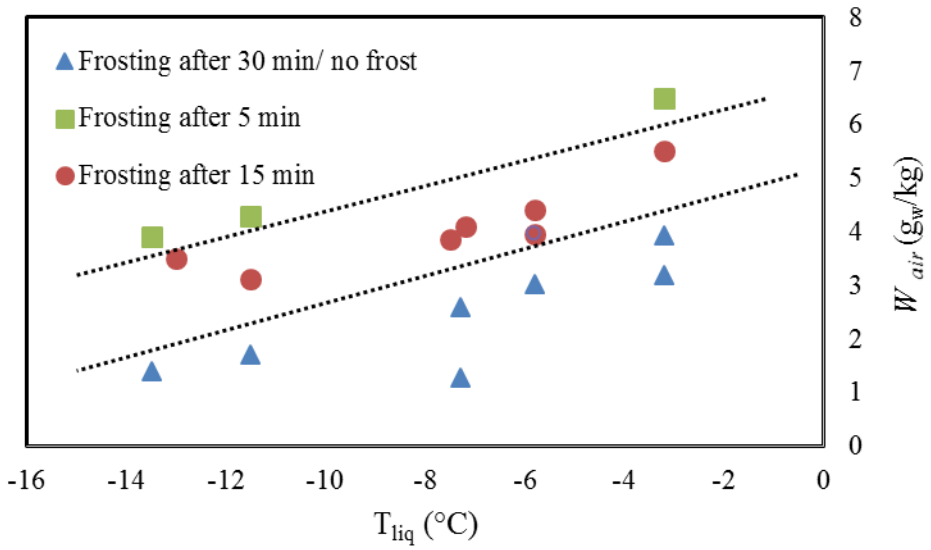

Figure 3.14. Time for frost to begin on a membrane as a function of $W_{air,in}$ and T_{liq}.

3.6.7 The Effect of W_{liq} on the frosting limit and the initiation time for frosting

The membrane has been shown to reduce the risk of condensation/frost occurring on a surface, due to the moisture transfer through the membrane, which reduces the humidity ratio of the air. The difference in the humidity ratio of the air, $W_{air,in}$, and the equivalent humidity ratio of the liquid desiccant, W_{liq}, is the driving potential for this moisture transfer. The results shown so far were for a liquid desiccant concentration (C_{liq}) of 22%, which results in a W_{liq} = 1.34 g_w/kg at T_{liq} = -7.5°C. Increasing the concentration of the liquid desiccant will decrease W_{liq}, which creates a larger driving potential for moisture transfer.

Figure 3.15 shows the membrane, after 150 min, at the same operating conditions as Figure 3.9, the partial frosting case, but with a liquid desiccant concentration of 35% (W_{liq} = 0.55 g_w/kg). It can be seen that only a few small ice particles formed on the membrane at the lower liquid humidity ratio. In addition, the initiation time for frost was after 30 min when C_{liq} = 35%, but only 20 min when C_{liq} = 22%. This confirms that increasing the moisture transfer through the membrane will further decrease the risk of frost formation on the surface.

Figure 3.15. Frost growth on a membrane at Time = 150 min, with $W_{air,in}$ = 3.4 g_w/kg_{air}, T_{liq} = - 7.5°C, and C_{liq} = 35% at the inlet (X_1), middle (X_2), and outlet (X_3) of the test section.

3.7 Conclusions

The experimental study reported in this chapter presents the frosting limits for a membrane and a plastic plate. It is found that a membrane, which can transfer both heat and moisture between two fluids, can be a promising solution to reduce frosting. The key findings are summarized as follows:

- A membrane can avoid frost formation compared to the plastic plate, under the same operating conditions ($W_{air,in}$, T_{liq}).
- Under some operating conditions, the plastic plate experiences complete condensation/frosting, while, the membrane experienced only partial condensation/frosting under the same conditions.
- The condensation/frosting limit for a membrane is lower than the condensation/frosting limit for the plastic plate by approximately 5 to 8°C.
- A membrane can delay the initiation time for condensation/frost formation.
- By increasing the amount of moisture transfer through the membrane, the risk of condensation/frost decreases.

CHAPTER 4

THE MECHANISMS OF FROST FORMATION ON A MEMBRANE

4.1 Overview

This chapter focuses on the mechanism of frost formation on membranes to meet the third objective of this thesis (*i.e.* to evaluate the mechanisms of frost formation on a semipermeable membrane). The initiation and growth of frost on the membrane is visualized during the experiment to determine if the frost formation process is different on the membrane than on a plastic plate, which has been well-established in the literature. The different stages of the frost formation on the membrane are detected and explained based on the classic explanation of the frost formation in the literature.

The manuscript included in this chapter is submitted to the Langmuir. The first author (Ph.D. student. Ms. Shirin Niroomand) performed the experiments, and analyzed the data and wrote the manuscript. The second author, Dr. Melanie Fauchoux, contributed to this manuscript by proofreading the manuscript, and providing guidance to clarify the discussions in this manuscript. Prof. Carey J. Simonson (supervisor) critically reviewed the manuscript.

The mechanism of frost formation on a semipermeable membrane

S. Niroomand, M.T. Fauchoux, C. J. Simonson

4.2 Abstract

Recent research has shown that the initiation of frost formation on a membrane is delayed, and the structure of the frost formed is different, when compared to frost growth on an impermeable surface. In this paper, the mechanism of frost formation on a membrane is investigated, and compared with that of frost formation on an impermeable surface. Both surfaces go through three stages: condensation, freezing and frosting, however the size of condensed water droplets, the length of condensation stage and the shape of the frost layer are different on two surfaces. Through photographs of these processes, it is found that the plastic plate is covered with a layer of frost after only 5 min. With the membrane, the photographs show the formation of large and distinct water droplets on the surface, followed by freezing of the individual water droplets, then crystal growth on top of the frozen droplets, and finally propagation of the frost to the entire surface. However, after two hours of testing, a mixture of water droplets and ice particles are still found on the surface of the membrane. The delay of frost formation using a membrane has many benefits for applications in cold climates.

4.3 Introduction

In Chapter 3, the frosting limit (the operating conditions that lead to frost formation) of a membrane and a plastic plate, were compared, and it was shown that under certain conditions when the plastic plate was frosted, frost formation on the membrane was delayed or avoided entirely. Therefore, it can be concluded that membranes are promising in developing anti-frost surfaces. In this chapter, the process of frosting is observed to understand the fundamental mechanism of the frost formation on a membrane.

As mentioned in Section 1.2.1, frost can grow on a cold surface through two possible processes; condensation frosting or deposition frosting [2,12,13]. The environmental conditions of interest in this thesis will lead to condensation frosting. The mechanisms of condensation frosting have been addressed in the literature [2,18,28,31,42,53]. It has been found that condensation frosting can be divided into the following stages: (1) condensing of water vapour into supercooled water droplets,

(2) phase change of water droplets into ice, when the temperature drops below the equilibrium freezing temperature, (3) crystal growth, (4) freezing propagation, and finally (5) frost layer growth and frost layer densification.

Based on the classic description of condensation frosting, the vapour pressure must have passed the saturation point before condensation will nucleate on a surface. Sometimes, the phase change process is delayed and a degree of supersaturation near the surface is needed to initiate nucleation [53] [87]; however, the bulk air flow does not need to be supersaturated [145]. When the first nucleus of water droplets form on the surface, they continue to grow and sometimes coalescent with neighboring condensed droplets until freezing begins. Freezing does not always begin at the datum freezing temperature of water, which is 0 °C. Whereas, water droplets might remain in the liquid state under metastable conditions in a supercooled state before freezing occurs. The onset of the freezing needs a degree of supercooling to overcome the energy barrier for freezing. When the required energy barrier is overcome, icing of droplets begins in a probabilistic pattern.

The rate of formation of embryos that can turn into droplets or ice crystals on a smooth surface is expressed as Eq. (4.1) [37],

$$I = I_0 \exp(-\frac{\Delta G_c}{k_1 T_{surf}}) \tag{4.1}$$

where, I_0 is the kinetic prefactor accounting for the flux of water molecules across the ice interface, ΔG_c is the critical Gibbs energy change for nucleation, T_{surf} is the surface temperature, and k_1 is the Boltzmann constant (1.38×10^{-23} J/K). Gibb's energy change is given by Eq. (4.2),

$$\Delta G_c = \frac{4\pi\sigma^3 V_m^2 (2 - 3\cos\theta + cos^3\theta)}{3(\bar{R}T_{surf}\ln(\frac{P}{P_{ws}}))^2} \tag{4.2}$$

where, σ is either the liquid-vapour or the ice-vapour surface energy, $\bar{R}$ is the ideal gas constant, V_m is the molar volume of the liquid, P is the partial pressure of water vapour in the surrounding

air, P_{ws} is the water vapour saturation pressure at T_{surf}, and θ is the contact angle of the embryo in contact with the solid.

When the nucleation of ice begins in each supercooled droplet, frost halos form on the frozen water droplet [157][158]. It should be noted that all the water droplets do not begin to freeze at the same time at temperatures above -40°C [2]. Instead, freezing propagates from a frozen droplet to the neighboring supercooled water droplets through interdroplet interactions and creates ice bridging and dry zones [2,18,43,54,139,159]. Then, frost spreads through the freezing wave propagation over the surface, followed by densification of the frost layer, due to growing of the individual ice crystals through desublimation. The process of densification and growth of the frost layer is investigated in the literature experimentally and numerically[14,48,71,97].

In order to delay or preventing frost formation, the rate of formation of embryos, I should be decreased. Looking at Eq. (1) and (2), this can be achieved by either (a) reducing the possibility of the adhesion of water droplets to the surface by increasing the contact angle, θ [37,44,51,52,59,77,83,139,145]; or (b) reducing the vapour pressure above the surface [13,28,32,34,36,45,135] Both of these methods have been investigated in the literature recently, however, formation of the frost is not eliminated completely on these surfaces.

The first approach is addressed in the literature by developing superhydrophobic surfaces ($\theta > 150$). The literature has shown that the formation of supercooled water droplets on superhydrophobic surfaces delays the nucleation of freezing, because water droplets are continually removed from the surface by jumping off or sliding. It has been found that not only the onset of freezing of an individual water droplet is delayed on superhydrophobic surfaces, but the interdrop ice bridging formation is also depressed on superhydrophobic surfaces. The interdrop ice bridging is the phenomena that leads to the propagation of freezing over a surface due to a difference in water vapour pressure above a frozen droplet and a unfrozen water droplet [15]. Also, the existence of microscale roughness on a surface might supress the freezing wave prorogation due to the structural barrier of micro/nanoscale roughness[19].

In the second approach, to alter the vapour pressure above the surface above a surface, new surfaces with an infusion of hygroscopic liquid into the surface have been developed based on the humidity sink effect. It has been shown that the hygroscopic liquid is able to absorb water vapour,

which depresses the nucleation of water droplets and even prevents the ice bridging. However as the hygroscopic liquid becomes diluted, its ability to absorb water vapour is reduced, decreasing its effectiveness at preventing frost.

Another technique that could reduce the amount of water vapour above a surface is using a membrane, which is the focus of this thesis. In this chapter, the mechanism of frost formation on a membrane is further investigated, and compared to frost formation on a plastic plate to find the difference between frosting process on a membrane and a plastic plate.

4.4 Frosting experiments

4.4.1 Test facility

The frosting experiments are conducted on two surfaces (a membrane and a plastic plate). The details of the test setup are presented in Chapter 3 (Section 3.4)

As mentioned in Section 3.4.1, a camera with a super macro lens (Canon EOS M3, Canon macro 28 mm), with a resolution of about 5 µm was set up to capture the top view photographs of the test section. The photographs were taken at three locations along the length of the test section (shown in Figure 3.1); X_1, X_2, and X_3 from the start of the test section. Side view photographs of the surfaces are also taken during the experiments. To capture the side view photographs, the camera was mounted on a rail tripod, which enabled the camera to move along the test section at a constant height.

The surface temperature at the air-surface interface is measured at three distances from the leading edge, at locations X_1, X_2, and X_3. Previously, it has been shown that the $T_{surf,air}$ at each location are very close for both test samples, within measurement uncertainty (Chapter 3).

Before each experiment was started, the surface of the test section was covered completely with an aluminum plate to avoid moisture transfer between the air and the liquid. Once the inlet air conditions (temperature and humidity ratio) and liquid temperature reached the set values, the surface was uncovered and exposed to the humid air. This was considered the start of the experiment (Time = 0 min). The temperature of the surface would initially spike at the beginning of the experiments (within the first 5 min), as the surface was exposed to the air flow, and then the

temperature would gradually reduce until it reached a steady temperature. Figure 4.1 shows the results of surface temperatures measurements, at three locations along the test section (X_1, X_2, X_3) over the duration of one test, when T_{liq} = -7.5°C and $W_{air,in}$ = 7 g_w/kg_{air}. It should be noted that the surface temperature, at all three locations, is below 0°C, which is the datum freezing temperature of water. Thus, the formation of the frosting is predicted on the surface based on the general knowledge of frost formation.

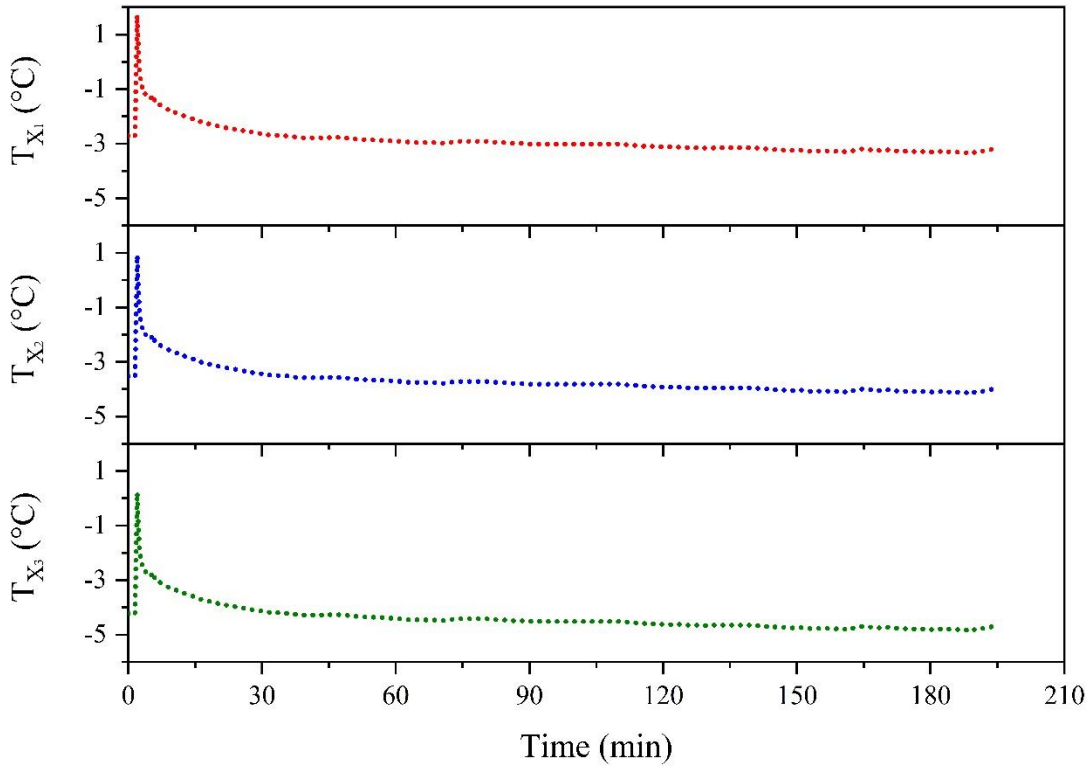

Figure 4.1. Change in surface temperature during a test when T_{liq} = -7.5°C and $W_{air,in}$ = 7 g_w/kg_{air}.

4.4.2 Surface materials

The physical properties of the membrane and plastic plate used in this study are provided in section 3.4.2. As it can be seen in Figure 4.2, there are evenly spaced pores in the fabric to allow for the moisture transfer through the membrane. The lighter parts of the photograph are the fabric,

while the dark rhombuses are the membrane. The fabric backing creates a rough surface on the air side. The plastic plate is a polyethylene vapour barrier sheet, with a relatively smooth surface.

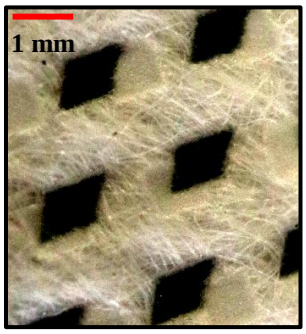

Figure 4.2. Top view photographs of the membrane (facing the fabric side).

4.5 Results and discussion

4.5.1 Mechanism of frost formation on a membrane

A test was conducted on the membrane with a liquid desiccant temperature of -7.5°C and a concentration of 22% (W_{liq} = 1.34). The air humidity ratio was 7 g_w/kg_{air} and the air temperature was 22 °C (43 % RH). The test was run for 120 min. Photographs of the frost initiation and development over the length of the test are shown in Figure 4.3 at the three locations identified as X_1, X_2, and X_3. An overview of the process will be presented here first, followed by details of coalescing of droplets, and the process of freezing of individual droplets.

The photographs at the top of the Figure 4.3 are taken at Time = 16 min and show that droplets of liquid water have formed on the membrane by this time. At location X_1, near the leading edge, the diameter of the liquid water droplets ranges between 0.1 mm and 0.26 mm. Smaller liquid droplets with diameters between 0.1 mm and 0.18 mm have formed at X_2 and X_3. At Time = 34 min, the water droplets have grown to between 0.2 mm and 0.62 mm at X_1, and between 0.2 mm and 0.8 mm at X_2 and X_3. At this time (34 min) and location X_1, the freezing of the deposited condensed droplets has begun probabilistically, whereas, there is still no freezing at X_2 and X_3. The sudden appearance of the ice crystals on a surface based on a probabilistic event is also reported by Boreyko et. al. [2][54].

After 45 min, freezing of water droplets at X_1 continues and the frost has begun to propagate throughout the test section (red circles in Figure 4.3, Time = 45 min). It can be seen that the frost begins to form at the edges of the pores in the fabric that will be discussed in more detail later. This shows that the fabric part of the membrane is a good site for nucleation.

At Time = 60 min, the frost has further propagated and the fabric pores at X_1 are almost completely full of frost. At X_2 and X_3, the freezing wave begins to front which is seen at the lower side of the photo and then spreads over the surface as indicated by the red arrow. At X_2 and X_3, a mixture of supercooled water droplets and ice particles still exists on the membrane. It can be seen that as the test continues (at Time = 90 min and Time = 120 min) the frost continues to propagate, covering more of the membrane. However, even after 120 minutes, there are still some parts of the surface which are not fully covered with ice.

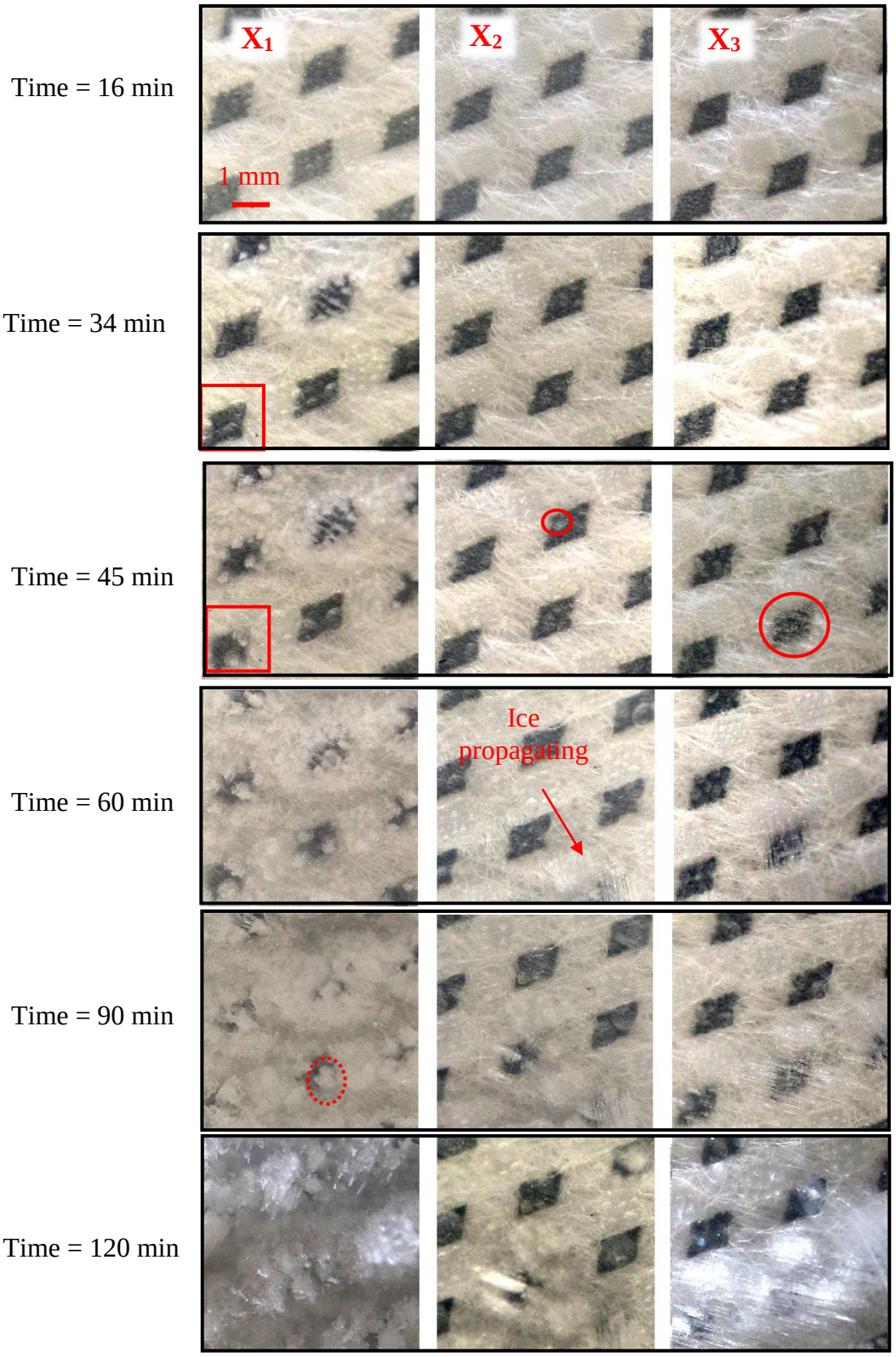

Figure 4.3. Frost accumulation on the membrane at three distances from the leading edge, with T_{liq} = -7.5°C and W_{air} = 7 $g_w/kg_{air.}$(at Time = 120 min, because of the reflection of the light off the ice surface, the color of the photos are different at X_1 and X_3).

To further investigate the mechanism of frost formation on the membrane, Figure 4.4 shows a magnified view of one pore, at Time = 34 min and at Time = 45 min. These photographs are a top view of the pore in the bottom left corner of the test section, highlighted by the red boxes Figure 4.3. In each photograph, the individual water droplets have been highlighted with white circles, to make them easier to see. At Time = 34 min there are four distinct water droplets. Two of the water droplets, labeled droplet #1 and droplet #2, had diameters of 0.34 mm and 0.38 mm, respectively, and were measured to be 0.04 mm apart using the photo imaging. At Time = 45 min these two droplets coalesced to become one larger droplet before beginning to freeze. These photographs also show that the water droplets first form along the edges of the pores. As the droplets grow larger and begin to freeze they expand into the pore. This is important as the ability of the membrane to transfer moisture between the air flow and the liquid desiccant will start to decline as the pore becomes blocked with frost. However, this shows that even under conditions where frost begins to grow, the pore is not fully blocked, and there will still be moisture transfer through the membrane.

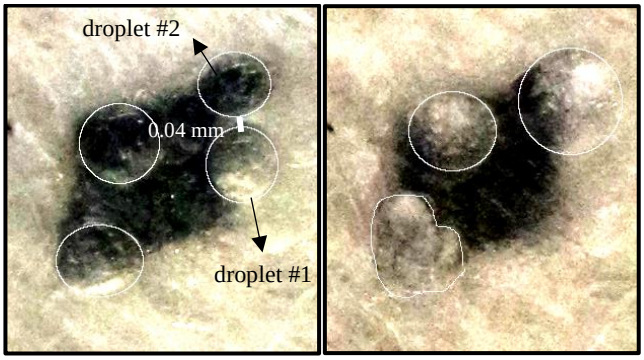

(a) Time = 34 min (b) Time = 45 min

Figure 4.4. Magnification of one pore (highlighted in Figure 4.3) at (a) Time = 34 min and (b) Time = 45 min.

The process of freezing of an individual water droplet on the membrane is depicted from the side view in Figure 4.5. The water droplet shown corresponds to the pore that is highlighted by the red dashed circle in Figure 4.3 (at Time = 90 min). The photographs in Figure 4.5 show how the water droplet changes over time. The first photo on the left side shows the side view of a water droplet at Time = 10 min. The water droplet is initially 0.2 mm high. At Time = 20 min, the droplet is frozen, and a small perturbation can be seen on the top of the frozen droplet, which is sign of

heterogeneous nucleation. As time goes on, ice crystals begin to form on the outer surface of the frozen droplet, as seen at Time = 50 min. At this point the water droplet has grown to a height of 0.5 mm, while maintaining approximately the same diameter. By Time = 80 min, the ice crystals have continued to grow on the droplet and create a column of ice crystals with height of 1.2 mm. The top view of this frost droplet has an irregular hexagon shape, as indicated in Figure 4.3.

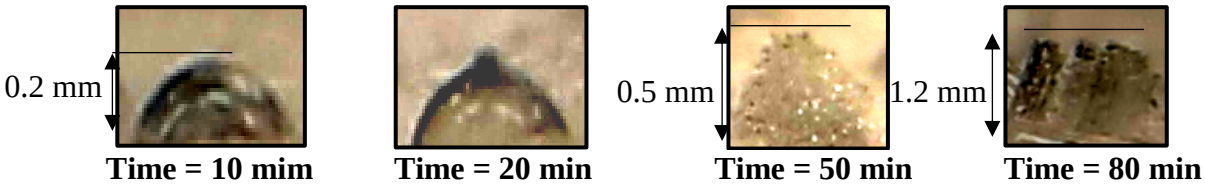

Figure 4.5. The process of the freezing and ice crystal growth on a frozen droplet.

The freezing of discrete and comparatively large water droplets on the membrane results in a cluster of irregular ice crystals as explained in Figure 4.5. When frozen water droplets are far from each other, the ice crystals grow in the horizontal direction. This process is further demonstrated in Figure 4.6, showing one of the pores created by the supporting fabric of the membrane at X_2 and the same conditions of the Figure 4.3. At t = 40 min (left picture), frozen water droplets have formed on the edge of the pore and ice crystals are growing on the outer surface of the frozen droplets (similar to Figure 4.5). As time goes on, it can be seen that ice crystals with sharp tips are protruding from the smaller frozen droplets to the larger frozen droplets, and consequently, the horizontal growth of ice crystals, probably driven by desublimation, connect all the frozen droplets together. At t = 60 min the horizontal ice crystals can be seen, as highlighted with the red dashed circle in Figure 4.6. At this time, frost covers most of the pore, which is expected to significantly decrease the moisture transfer through the pore. At t = 90 min, the pore is almost completely covered with frost. It can be seen that for two frozen droplets that are closer to each other, the interdrop frost branching produce a bushy matrix of ice crystals, whereas, horizontal ice crystals.

Time = 40 min Time = 60 min Time = 90 min

Figure 4.6. Photographs showing ice growth in the horizontal direction that eventually connects frozen droplets.

These results show that the membrane experiences all three stages of frosting that are known in the literature for frosting on impermeable surfaces; that is, water droplets form on the surface, the water droplets freeze, and then frost grows. It also confirms that not all of the water droplets freeze at the same time. Water droplets formed on the membrane remain in the liquid phase for a longer time compared to that on the plastic plate. It is believed that the moisture transfer through the membrane, that changes the vapour pressure on the surface, and also the roughness of the surface creating by the supporting fabric that might affect the freezing time and interdroplet ice bridging, are the reasons for the observed pattern of frosting.

4.5.2 Frost formation on a plastic plate

Frost formation on a plastic plate follows the same process as on the membrane; condensation, freezing and frosting. However, the transition time from condensation to freezing is very short, and is not detectable with the test facilities used in this research. After just 5 min. a very thin layer of frost forms on the plastic plate. Figure 4.7 shows a fresh plastic plate, and the frost layer on the plastic plate at Time = 15 min and Time = 120 min, for a test with the same operating conditions as the membrane (T_{liq} = -7.5°C and W_{air} = 7 gw/kgair). The frozen water droplets seen on the membrane, resulting from the freezing of distinct water droplets, are not observed on the plastic plate. Instead, ice crystals form on the plastic plate and formed a bushy matrix of ice crystals. The frost layer on the plastic plate has a more uniform shape at each location compared to the membrane. The frost layer at X_1 is thicker and consists of needle shaped crystals, while the frost layer is thinner at X_2 and X_3 and consists of plastic plate shaped crystals.

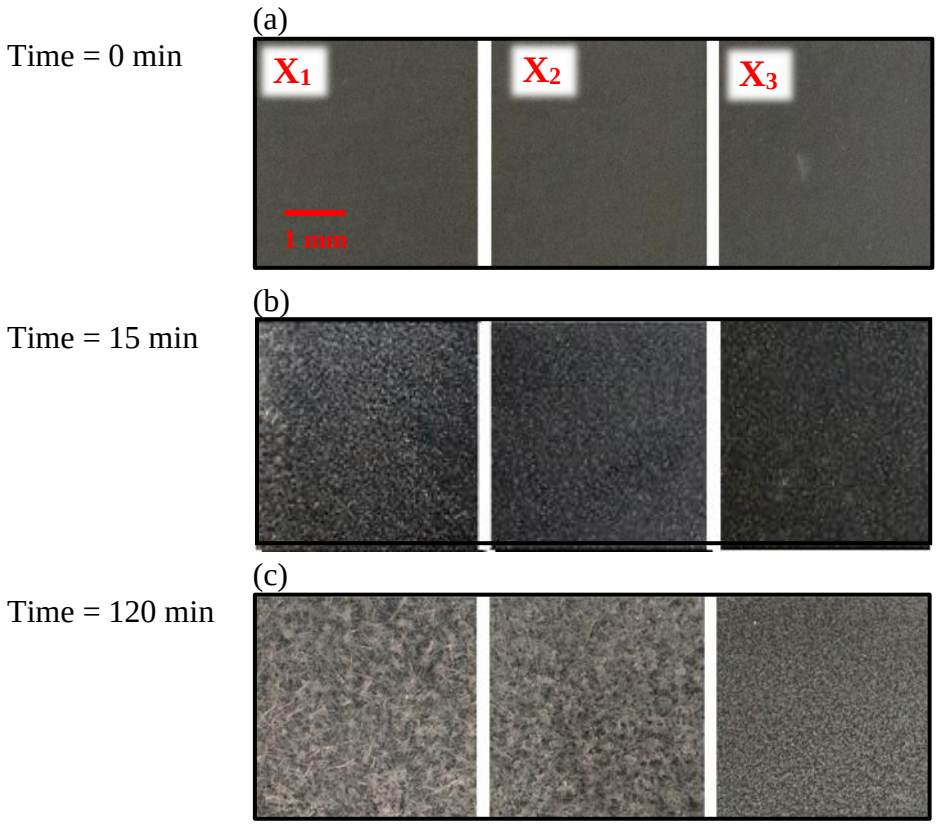

Figure 4.7. Top view photographs of a plastic plate at (a) the start of a test, (b) 15 min and (c) 120 min of the start of a test.

4.6 Conclusions

The mechanism of frost growth on a membrane is observed and compared with the process of frost formation on a plastic plate. On the membrane, isolated water droplets formed first, then froze and then ice crystals grew on the surface of the frozen droplets. The ice crystals grew horizontally between district frozen droplets, making bridges that connected the frozen water droplets together. It was observed that after 2 hr, some of the water droplets continued to grow and form larger droplets, with a mixture of supercooled water droplets and ice particles observed on the membrane. On the plastic plate, under the same environmental conditions, a layer of frost was formed quickly, and continued to grow as a full layer. This finding suggests that using membranes could delay the process of freezing (freezing depression), allowing the moisture transfer through the membrane to continue, even under conditions where frost exists.

CHAPTER 5

COMPARISON OF FROST PROPERTIES ON A PLASTIC PLATE AND A MEMBRANE

5.1 Introduction

The results presented in Chapter 3 and 4 show that the formation of frost on a membrane is delayed compared to a plastic plate. However, at severe conditions, frost formation cannot be avoided completely. In this chapter, the properties of the frost layer on a membrane are evaluated both qualitatively and quantitatively. The thickness, the area of the membrane covered with frost, and mass of the frost layer on a membrane are measured and compared with those on a plastic plate, at the same operating conditions. Moreover, the effect of operating conditions (air humidity ratio, air mass flow rate, liquid desiccant temperature and salt concentration) on the thickness and mass of accumulated frost are investigated.

This chapter completes the first objective of this thesis (*i.e.* to apply image processing to characterize frost properties on a surface) and addresses the fourth objective (*i.e.* To identify the effect of moisture transfer on frost properties on a membrane). In this chapter, the main goal is to compare frost properties on the membrane with those on the plastic plate. This chapter also aims to find the effect of operating conditions on the frost layer shape, thickness and mass of the frost layer on the membrane. Because the process of frost formation on both a membrane and plastic plate, have been presented in Chapter 3 and 4, only photographs of the frost layer at the end of the experiments are shown in this chapter for better understanding of the results.

In this chapter, the test facility that is presented in Chapter 3, Figure 3.1, is modified to measure the properties of a frost layer on a membrane and a plastic plate. Two micro rulers are added to the test section at d_1 and d_2 for image processing purposes in order to measure frost thickness accurately at these points. The details of the experimental procedure and material properties have been provided previously in Section 3.4.

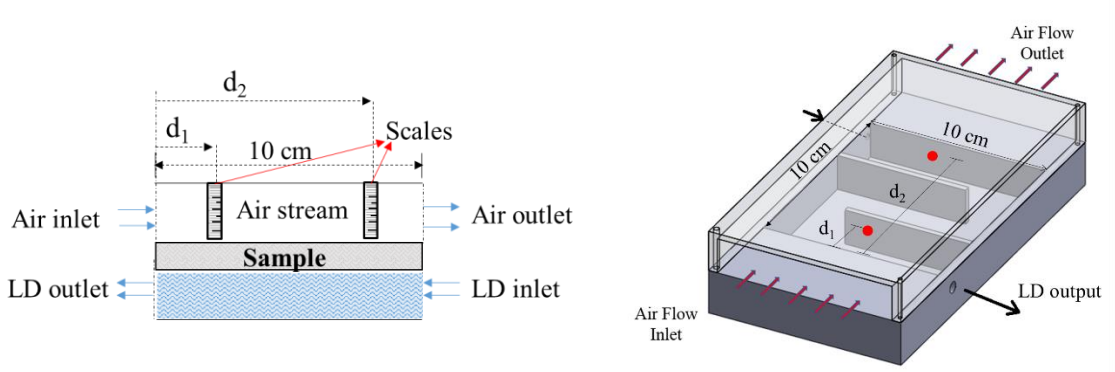

Figure 5.1. Schematic of the experimental test section for study of frost formation on a membrane; Locations of two scale are shown in red circles in left picture. Note: The diagrams are not drawn to scale.

Experiments are conducted to measure the thickness, the frosted area of the membrane and mass of the frost layer formed on the plastic plate and the membrane. Top view photos are taken at three locations shown in Figure 3.1 (X_1, X_2, and X_3,) to visualize the frost layer shape at different locations. The methodologies to measure thickness and mass are presented in the following sections.

In Chapter 3, it was found that the initiation of frost formation is delayed on the membrane compared to the plastic plate, because a membrane reduces the dew point temperature of the air. The process of frost formation was evaluated visually in Chapter 4, in detail, to explain the difference between the mechanisms of the frost formation on the membrane and the plastic plate. It is found that the fundamentals of the process of frost formation on the two surfaces are similar: condensation, freezing, and frosting. However, comparatively large and distinct water droplets formed on the membrane, and these remain in the liquid state for a longer time compared to the dropwise condensation formed on the plastic plate. After freezing of water droplets, ice crystals grow on the outer surface of frozen droplets, and sometimes the frozen droplets connect to each other with a lateral bridging of ice crystals (Figure 4.6).

It should be noted that the surface roughness of the frost on the membrane is not presented in this Chapter. The horizontal growth of the ice crystals results in unreliable measurement of the surface roughness because of the existence of re-entered surfaces (Sections 2.4.2.3 and 2.4.2.2). Figure 5.2(a) shows the surface profile of a frost layer on a membrane where the lateral growth of

ice crystals are clear. Figure 5.2(b) shows the generated surface profile used to measure frost surface roughness. It can be seen that the details of the horizontal growth of ice crystals, which is a main characteristic of frost growth on a membrane, is ignored completely. Moreover, it is discussed in Chapter 2 that the density of the frost layer on a plastic plate is a function of the ice crystals shape that is quantified with frost surface roughness. Because large water droplets form on the membrane, and the density of water is at least twice the density of the frost, the density of the frost layer is mainly dependant on the size of water droplets, not the shape of the frost crystals. From this discussion, it can be concluded that frost roughness might not be a valuable parameter to characterize the frost layer on a membrane. Therefore, the frost thickness and the area of the membrane covered with the frost crystals are chosen as two parameters that characterize frost growth on a membrane.

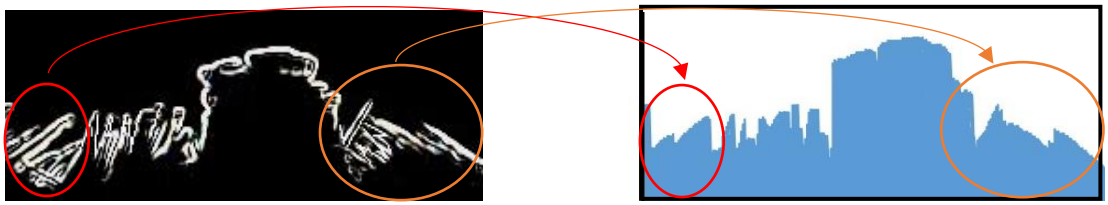

Figure 5.2. Images of (a) real profile of a frost layer on the membrane, and (b) generated profile for roughness measurement.

5.2 Frost thickness measurements

The thickness of the frost layer on the surface is measured by taking photographs of the side of the test section, and analyzing these images using a computer software, Image J[156]. Ref. [11] showed that frost growth begins from the top surface of the membrane, not within the membrane. Therefore, side view images of the frosted membrane is a good indication of frost layer thickness. Since the thickness of the frost layer changes along the test section, under forced convection conditions, the thickness of frost is measured at two different locations from the leading edge. Therefore, a camera was mounted on a rail tripod, making the movement of the camera along the test section possible. The tripod was aligned with on the test section before each experiment and was fixed to avoid any movement. The membrane budges when liquid desiccant is flowing in the

test section, despite the pre-stretching of the membrane before gluing to the test section. It should be noted that gluing the membrane on two baffles shown in Figure 3.1, produces three small deflections at X_1, X_2, and X_3. The thickness of the frost at the apex points of the membrane deflection curves at two locations (x^* = 0.2 and x^* = 0.8, where $x^* = \frac{d}{L}$, shown in Figure 5.1) is measured and reported. Two small scales are hanging from the top of test section at d_1 and d_2 which are used to convert pixel size to mm, as explained in Chapter 2 (Section 2.4.2.2).

In this chapter the frost thickness is assumed as the average detected value for a range of 2 mm around at d_1 and d_2. The frost-air interface is detected and the average distance between frost-air interface and a base line is measured by using an imaging technique to find the frost thickness at each time. A detailed description of detecting frost-air interface was provided in Chapter 2. The total uncertainty in the thickness measurement was found to be ±0.02 mm.

5.3 Frost mass measurement

The mass of frost accumulated on the membrane is equal to the difference between the total reduction in moisture content in the air flow through the test section, and the total moisture transferred to the liquid desiccant, as shown in Eq.(5.1):

$$m_{frost} = \int_0^t \dot{m}_{air}(W_{air,in} - W_{air,out})dt - \Delta mass_{\mathrm{liq}} \tag{5.1}$$

Where, t(s) is the total duration of the experiment. The total change in mass of liquid desiccant over the length of the test ($\Delta mass_{liq}$) is measured, by measuring the change in mass of the liquid desiccant inside the liquid container, shown in Figure 3.1.

The uncertainty in frost mass measurement is calculated by propagating the uncertainties in the inlet and outlet humidity ratios and $\Delta mass_{\mathrm{liq}}$. The total uncertainty is ±0.25 g. To measure the mass of frost on the plastic plate, $\Delta mass_{\mathrm{liq}} = 0$, as no moisture transfers through the plastic plate. The total uncertainty of the mass measurement for the plastic plate is equal to ±0.2 g.

5.4 Results and discussion

5.4.1 Comparison between frost properties on a membrane and a plastic plate

To find the difference between frost growth on the membrane and the plastic plate, two experiments are conducted, one with the plastic plate, and another with the membrane, at the same operating conditions. Top-view photos of the frost layer on the membrane and plastic plate are shown in Figure 5.3. The frost layer on the plastic plate, consists of a uniform layer of needle shape crystals at X_1, and more plastic plate shape crystals at X_2 and X_3 (Figure 5.3(a)). However, the frost layer on the membrane mostly consists of irregular hexagonal shape ice clusters which are connected to each other with horizontal ice crystals, because of the formation of large and distinct water droplets as explained in Chapter 4 (Figure 5.3(b)). It is clear that frost layer covers the entire plastic plate, however, for the permeable membrane, there are some parts (at X_2 and X_3) which are not covered with frost (red circles in Figure 5.3(b)). Approximately, 63% and 50% of the area of the membrane at X_2 and X_3 is covered by the frost crystals.

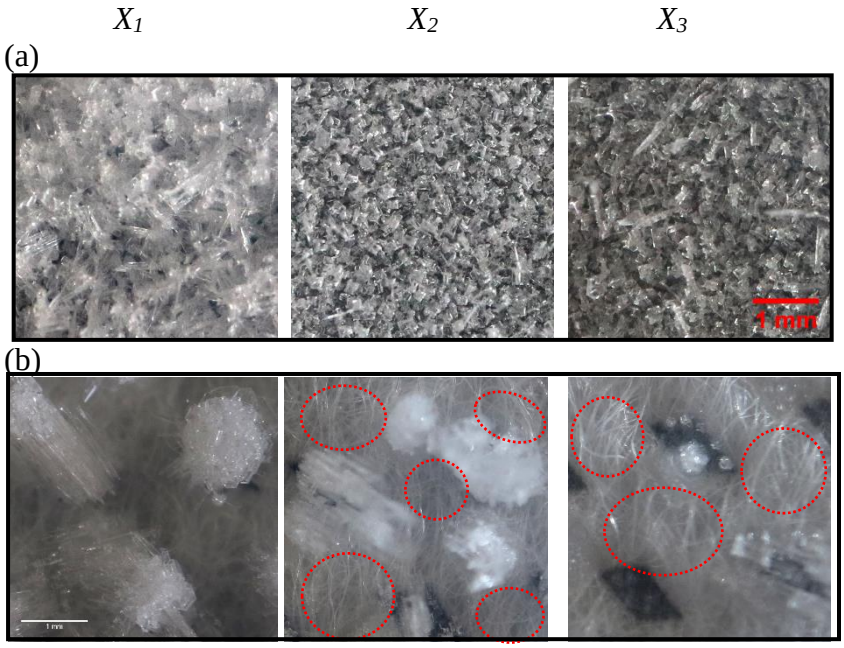

Figure 5.3. Top- view photos of the frost layer at X_1, X_2, and X_3, and on (a) plastic plate, (b) membrane, when $T_{air,in}$ = 22 °C, $W_{air,in}$ = 7.5 g_w/kg_{air}, and T_{liq} = -10.5 °C. Note: all photos have the same scale. Red circles show the unfrosted parts of the membrane

5.4.2 Frost thickness

The measurement of the frost thickness on the membrane and plastic plate at x^* = 0.2 and x^* = 0.8, is shown in Figure 5.4. It can be seen that, for both surfaces, the frost thickness increases with time. For the membrane, the frost thickness is greater at x^* = 0.2 than at x^* = 0.8. In Chapter 3, it was shown that frost growth begins from the entrance of the test section and then spread over the entire surface, due to the undeveloped thermal and mass boundary layer. Therefore, a thicker frost layer formed at x^* = 0.2 compared to x^* = 0.8. Moreover, it can be seen that a thicker frost layer formed on the plastic plate compared to the membrane at all data points.

Within the first 60 min of the test, the rate of the frost growth on the membrane (0.1 mm at x^* = 0.2 and 0.05 mm at x^* = 0.8) is smaller compare to the frost growth on the plastic plate (1 mm at x^* = 0.2 and 0.85 mm at x^* = 0.8). However after 60 min, the rate of frost growth increases rapidly for the membrane compare to the plastic plate. This finding suggests that even when frost begins to form in a membrane energy exchanger, it might take time until frost growth affects the performance of the exchanger. However, in a plate heat exchanger, frost growth may degrade the heat exchanger's performance at the early stages of the frost formation.

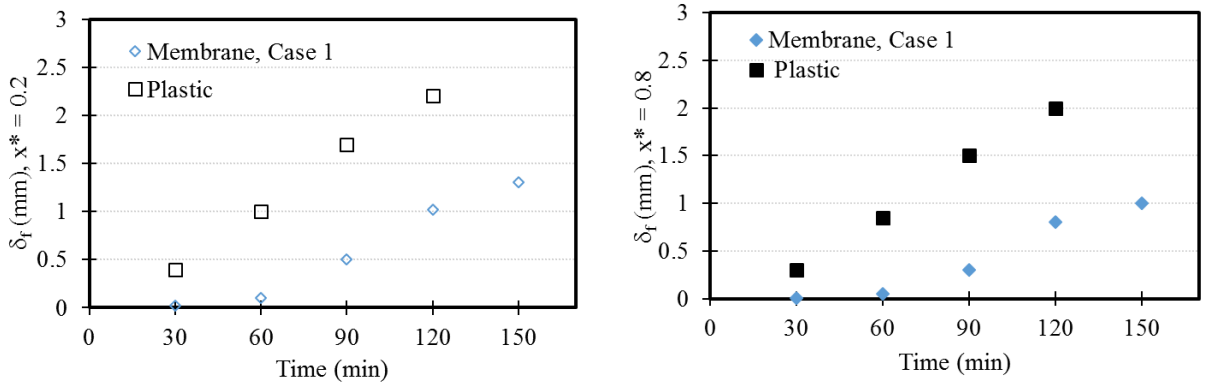

Figure 5.4. The thickness of a frost layer on the membrane and plastic plate at x^* = 0.2 and 0.8, when $T_{air,in}$ = 22 °C, $W_{air,in}$ = 7.5 g_w/kg_{air}, and T_{liq} = -10.5 °C (error bars are not shown for the frost thickness because the uncertainty (±0.02 mm) is smaller than the symbols).

5.4.3 Frost mass

The mass of the frost layer on two surfaces (membrane and plastic plate) are measured and results are presented in Table 5.1.

Table 5.1. Frost mass after 150 min (g).

Plastic plate	3.2 ± 0.2
Membrane	1.6 ± 0.25

The mass of frost on the membrane is 50% lower than the mass of frost on the plastic plate. Therefore, it can be concluded that the frost layer accumulated on the membrane is thinner and has lower mass than a frost layer formed on the plastic plate at the same operating conditions.

5.5 The influence of operating conditions on frost properties on the membrane

Now that it has been shown that less frost formed on the membrane compared to the plastic plate at the same operating conditions, it is interesting to see the effect of operating conditions on the properties of the frost layer on the membrane. It was shown in Chapter 2 that decreasing the surface temperature and increasing the air humidity ratio increases the frost layer thickness on a plastic plate. On the other hand, it is believed that increasing the moisture transfer rate through the membrane may decrease the amount of frost formation on the membrane. It should be noted that the change in the diffusivity of a membrane and also the operating conditions (increasing the difference between the humidity ratio of the air inlet and solution) could change the rate of the moisture transfer rate through the membrane; however, changing in the membrane diffusivity is not investigated in this research. Therefore, the influence of the humidity ratio of the air and liquid desiccant on the frost growth is evaluated.

The tested operating conditions in this section are given in Table 5.2. The shaded cells indicate the values that have changed from the base case (case 1). The effect of T_{liq}, $W_{air,in}$, W_{liq}, and $\dot{m}_{air}$ on the frost thickness and mass are evaluated in the following subsections.

Table 5.2. The tested operating conditions.

Case #	$T_{air,in}$ (°C)	$W_{air,in}$ (g_w/kg)	T_{liq} (°C)	C_{liq} (%)	W_{liq} (g_w/kg)	$\dot{m}_{air}$ (kg/s)
Case 1	22	6.5	-10.5	33	0.51	0.2
Case 2	22	6.5	-10.5	17	1.3	0.2
Case 3	22	6.5	-19.5	20.5	0.54	0.2
Case 4	22	7.5	-10.5	33	0.51	0.2
Case 5	23	6.5	-10.5	32.5	0.51	0.5

5.6 Effect of liquid desiccant concentration

Decreasing of C_{liq}, increases the equivalent humidity ratio of the liquid desiccant (W_{liq}), which decrease the difference between the inlet air humidity ratio and the equivalent liquid humidity ratio ($W_{air,in}$– W_{liq}) for the same $W_{air,in}$. Two experiments for two different value of W_{liq}; Case 1, W_{liq} = 0.5 g_w/kg when, and Case 2, when W_{liq} = 1.3 g_w/kg, are conducted in order to determine the effect of W_{liq} on frost growth. Figure 5.5 shows top view photos of the frost layer at two values of W_{liq}. As it can be seen in Figure 5.5, at higher W_{liq}, the coverage of frost on the surface increases at locations X_2 and X_3; approximately 99% and 90% of the membrane area at X_2 and X_3 is covered with the frost crystals, while, at lower W_{liq}, only 63% and 50% of the membrane area at X_2 and X_3 is covered with the frost crystals. Also, the distinct ice crystals clusters are obvious at the lower W_{liq}, compare to the higher W_{liq}.

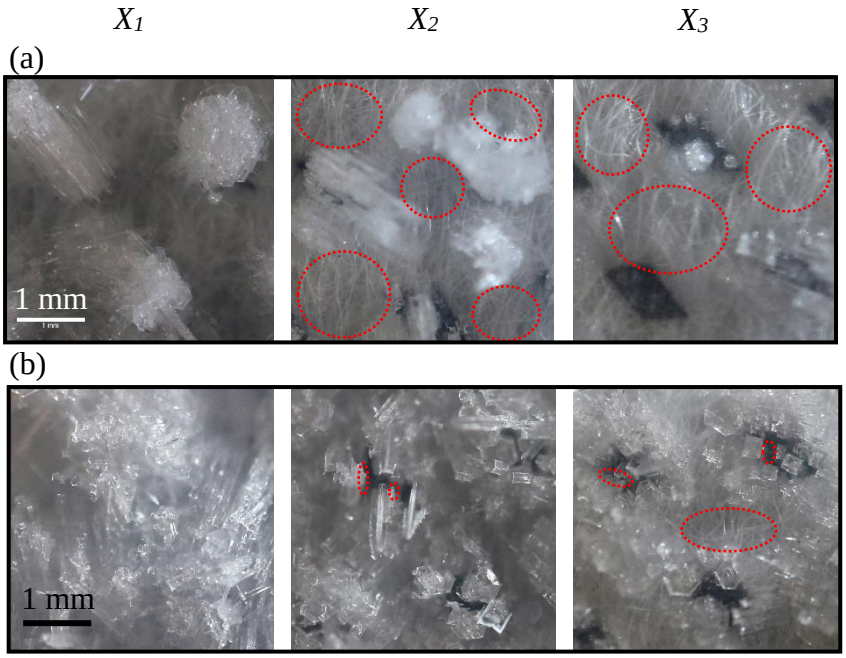

Figure 5.5. Top- down photos of frost later at X_1, X_2, and X_3 on (a) Case 1, W_{liq} = 0.5 g_w/kg_{air} (b) and Case 2, W_{liq} = 1.27 g_w/kg_{air}. Note: all photos have the same scale. Red circles show the unfrosted parts of the membrane

The thickness of the frost layer, at x^* = 0.2 and 0.8 at two conditions are measured and results are shown in Figure 5.6. As mentioned in Section 5.5, after 60 min of the beginning of the test, frost growth accelerate, which at W_{liq} = 1.3 g_w/kg, the rapid growth of the thickness of the frost layer begins after 30 min as Figure 5.6 reveals. However, after 60 min, the rate of frost growth at two conditions are almost the same. Generally, the thickness of the frost layer is higher when W_{liq} = 1.3 g_w/kg. Findings suggest that increasing in the amount of moisture transfer by decreasing of W_{liq} would depress the formation of the frost accumulation on the membrane.

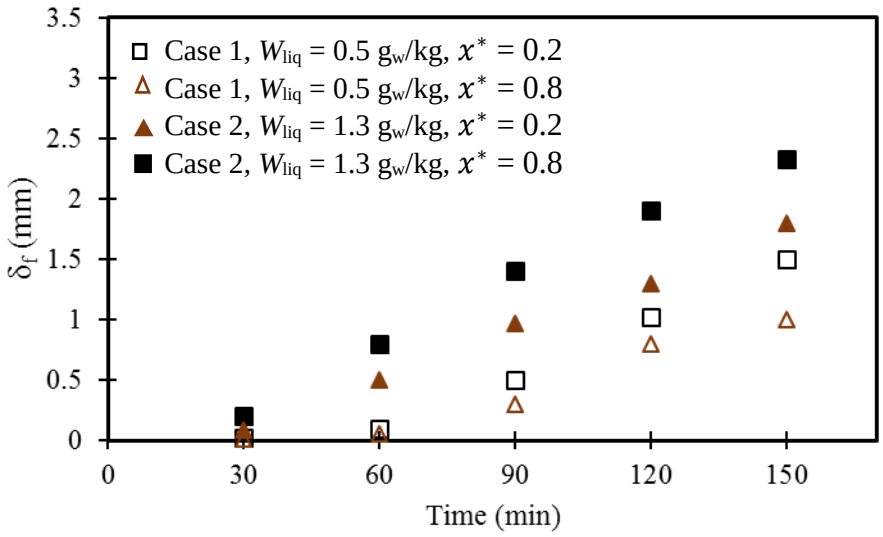

Figure 5.6. The thickness of a frost layer on the membrane at x^* = 0.2 and 0.8, when W_{liq}= 0.5 g_w/kg_{air} and W_{liq} = 1.27 g_w/kg_{air} (error bars are not shown for the frost thickness because the uncertainty (±0.02 mm) is smaller than the symbols).

5.7 Effect of the temperature of the liquid desiccant

To determine the influence of the T_{liq} on the frost growth on the membrane, two experiments at T_{liq} = -19.5 °C and T_{liq} = -10.5 °C have been done. Top view photos of the frosted membrane at the end of the experiments are shown in Figure 5.7. The lower liquid temperature, the membrane is completely covered with frost. Also, irregular hexagonal ice clusters appear at Figure 5.7(a), do not appeare at T_{liq} = -19.5 °C; whereas, needle shape crystals formed at X_1, and mixture of needle shape and plastic plate shape crystals at X_2 and X_3, which is similar to the frost layer shape on the plastic plate. The thickness of the frost layer formed on the membrane at x^* = 0.2 and 0.8 when T_{liq} = -19.5 °C and T_{liq} = -10.5 °C is presented in Figure 5.8. The thickness of the frost layer at T_{liq}= -19.5 °C is higher than that at T_{liq}= -10.5 °C. For case 1, where T_{liq} = -10.5 °C, the frost layer is very thin at first 60 min of the test, and then the rate of frost thickness growth increases. However, for case 3, frost begins to grow rapidly from the beginning of the test.

Figure 5.8, also compares case 2, where W_{liq} = 1.3 g_w/kg and T_{liq} = -10.5 °C, with case 3, where both W_{liq} and T_{liq} are lower than case 2. As it can be seen, although ($W_{air,in}$– W_{liq}) is higher for case 3, and higher amount of moisture transfer through the membrane is expected, the frost thickness

is higher at two x* values compare to the case 2. This is because T_{liq} is lower for case 3 compare to case 2. Thus, it can be concluded that at lower liquid temperatures, the effect of the moisture transfer on frost growth is negated.

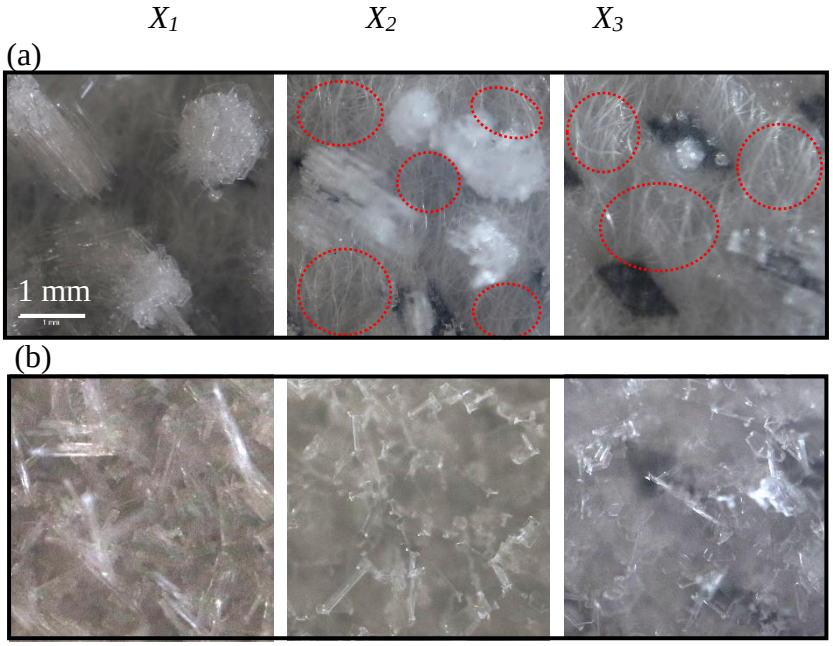

Figure 5.7. Top- down photos of frost later at X_1, X_2, and X_3 on (a) Case 1, T_{liq} = -10.5 °C (b) and Case 3, T_{liq} = -19.5 °C. Note: all photos have the same scale. Red circles show the unfrosted parts of the membrane.

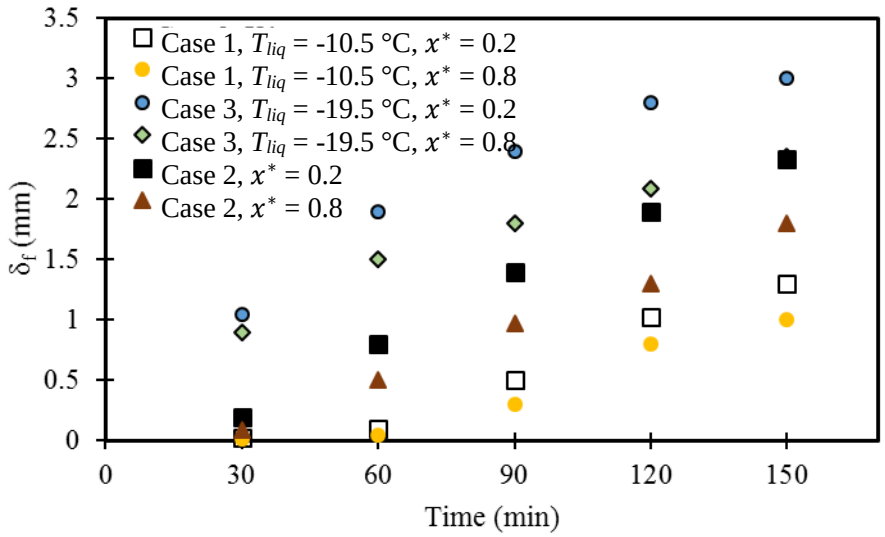

Figure 5.8. The thickness of a frost layer on the membrane at x^* = 0.2 and 0.8 when T_{liq} = - 10.5 °C and T_{liq} = -19.5 °C (error bars are not shown for the frost thickness because the uncertainty (±0.02 mm) is smaller than the symbols).

5.8 Effect of inlet air Humidity ratio on the Thickness of the Frost Layer

Increasing the air inlet humidity ratio increases the moisture transfer through the membrane and the potential for the frost growth (in Chapter 2 it is shown that thicker frost layer form at higher air humidity ratios). The top view photos of frosted membranes at two air humidity ratios are presented in Figure 5.9. The frost layer shape is similar for theses two cases; however, the coverage of the surface by frost increases at the higher humidity ratio ($W_{air,in}$ = 7.5 g_w/kg); the membrane surface is mostly covered with frost crystals at X_1 and X_2 and about 70% of the area is covered at X_3. Figure 5.10 presents the thickness of the frost layer on the membrane for the two different values of $W_{air,in}$. It can be seen that thickness of the frost layer is higher when $W_{air,in}$ = 7.5 g_w/kg compared to $W_{air,in}$ = 6.5 g_w/kg. Also, the rapid growth in the frost layer thickness begins earlier at higher $W_{air,in}$ compared to the lower $W_{air,in,}$. It shows that despite the higher rate of moisture transfer at the higher $W_{air,in}$ at the beginning of the test, the frost layer at higher $W_{air,in}$ is thicker than the frost layer at lower $W_{air,in}$.

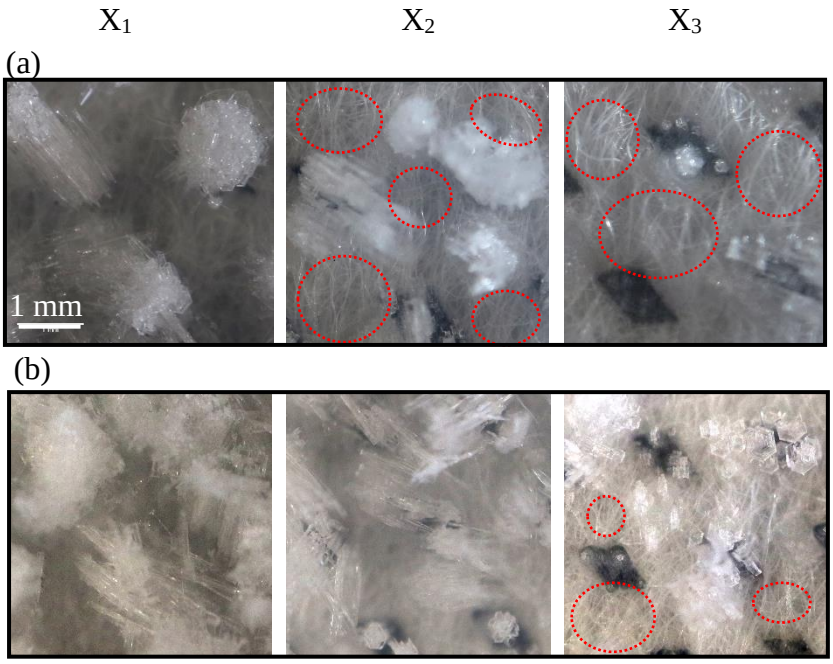

Figure 5.9. Top- down photos of frost later at X_1, X_2, and X_3 on (a) Case 1, $W_{air,in}$= 6.5 g_w/kg_{air}, and (b) Case 4, $W_{air,in}$ = 7.5 g_w/kg_{air}. Note: all photos have the same scale. Red circles show the unfrosted parts of the membrane.

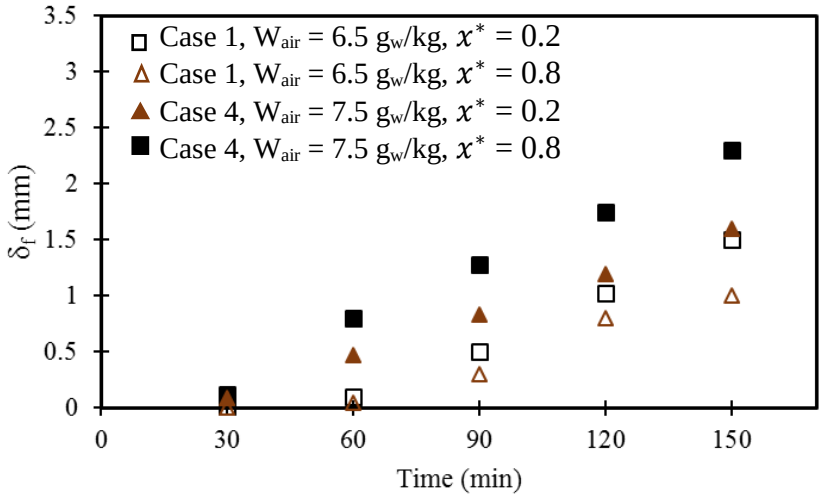

Figure 5.10. The thickness of a frost layer on the membrane at x^* = 0.2 and 0.8 when $W_{air,in}$ = 6.5 g_w/kg_{air} and $W_{air,in}$ = 7.5 g_w/kg_{air} (error bars are not shown for the frost thickness because the uncertainty (±0.02 mm) is smaller than the symbols).

5.9 Effect of air mass flow rate on the thickness of the frost layer

To determine the effect of the air mass flow rate on the frost growth, experiments are conducted at $\dot{m}_{\text{air}} = 0.2$ kg/s and $\dot{m}_{\text{air}} = 0.5$ kg/s, and top view photos are shown in Figure 5.11. As can be seen, the frost layer covers the membrane completely at the higher air mass flow rate, as no free space can be seen between ice crystals at X_2 and X_3. Again, the overall shape of frost layer at $\dot{m}_{air} =$ 0.5 kg/s is similar to the frost layer on the plastic plate. Also, the thickness of frost layer at two conditions is presented in Figure 5.12. The thickness measurement shows that increasing $\dot{m}_{air}$, increases the thickness of the frost layer. If the test section is considered as an energy exchanger, based on the heat and moisture exchangers theory, the latent effectiveness of an energy exchanger is a function of NTU_m and Cr, where, NTU_m is the number of mass transfer units, and Cr is the heat capacity ratio of the energy exchanger. For the tests performed in this thesis, $Cr \approx 0$. Thus the latent effectiveness of the energy exchanger could be found by the following Eqs.[160]:

$$\epsilon_{latent} = 1 - \exp(-NTU_m) \tag{5.2}$$

$$NTU_m = \frac{U_m A}{\dot{m}_{air}} \tag{5.3}$$

where, U_m is the overall mass transfer coefficient of the exchanger ($kg_{air}/(m^2.s)$) and A is the area of the surface. Based on Eq. (5.3), higher $\dot{m}_{air}$, results in lower $NTU_{m,}$ which means the ε_{latent} decreases. The reduction of the latent effectiveness means the reduction of the moisture transfer, which results in higher values of W_{air} along the exchanger. As results shows in Section 5.8, higher air humidity ratio results in thicker frost layer.

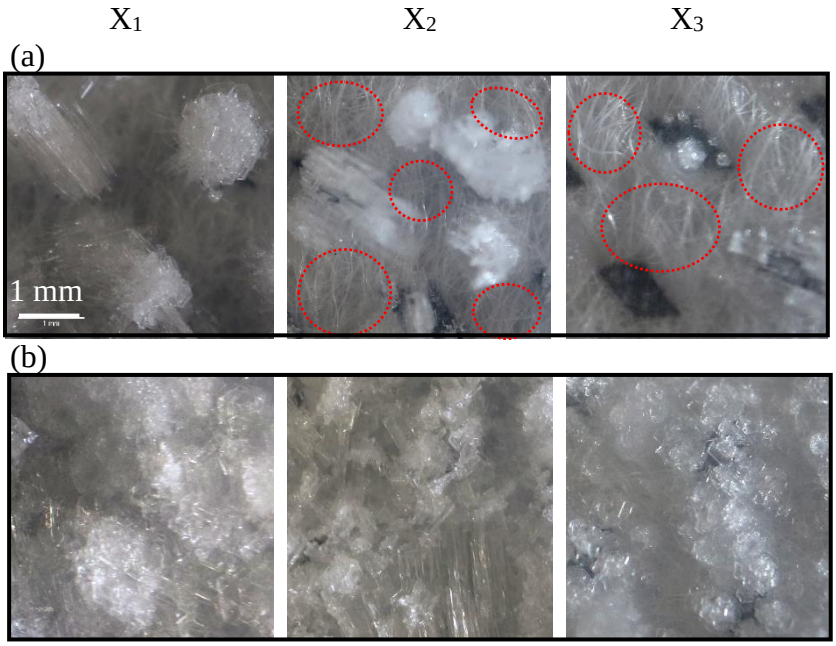

Figure 5.11. Top- down photos of frost later at X_1, X_2, and X_3 on (a) Case 1, $\dot{m}_{air}$= 0.2 kg/s, and (b) Case 5, $\dot{m}_{air}$= 0.5 kg/s. Note: all photos have the same scale. Red circles show the unfrosted parts of the membrane.

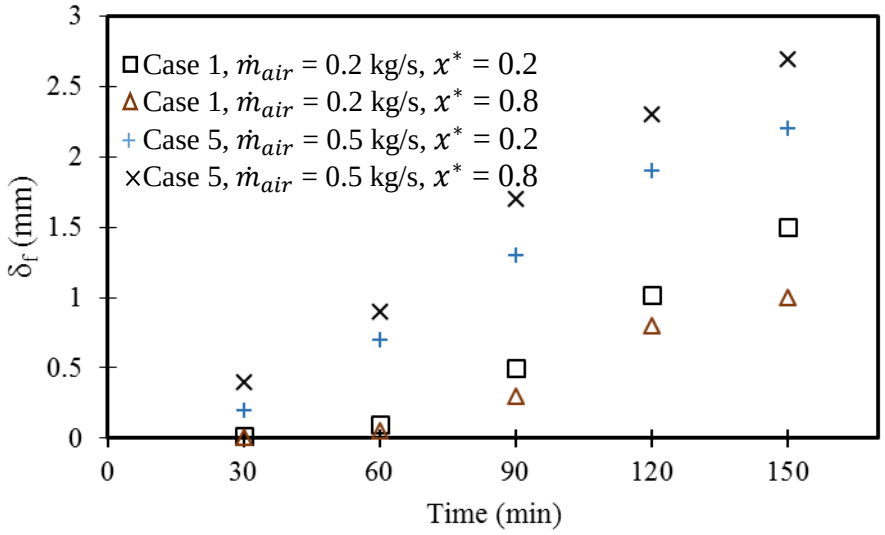

Figure 5.12. The thickness of a frost layer on the membrane x^* = 0.2 and 0.8 when $\dot{m}_{air}$ =0.2 kg/s and $\dot{m}_{air}$ = 0.5 kg/s (error bars are not shown for the frost thickness because the uncertainty (±0.02 mm) is smaller than the symbols).

5.10 Frost mass

The mass of accumulated frost on the membrane after 150 min for all cases are presented in Table 5.3. Results show that the mass of the frost accumulated on the membrane increases when the air humidity ratio, the air mass flow rate, and the humidity ratio of the liquid desiccant increases and the temperature of the liquid desiccant reduces. However, as it can be seen, the uncertainty in mass measurement is higher than the difference between the frost mass in the different cases, which make it difficult to investigate the effect of operating conditions on the frost mass. Therefore, a more accurate mass measurement with lower uncertainty is suggested for future studies.

Table 5.3. Frost mass at different operating conditions on the membrane after 150 min (g).

Case	Frost mass
Case 1	1.36 ± 0.25
Case 2	1.60 ± 0.25
Case 3	1.90 ± 0.25
Case 4	2.00 ± 0.25
Case 5	1.90 ± 0.25

5.11 Conclusions

The experimental study in this chapter presents the measured thickness and mass of frost accumulated on a plastic plate and membrane. All the test are accompanied by visual observation to help explain the influence of the operating conditions on the frost formation process. It is found that frost growth on a membrane can be reduced because of moisture transfer through the membrane. The key findings are summarized as follows:

- The frost deposition can be delayed on the membrane, for 30 to 60 min, depending on the operating conditions, compared to the plastic plate.
- The following changes to the operating conditions will result in thicker frost layer on the membrane
    - Increasing W_{liq},
    - Decreasing T_{liq},
    - Increasing $W_{air,in}$, or

    - Increasing $\dot{m}_{air}$.
- The effect of decreasing T_{liq} or increasing $\dot{m}_{air}$ are significant enough that the frost layer on the membrane was similar to the frost layer on the impermeable plastic plate, indicating that under extreme weather conditions, the membrane may become completely blocked and act as an impermeable plastic plate.

CHAPTER 6

SUMMARY, CONCLUSIONS, CONTRIBUTIONS AND FUTURE WORK

The main objectives of this Ph.D. thesis are to investigate the effect of moisture transfer through a membrane on the frosting limit and the onset and growth of frost on a membrane through an experimental approach. This chapter will summarize the research and important results presented in this thesis, as well as potential areas for future research.

6.1 Summary and conclusions

Frosting is a physical phenomenon that occurs when humid air is in contact with a cold surface that has a surface temperature below the dew point temperature and freezing temperature of the humid air. Due to the difficulties of defrosting processes, it is desired to develop anti-frosting surfaces, which requires a comprehensive knowledge about the process of the frost formation on such a surface. Membrane exchangers are gaining interest in HVAC (Heating, ventilating and air-conditioning) applications because the vapour permeability of the membranes allows the control of both temperature and humidity of the air in buildings. The literature has shown that membrane exchangers can tolerate lower temperatures without frosting occurring inside the exchangers. However, no information is available on the conditions that lead to frost formation, the initiation time of frost, the mechanism of frost formation, and the characteristics of frost on a membrane. In this Ph.D. thesis, the following objectives are set to investigate the effect of moisture transfer through a membrane on frosting:

1. To apply image processing to characterize frost properties (Chapter 2 and Chapter 5).
2. To identify the effect of moisture transfer on frosting limit (Chapter 3).
3. To determine the mechanisms of frost formation on a membrane (Chapter 4).
4. To identify the effect of moisture transfer on frost properties on a membrane (Chapter 5).

The thesis compares frost growth on a membrane and a plastic plate to investigate the effect of moisture transfer through the membrane on frosting.

In Chapter 2, the image processing is applied to characterize a frost layer on a plate. A test facility to evaluate the frost layer formed on a plate under natural convection conditions are developed and explained in detail (*i.e*. calibrations, uncertainty measurements, measurements methodologies). Natural convection was chosen because it results in an approximately uniform frost layer on the surface. Image processing is used to measure the thickness and roughness of the frost layer on the plate. The mass and density of the frost layer are also measured in this chapter. In this chapter, frost layer shape is quantified with frost surface roughness and a relation between frost surface roughness and density is presented. Moreover, the effects of the operating conditions (air temperature, surface temperature, air relative humidity) on the frost properties formed on a plate are studied both qualitatively and quantitatively.

The following are the major conclusions related to this chapter:

- The thickness and mass of the frost increase on a plate with time; however, the rate of the growth is highly dependent on the operating conditions.
- The surface of the frost layer is very rough, which can be defined with the arithmetic roughness parameter (R_a) and the skewness of the roughness of the frost surface (R_{sk}). The shape of frost crystals is quantified with R_a and R_{sk}.
- The surface temperature has the greatest effect on the frost layer structure and the density of the frost layer.
- Frost density and frost surface roughness are related to each other independent to the operating conditions; higher frost roughness results in frost layer with lower density. Also, negative skewness corresponds to the frost layer with very low density.

In Chapter 3, a test facility is developed to study frost formation on a surface under forced convection conditions. The details of the test facility, uncertainty analyses, the experimental procedure, and test apparatus are explained in this chapter. The main focus of this chapter is to visually identify and compare the operating conditions (air humidity ratio and the cold temperature) that lead to condensation/frosting on a membrane and plastic plate (the condensation/frosting limit). The initiation time for the frost to form on the membrane is also investigated further, and the effect of the moisture transfer rate on the frosting limit is presented. The principal conclusions related to this chapter are:

- Condensation/frost appears at the inlet of the test section, then spreads over the entire surface for both the membrane and plastic plate.
- There are some operating conditions where frost appears only at the entrance of the test section for the membrane.
- The condensation/frosting limit for the membrane is lower than the condensation/frosting limit for the plastic plate by approximately 5 to 8°C.
- The initiation time for condensation/frost formation on the membrane is longer than on the plastic plate and the delayed time is quantified for the membrane.
- Increasing the moisture transfer rate through the membrane decreases the risk of condensation/frost.

In Chapter 4, the mechanism of the frost formation on a membrane is investigated in detail. The process of frosting on the membrane is monitored during the experiment using top view photographs. The different stages of frosting (condensation, freezing and frosting) on the membrane are detected and are compared with those on the plastic plate. The main conclusions related to this chapter are:

- The mechanism of frost growth on a membrane follows the same process as the well-known frost growth on a plastic plate: condensation, freezing, frosting, however there are differences in each stage.
- On the membrane, isolated and large water droplets form first, then freeze and then ice crystals grow on the frozen droplets. Sometimes, lateral growth of ice crystals connect frozen droplets.
- After 2 hours of the experiment, a mixture of supercooled water droplets and frost is observed on the membrane, whereas, the plastic plate is covered with a layer of frost.

In Chapter 5, the properties of the frost layer on the membrane and plastic plate are compared. Furthermore, the effect of operating conditions and moisture transfer rate on the properties of the frost layer on the membrane are investigated quantitatively and qualitatively. The main conclusions related to this chapter are:

- The thickness and mass of the frost accumulated on a membrane is lower than the frost mass and thickness formed on the plastic plate at the same operating conditions.
- The frost growth on the membrane is very slow at the beginning of the experiment (30 ~ 60min) followed by a rapid increase in the frost thickness.
- The time at which the rapid growth of frost on the membrane begins could be delayed by 30 min to 60 min, depending on the operating conditions.
- Increasing the moisture transfer rate can reduce the frost growth on the membrane.
- Increasing the air humidity ratio, air mass flow rate and reducing the liquid temperature increases the frost growth on the membrane.

6.2 Contributions

The outcomes of this research contribute to the scientific literature as follows:

6.2.1 Objective 1: To apply image processing to characterize frost properties

The well-defined test method to characterize frost properties is developed and explained in details;

- Image processing technique is applied to measure roughness of the frost layer on a plastic plate. The imaging technique is highly accurate, simple to use and avoids damaging of the frost layer compared to the contact measurement techniques. The methods to measure frost surface roughness by using image processing has not been previously established.
- A relationship between density and surface roughness is presented which can be used by numerical researchers to predict surface roughness, rather than assuming smooth frost surface which is used in the literature.
- The thickness of a frost layer on a membrane and the the area of the surface that is covered with frost are measured using image processing technique. This is new contribution to the literature because there is no information available about the properties of frost layer on a membrane.
- It is found that the definition of frost surface roughness used in Chapter 2, does not describe the properties of frost layer form on a membrane.

6.2.2 Objective 2: To identify the effect of moisture transfer on frosting limit

- Condensation/frosting limit for a plastic plate and membrane are quantified, which can used by manufacturers as benchmarks of the operating conditions where frost will form in a heat/energy exchanger.
- The effect of increasing moisture transfer on the condensation/frosting limit for a membrane is presented. The results demonstrate that increasing the moisture transfer rate through the membrane lowers the condensation/frosting limit

6.2.3 Objective 3: To determine the mechanisms of frost formation on a membrane

An in-depth experimental investigation, which is new to the literature, is conducted in this thesis to evaluate the mechanism of the frost formation on a membrane. The frost growth stages on a membrane are identified and compared with those observed on a plastic plate. The results prove that the fundamental of frost growth process is similar for both membrane and plastic plate; however, the size of water droplets and also the length of condensation stage are different. This is an important contribution to the literature, as it shows moisture transfer through a membrane results in freezing point depression. After two hours experiment at the same conditions for both membrane and plastic plate, the frost layer on the membrane consists of a mixture of supercooled water droplets and a cluster of irregular hexagonal shape crystals, whereas the frost layer on the plastic plate is a bushy layer of ice crystals that covers the whole surface of the plastic plate.

6.2.4 Objective 4: To identify the effect of moisture transfer on frost properties on a membrane

Frost properties (frost thickness, the frosted area and frost mass) on a membrane are determined and compared with those on a plastic plate. Also the effect of operating conditions and the moisture transfer rate on the frost properties on a membrane is shown, which is a new contribution to the literature.

6.3 Future work and recommendations

The following recommendations are presented for future research on frosting:

- More experiments need to be conducted on the test facility presented in Chapter 2 for frost on a plastic plate under natural convection conditions, under different operating conditions, to provide more data to determine the relationship between frost density and frost surface roughness.
- More experiments are needed to fill in the gaps on the condensation/frosting limit graphs shown in Figure 3.13 and Figure 3.12, for frost growth on a plastic plate and membrane under forced convection conditions.
- In Chapter 4, it has been shown that large water droplets form on a membrane, then frost forms around the frozen water droplets. It can be concluded that the initial size of the water droplets could have a great impact on the density of the frost layer. On the other hand, the water droplets formed on a plastic plate are very small, and the density of the frost layer is mainly a function of the frost layer shape as shown in Chapter 2. Therefore, modeling frost formation on a semipermeable membrane to find the nucleation rate, the transition times for condensation and freezing periods and the size of water droplets using the classic description of the condensation frosting would be beneficial. Furthermore, the result may be helpful for improving the anti-frosting properties of membranes.
- It is recommended to investigate the effect of the diffusivity of the membrane and the size and distribution of the pores of the membrane on frost formation experimentally.
- It is recommended to monitor the process of frost formation on a membrane using high speed imaging, and also, expanding the experiments to measure the temperature and humidity ratio gradient of the air close to the surface, to be integrated with the digital microscopy. The results will reveals details about the initiation of the condensation and freezing and freezing propagating on a membrane. Also, using high speed imaging would help to capture the initiation of condensation on the plastic plate. The condensation stage was not detected with test facility in Chapter 4 because condensation happens too fast (within the first 5 min).
- Investigate defrosting processes for the frost layer accumulated on a membrane has not been investigated in this thesis that could be an interesting topic for future research.

REFERENCES

[1] M. Rafati Nasr, M. Fauchoux, R.W. Besant, C.J. Simonson, A review of frosting in air-to-air energy exchangers, Journal of Renewable and Sustainable Energy Reviews. 30 (2014) 538–554.

[2] S. Nath, S.F. Ahmadi, J.B. Boreyko, A review of condensation frosting, Journal of Nanoscale and Microscale Thermophysical Engineering. 21 (2017) 81–101.

[3] O. Parent, A. Ilinca, Anti-icing and de-icing techniques for wind turbines: Critical review, Cold Regions Science and Technology. 65 (2011) 88–96.

[4] T.H. Lee, The effects of frost formation in a flat plate finned-tube heat exchanger, in: International Refrigeration and Air Conditioning Conference, purdue, 1996: pp. 205–210.

[5] D. Seker, H. Karatas, N. Egrican, Frost formation on fin-and-tube heat exchangers. Part I - Modeling of frost formation on fin-and-tube heat exchangers, International Journal of Refrigeration. 27 (2004) 367–374.

[6] L. Huang, Z. Liu, Y. Liu, Y. Gou, J. Wang, Experimental study on frost release on fin-and-tube heat exchangers by use of a novel anti-frosting paint, Journal of Experimental Thermal and Fluid Science. 33 (2009) 1049–1054.

[7] A.F. Emery, B.L. Siegel, Experimental measurements of the effects of frost formation on heat exchanger performance, United States: American Society of Mechanical Engineers. (1990) 1–7.

[8] P. Liu, M. Rafati Nasr, G. Ge, M. Justo Alonso, H.M. Mathisen, F. Fathieh, C. Simonson, A theoretical model to predict frosting limits in cross-flow air-to-air flat plate heat/energy exchangers, Journal Energy and Buildings. 110 (2016) 404–414.

[9] M. Justo Alonso, H.M. Mathisen, S. Aarnes, P. Liu, Performance of a lab-scale membrane-based energy exchanger, Journal of Applied Thermal Engineering. 111 (2017) 1244–1254.

[10] I. Wiik, Frost formation in membrane based flat plate heat exchangers, MSc Thesis, Norwegian University of Science and Technology, 2014.

[11] P. Navid, Numerical study of frost formation in a membrane for HVAC applications, MSc Thesis, University of saskatchewan, 2018.

[12] J.G. Georgiadis, J. Hoke, Quantitative visualization of early frost growth with scanning confocal microscopy, in: Proceedings of the 10th Brazilian Congress of Thermal Sciences and Engineering, Rio de Janeiro, Brazil, November 30-December 4, 2004., n.d.

[13] X. Sun, K. Rykaczewski, Suppression of frost nucleation achieved using the nanoengineered integral humidity sink effect, ACS Nano. 11 (2017) 906–917.

[14] S. Y. Hayashi, A. Aoki, S. Adaohi, K. Hori, Study of frost properties correlating with frost formation types, ASME Journal of Heat Transfer. 99 (1977) 239–245.

[15] J.B. Dooley, Determination and characterization of ice propagation mechanisms on surfaces undergoing dropwise condensation, PhD. thesis, Texas A&M University, 2010.

[16] J. Guadarrama-Cetina, A. Mongruel, W. González-Viñas, D. Beysens, Percolation-induced frost formation, EPL (Europhysics Letters). 101 (2013) 16009.

[17] M. Song, C. Dang, Review on the measurement and calculation of frost characteristics, International Journal of Heat and Mass Transfer. 124 (2018) 586–614.

[18] S. Nath, J.B. Boreyko, On localized vapor pressure gradients governing condensation and frost phenomena, Langmuir. 32 (2016) 8350–8365.

[19] X. Chen, R. Ma, H. Zhou, X. Zhou, L. Che, S. Yao, Z. Wang, Activating the microscale edge effect in a hierarchical surface for frosting suppression and defrosting promotion, Scientific Reports. 3 (2013) 1–8.

[20] K. Kim, K.-S. Lee, Frosting and defrosting characteristics of a fin according to surface contact angle, International Journal of Heat and Mass Transfer. 54 (2011) 2758–2764.

[21] K.K. Varanasi, T. Deng, J.D. Smith, M. Hsu, N. Bhate, Frost formation and ice adhesion on superhydrophobic surfaces, Applied Physics Letters. 97 (2010) 23–26.

[22] J.L. Hoke, J.G. Georgiadis, A.M. Jacobi, Effect of substrate wettability on frost properties, Journal of Thermophysics and Heat Transfer. 18 (2004) 228–235.

[23] Z. Liu, Y. Gou, J. Wang, S. Cheng, Frost formation on a super-hydrophobic surface under natural convection conditions, International Journal of Heat and Mass Transfer. 51 (2008) 5975–5982.

[24] N. Seki, S. Fukisako, K. Matsuo, S. Uemura, Incipient phenomena of frost formation, Bulletin of JSME. 27 (1984) 2476–2482.

[25] H. Lee, J. Shin, S. Ha, B. Choi, J. Lee, Frost formation on a plate with different surface hydrophilicity, International Journal of Heat and Mass Transfer. 47 (2004) 4881–4893.

[26] R. Karmouch, G.G. Ross, Experimental study on the evolution of contact angles with temperature near the freezing point, Journal of Physical Chemistry C. 114 (2010) 4063–4066.

[27] J. Shin, A. V. Tikhonov, C. Kim, Experimental study on frost structure on surfaces with different hydrophilicity: density and thermal conductivity, Journal of Heat Transfer. 125 (2003) 84–94.

[28] X. Sun, V.G. Damle, A. Uppal, R. Linder, S. Chandrashekar, A.R. Mohan, K. Rykaczewski, Inhibition of condensation frosting by arrays of hygroscopic antifreeze drops, Langmuir. 31 (2015) 13743–13752.

[29] J. Guadarrama Cetina, R.D. Narhe, D.A. Beysens, W. González-Viñas, Droplet pattern and condensation gradient around a humidity sink, Physical Review E - Statistical, Nonlinear, and Soft Matter Physics. 89 (2014) 1–10.

[30] M.G. Medici, A. Mongruel, L. Royon, D. Beysens, Edge effects on water droplet condensation, Physical Review E. 90 (2014) 062403.

[31] L. Oberli, D. Caruso, C. Hall, M. Fabretto, P.J. Murphy, D. Evans, Condensation and freezing of droplets on superhydrophobic surfaces, Advances in Colloid and Interface Science. 210 (2014) 47–57.

[32] R. Williams, J. Blanc, Inhibition of water condensation by a soluble salt nucleus, The Journal of Chemical Physics. 74 (1981) 4675–4677.

[33] M. Rahman, A. Jacobi, Condensation, frost formation, and frost melt-water retention characteristics on microgrooved brass surfaces under natural convection, Heat Transfer Engineering. 34 (2013) 1147–1155.

[34] J. Guadarrama Cetina, A. Mongruel, W. González Viñas, D. Beysens, Frost formation with salt, Journal of Exploring the Frontiers of Physics. 110 (2015) 1–5.

[35] M.A. Rahman, A.M. Jacobi, Experimental study on frosting/defrosting characteristics of microgrooved metal surfaces, International Journal of Refrigeration. 50 (2015) 44–56.

[36] X. Sun, V.G. Damle, S. Liu, K. Rykaczewski, Bioinspired stimuli-responsive and antifreeze-secreting anti-icing coatings, Advanced Materials Interfaces. 2 (2015) 25–27.

[37] N.H. Fletcher, Size effect in heterogeneous nucleation, The Journal of Chemical Physics. 29 (1958) 572–576.

[38] H. Lee, M.L. Alcaraz, M.F. Rubner, R.E. Cohen, Zwitter-wettability and antifogging

capabilities, ACS Nano. 7 (2013) 2172–2185.

[39] M.A. Rahman, A.M. Jacobi, Effects of microgroove geometry on the early stages of frost formation and frost properties, Applied Thermal Engineering. 56 (2013) 91–100.

[40] E. Moallem, L. Cremaschi, D.E. Fisher, S. Padhmanabhan, Experimental measurements of the surface coating and water retention effects on frosting performance of microchannel heat exchangers for heat pump systems, Journal of Experimental Thermal and Fluid Science. 39 (2012) 176–188.

[41] D. Kim, H. Kim, S.W. Kim, D.R. Kim, K.-S. Lee, Experimental investigation of frost retardation for superhydrophobic surface using a luminance meter, International Journal of Heat and Mass Transfer. 87 (2015) 491–496.

[42] S. Jung, M.K. Tiwari, N.V. Doan, D. Poulikakos, K.T. Manish, V. Doan, D. Poulikakos, M.K. Tiwari, N.V. Doan, D. Poulikakos, Mechanism of supercooled droplet freezing on surfaces, Nature Communications. 3 (2012) 1–8.

[43] Q. Hao, Y. Pang, Y. Zhao, J. Zhang, J. Feng, S. Yao, Mechanism of delayed frost growth on superhydrophobic surfaces with jumping condensates : more than interdrop freezing, American Chemical Society. 30 (2014) 15415–15422.

[44] F. Wang, C. Liang, X. Zhang, Research of anti-frosting technology in refrigeration and air conditioning fields: A review, Renewable and Sustainable Energy Reviews. 81 (2018) 707–722.

[45] W. Fisk, R. Chant, K. Archer, D. Hekmat, F. Offermann, B. Pedersen, Onset of freezing in residential air-to-air heat exchangers, ASHRAE Transactions. 91 (1985) 159–172.

[46] A.D. Sommers, Methodology for calculating the volume of condensate droplets on topographically modified, microgrooved surfaces, Langmuir. 27 (2011) 5523–5533.

[47] A.D. Sommers, J. Ying, K.F. Eid, Predicting the onset of condensate droplet departure from a vertical surface due to air flow—Applications to topographically-modified, micro-grooved surfaces, Journal Experimental Thermal and Fluid Science. 40 (2012) 38–49.

[48] J.L. Hoke, J.G. Georgiadis, A.M. Jacobi, H. Phoenix, The Interaction between the substrate and frost layer through condensate distribution, Urbana-Champaign, p. 135, 2000.

[49] Y. Chen, P. Lu, C. Shen, Q. Zhang, Experimental study on frost formation on a cold surface in low atmospheric pressure, Journal of Applied Thermal Engineering. 90 (2015) 86–93.

[50] Z. Liu, X. Zhang, H. Wang, S. Meng, S. Cheng, Influences of surface hydrophilicity on

frost formation on a vertical cold plate under natural convection conditions, Experimental Thermal and Fluid Science. 31 (2007) 789–794.

[51] A. Alizadeh, M. Yamada, R. Li, W. Shang, S. Otta, S. Zhong, L. Ge, A. Dhinojwala, K.R. Conway, V. Bahadur, A.J. Vinciquerra, B. Stephens, M.L. Blohm, Dynamics of ice nucleation on water repellent surfaces, Langmuir. 28 (2012) 3180–3186.

[52] J.B. Boreyko, C.P. Collier, Delayed frost growth on jumping-drop superhydrophobic surfaces, ACS Nano. 7 (2013) 1618–1627.

[53] B. Na, R.L. Webb, A fundamental understanding of factors affecting frost nucleation, International Journal of Heat and Mass Transfer. 46 (2003) 3797–3808.

[54] J.B. Boreyko, R.R. Hansen, K.R. Murphy, S. Nath, S.T. Retterer, C.P. Collier, Controlling condensation and frost growth with chemical micropatterns, Scientific Reports. 6 (2016) 1–15.

[55] Y. Zhao, R. Wang, C. Yang, Interdroplet freezing wave propagation of condensation frosting on micropillar patterned superhydrophobic surfaces of varying pitches, International Journal of Heat and Mass Transfer. 108 (2017) 1048–1056.

[56] J. Feng, Y. Pang, Z. Qin, R. Ma, S. Yao, Why condensate drops can spontaneously move away on some superhydrophobic surfaces but not on others, ACS Applied Materials and Interfaces. 4 (2012) 6618–6625.

[57] D. Mangini, C. Antonini, M. Marengo, A. Amirfazli, Cold regions science and technology runback ice formation mechanism on hydrophilic and superhydrophobic surfaces, Cold Regions Science and Technology. 109 (2015) 53–60.

[58] Y.L. Hao, Y.X. Tao, J. Iragorry, D. Castro, Experimental study of frost formation on a flat surface under natural convection, in: ASME International Mechanical Engineering Congress, Washington, D.C., 2003: pp. 1–7.

[59] Z. Liu, H. Wang, X. Zhang, S. Meng, C. Ma, An experimental study on minimizing frost deposition on a cold surface under natural convection conditions by use of a novel anti-frosting paint. Part II. Long-term performance, frost layer observation and mechanism analysis, International Journal of Refrigeration. 29 (2006) 237–242.

[60] H. Kim, D. Kim, H. Jang, D.R. Kim, K.S. Lee, Microscopic observation of frost behaviors at the early stage of frost formation on hydrophobic surfaces, International Journal of Heat and Mass Transfer. 97 (2016) 861–867.

[61] P. Tsai, R.G.H. Lammertink, M. Wessling, D. Lohse, Evaporation-triggered wetting transition for water droplets upon hydrophobic microstructures, Physical Review Letters. 104 (2010) 1–4.

[62] X. Wu, W. Dai, W. Xu, L. Tang, Mesoscale investigation of frost formation on a cold surface, Journal of Experimental Thermal and Fluid Science. 31 (2007) 1043–1048.

[63] K. Rykaczewski, S. Anand, S.B. Subramanyam, K.K. Varanasi, Mechanism of frost formation on lubricant-impregnated surfaces, Langmuir. 29 (2013) 5230–5238.

[64] C.H. Jeong, D.H. Shin, V. Konduru, J.S. Allen, C.K. Choi, S.H. Lee, Quantitative measurements of nanoscale thin frost layers using surface plasmon resonance imaging, International Journal of Heat and Mass Transfer. 124 (2018) 83–89.

[65] Y. Mao, The measurement and analysis of frost accumulation on a flat plate with forced convection, M.Sc Thesis, University of Saskatchewan, 1991.

[66] A.D. Sommers, N.L. Truster, A.C. Napora, A.C. Riechman, E.J. Caraballo, Densification of frost on hydrophilic and hydrophobic substrates - examining the effect of surface wettability, Experimental Thermal and Fluid Science. 75 (2016) 25–34.

[67] H. Chen, Modeling and measurement of frost characteristics on heat exchanger surfaces, PhD Thesis, University of saskatchewan, 2000.

[68] M.Y. Lee, Y. Kim, D.Y. Lee, Experimental study on frost height of round plate fin-tube heat exchangers for mobile heat pumps, Energies. 5 (2012) 3479–3491.

[69] J. Iragorry, Y.X. Tao, Frost temperature relations for defrosting sensing system, Journal of Heat Transfer. 127 (2005) 344–351.

[70] Y.B. Lee, S.T. Ro, Frost formation on a vertical plate in simultaneously developing flow, Journal of Experimental Thermal and Fluid Science. 26 (2002) 939–945.

[71] M. Kandula, Frost growth and densification on a flat surface in laminar flow with variable humidity, International Communications in Heat and Mass Transfer. 39 (2012) 1030–1034.

[72] F.A. Kulacki, Experimental strategies for frost analysis, MSc Thesis, University of Minnesota, 2013.

[73] P.L.T. Brian, R.C. Reid, Y.T. Shah, Frost deposition on cold surfaces, Industrial & Engineering Chemistry Fundamentals. 9 (1970) 375–380.

[74] R. Yun, Y. Kim, M. Min, Modeling of frost growth and frost properties with airflow over a flat plate, International Journal of Refrigeration. 25 (2002) 362–371.

[75] C.H. Cheng, K.H. Wu, Observations of early-stage frost formation on a cold plate in atmospheric air flow, Journal of Heat Transfer. 125 (2003) 95–102.

[76] D.M. Carlson, P.S. Hrnjak, C.W. Bullard, Deposition, distribution, and effects of frost on a multi-row heat exchanger performance, Urbana-Champaign, 2001.

[77] Z. Liu, H. Wang, X. Zhang, S. Meng, C. Ma, An experimental study on minimizing frost deposition on a cold surface under natural convection conditions by use of a novel anti-frosting paint. Part I. Anti-frosting performance and comparison with the uncoated metallic surface, International Journal of Refrigeration. 29 (2006) 229–236.

[78] C.H. Cheng, C.C. Shiu, Frost formation and frost crystal growth on a cold plate in atmospheric air flow, International Journal of Heat and Mass Transfer. 45 (2002) 4289–4303.

[79] F. Wang, C. Liang, M. Yang, C. Fan, X. Zhang, Effects of surface characteristic on frosting and defrosting behaviors of fin-tube heat exchangers, Journa of Applied Thermal Engineering. 75 (2015) 1126–1132.

[80] M. Amini, A.R. Pishevar, M. Yaghoubi, Experimental study of frost formation on a fin-and-tube heat exchanger by natural convection, International Journal of Refrigeration. 46 (2014) 37–49.

[81] V.S. Nascimento, F.R. Loyola, C.J.L. Hermes, A study of frost build-up on parallel plate channels, Experimental Thermal and Fluid Science. 60 (2015) 328–336.

[82] M. Fossa, G. Tanda, Study of free convection frost formation on a vertical plate, Journal of Experimental Thermal and Fluid Science. 26 (2002) 661–668.

[83] E. Okoroafor, M. Newborough, Minimising frost growth on cold surfaces exposed to humid air by means of crosslinked hydrophilic polymeric coatings, Journal of Applied Thermal Engineering. 20 (2000) 737–758.

[84] Z. Liu, Y. Dong, Y. Li, An experimental study of frost formation on cryogenic surfaces under natural convection conditions, International Journal of Heat and Mass Transfer. 97 (2016) 569–577.

[85] J. Xiao, W. Wang, Q.C. Guo, Y.H. Zhao, An experimental study of the correlation for predicting the frost height in applying the photoelectric technology, International Journal of Refrigeration. 33 (2010) 1006–1014.

[86] R. Östin, S. Andersson, Frost growth parameters in a forced air stream, International Journal

of Heat and Mass Transfer. 34 (1991) 1009–1017.

[87] C.T. Sanders, The influence of frost formaation and defrosting on the performance of air coolers, PhD Thesis, Delf Technical University, 1974.

[88] C. J. Cremers, V.K. Mehra, Frost formation on vertical cylinders in free convection, Journal of Heat Transfer. 104 (1982) 3–7.

[89] S. Negrelli, C.J.L. Hermes, A semi-empirical correlation for the thermal conductivity of frost, International Journal of Refrigeration. 58 (2015) 243–252.

[90] R. Le Gall, J.M. Grillot, Modelling of frost growth and densification, International Journal of Heat and Mass Transfer. 40 (1997) 3177–3187.

[91] D.K. Yang, K.S. Lee, Modeling of frosting behavior on a cold plate, International Journal of Refrigeration. 28 (2005) 396–402.

[92] B. Na, R.L. Webb, New model for frost growth rate, International Journal of Heat and Mass Transfer. 47 (2004) 925–936.

[93] L.Z. Zhang, J.L. Niu, Effectiveness correlations for heat and moisture transfer processes in an enthalpy exchanger with membrane cores, Journal of Heat Transfer. 124 (2002) 922.

[94] D. Kim, C. Kim, K.S. Lee, Frosting model for predicting macroscopic and local frost behaviors on a cold plate, International Journal of Heat and Mass Transfer. 82 (2015) 135–142.

[95] K.-S. Lee, W.-S. Kim, T.-H. Lee, A one-dimensional model for frost formation on a cold flat surface, International Journal of Heat and Mass Transfer. 40 (1997) 4359–4365.

[96] F. Brèque, M. Nemer, Frosting modeling on a cold flat plate: comparison of the different assumptions and impacts on frost growth predictions, International Journal of Refrigeration. 69 (2016) 340–360.

[97] C.J.L. Hermes, An analytical solution to the problem of frost growth and densification on flat surfaces, International Journal of Heat and Mass Transfer. 55 (2012) 7346–7351.

[98] F.R. Loyola, V.S. Nascimento, C.J.L. Hermes, Modeling of frost build-up on parallel-plate channels under supersaturated air-frost interface conditions, International Journal of Heat and Mass Transfer. 79 (2014) 790–795.

[99] C.M. Robinson, a M. Jacobi, A Study of frost formation on a plain fin, Urbana-Champaign, 2001.

[100] Y.X. Tao, R.W. Besant, Prediction of spatial and temporal distributions of frost growth on

a flat plate under forced convection, ASME, Heat Transfer Division,. 115 (1993) 278–281.

[101] Y.X. Tao, R.W. Besant, K.S. Rezkallah, A mathematical model for predicting the densification and growth of frost on a flat plate, International Journal of Heat and Mass Transfer. 36 (1993) 353–363.

[102] K.A.R. Ismail, C.S. Salinas, Modeling of frost formation over parallel cold plates, International Journal of Refrigeration. 22 (1999) 425–441.

[103] W. Wang, Q.C. Guo, W.P. Lu, Y.C. Feng, W. Na, A generalized simple model for predicting frost growth on cold flat plate, International Journal of Refrigeration. 35 (2012) 475–486.

[104] J. Hwang, K. Cho, Numerical prediction of frost properties and performance of fin–tube heat exchanger with plain fin under frosting, International Journal of Refrigeration. 46 (2014) 59–68.

[105] E. Bartrons, C. Oliet, E. Gutiérrez, A. Naseri, C.D. Pérez-Segarra, A finite volume method to solve the frost growth using dynamic meshes, International Journal of Heat and Mass Transfer. 124 (2018) 615–628.

[106] A.D. Sommers, C.W. Gebhart, C.J.L. Hermes, The role of surface wettability on natural convection frosting: Frost growth data and a new correlation for hydrophilic and hydrophobic surfaces, International Journal of Heat and Mass Transfer. 122 (2018) 78–88.

[107] C.J.L. Hermes, A.D. Sommers, C.W. Gebhart, V.S. Nascimento, A semi-empirical model for predicting frost accretion on hydrophilic and hydrophobic surfaces, International Journal of Refrigeration. 87 (2018) 164–171.

[108] K. Prölss, G. Schmitz, Modeling of frost growth on heat exchanger surfaces, in: Proceedings of the 5th Modelica Conference, Vienna, Austria, 2006: pp. 509–516.

[109] B.W. Jones, J.D. Parker, Frost formation with varying environmental parameters, Journal of Heat Transfer. 97 (1975) 255–259.

[110] Y.W. Kuang, C.C. Yi, W. Wang, Numerical simulation of frosting behavior and its effect on a direct-contact ambient air vaporizer, Journal of Natural Gas Science and Engineering. 27 (2015) 55–63.

[111] G. Biguria, L.A. Wenzel, Measurement and correlation of water frost conductivity and density, Industrial & Engineering Chemistry Fundamental. 9 (1970) 129–138.

[112] B. Na, R.L. Webb, Mass transfer on and within a frost layer, International Journal of Heat and Mass Transfer. 47 (2004) 899–911.

[113] P. Verma, Y. Wu, D.M. Carlson, Experimentally validated model for frosting of plain-fin-round-tube heat exchangers, in: The International Conference of New Technologies in Commercial Refrigeration, Urbana-Champaign, 2002: pp. 152–162.

[114] M.A. Rahman, A.M. Jacobi, Study of frost properties and frost melt water drainage on microgrooved brass surfaces in multiple frost/defrost/refrost cycles, Applied Thermal Engineering. 64 (2014) 453–461.

[115] K.S. Lee, W.S. Kim, The effects of design and operating factors on the frost growth and thermal performance of a flat plate fin-tube heat exchanger under the frosting condition, KSME International Journal. 13 (1999) 973–981.

[116] N.C. Schmiesing, A.D. Sommers, Defrosting performance on hydrophilic, hydrophobic, and micro-patterned gradient heat transfer surfaces, Science and Technology for the Built Environment. 23 (2017) 946–959.

[117] A. Leoni, M. Mondot, F. Durier, R. Revellin, P. Haberschill, U. De Lyon, U. Lyon, C. Umr, State-of-the-art of frost deposition on flat surfaces, International Journal of Refrigeration. 68 (2016) 198–217.

[118] Y. Xia, Y. Zhong, P.S. Hrnjak, a. M. Jacobi, Frost, defrost, and refrost and its impact on the air-side thermal-hydraulic performance of louvered-fin, flat-tube heat exchangers, International Journal of Refrigeration. 29 (2006) 1066–1079.

[119] Z.S. Ahmet, Effective thermal conductivity of frost during the crystal growth period, Journal of Heat and Mass Transfer. 43 (2000) 539–553.

[120] W. Shang, H. Chen, R.W. Besant, Frost growth in regenerative wheels, Journal of Heat Transfer. 127 (2005) 1015–1026.

[121] K.S. Lee, S. Jhee, D.K. Yang, Prediction of the frost formation on a cold flat surface, International Journal of Heat and Mass Transfer. 46 (2003) 3789–3796.

[122] A.D. Sommers, A.C. Napora, N.L. Truster, E.J. Caraballo, C.J.L. Hermes, A semi-empirical correlation for predicting the frost density on hydrophilic and hydrophobic substrates, International Journal of Refrigeration. 74 (2017) 313–323.

[123] J. Iragorry, Y.X. Tao, S. Jia, Review article: a critical review of properties and models for frost formation analysis, HVAC&R Research. 10 (2004) 393–420.

[124] M.M. Chen, W. Rohsenow, Heat , mass , and momentum transfer inside frosted tubes — experiment and theory, Transaction of ASME Journal. (1964) 334–340.

[125] S. Mengjie, D. Chaobin, L. Shengchun, S. Zhili, M. Ning, Frost layer thickness measurement and calculation: a short review, Journal of Energy Procedia. 142 (2017) 3812–3819.

[126] D.L. O'Neal, The effect of frost formation on the performance of a parallel plate heat exchanger, PhD Thesis, Purdue University, 1982.

[127] J.-S. Park, D.R. Kim, K.S. Lee, Local frost behaviors of a scaled-up louvered fin heat exchanger, International Journal of Heat and Mass Transfer. 89 (2015) 1127–1134.

[128] B. Xu, C. Zhang, Y. Wang, J. Chen, K. Xu, F. Li, N. Wang, Experimental investigation of the performance of microchannel heat exchangers with a new type of fin under wet and frosting conditions, Applied Thermal Engineering. 89 (2015) 444–458.

[129] M. Justo Alonso, P. Liu, H.M. Mathisen, G. Ge, C. Simonson, Review of heat/energy recovery exchangers for use in ZEBs in cold climate countries, Journal of Building and Environment. 84 (2015) 228–237.

[130] M.F. Lundekvam, New type of energy exchanger for ventilation air, MSc Thesis, University of NTNU, 2016.

[131] W.J. Fisk, R. Chant, K. Archer, D. Hekmat, F. Offermann, B. Pedersen, Onset of freezing in residential air-to-air heat exchangers, ASHRAE Transactions. 91 (1984) 145–158.

[132] M. Rafati nasr, G. Ge, M. Kassai, C.J. Simonson, Evaluation of defrosting methods for air-to-air heat/energy exchangers on energy consumption of ventilation, Journal of Energy and Buildings. 151 (2015) 32–40.

[133] M. Rafati Nasr, F. Fathieh, D. Kadylak, R. Huizing, R.W. Besant, C.J. Simonson, Experimental methods for detecting frosting in cross-flow air-to-air energy exchangers, Journal of Experimental Thermal and Fluid Science. 77 (2016) 100–115.

[134] S. Bilodeau, P. Brousseau, M. Lacroix, Y. Mercadier, Frost formation in rotary heat and moisture exchangers, International Journal of Heat and Mass Transfer. 42 (1999) 2605–2619.

[135] R.B. Holmberg, Prediction of condensation and frosting limits in rotary wheels for heat recovery in buildings, ASHRAE Transactions. 99 (1993) 64–69.

[136] N.F. Aljuwayhel, Numerical and experimental study of the influence of frost formation and defrosting on the performance of industrial evaporator coils, PhD Thesis, University of Wisconsin-Madison, 2006.

[137] T. Bharathidasan, S.V. Kumar, M.S. Bobji, R.P.S. Chakradhar, B.J. Basu, Effect of wettability and surface roughness on ice-adhesion strength of hydrophilic, hydrophobic and superhydrophobic surfaces, Applied Surface Science. 314 (2014) 241–250.

[138] W. Zhang, S. Wang, Z. Xiao, X. Yu, C. Liang, Y. Zhang, Frosting behavior of superhydrophobic nanoarrays under ultralow temperature, Langmuir. 33 (2017) 8891–8898.

[139] J.B. Boreyko, B.R. Srijanto, T.D. Nguyen, C. Vega, M. Fuentes-Cabrera, C.P. Collier, Dynamic defrosting on nanostructured superhydrophobic surfaces, Langmuir. 29 (2013) 9516–9524.

[140] X.M. Wu, R.L. Webb, Investigation of the possibility of frost release from a cold surface, Journal of Experimental Thermal and Fluid Science. 24 (2001) 151–156.

[141] X. Xu, Z. Zhang, J. Yang, Fabrication of biomimetic superhydrophobic surface on engineering materials by a simple electroless galvanic deposition method, Langmuir. 26 (2010) 3654–3658.

[142] P. Kim, T.S. Wong, J. Alvarenga, M.J. Kreder, W.E. Adorno-Martinez, J. Aizenberg, Liquid-infused nanostructured surfaces with extreme anti-ice and anti-frost performance, ACS Nano. 6 (2012) 6569–6577.

[143] K. Golovin, S.P.R. Kobaku, D.H. Lee, E.T. DiLoreto, J.M. Mabry, A. Tuteja, Designing durable icephobic surfaces, Science Advances. 2 (2016) 1–12.

[144] S.A. Kulinich, S. Farhadi, K. Nose, X.W. Du, Superhydrophobic surfaces: Are they really ice-repellent?, Langmuir. 27 (2011) 25–29.

[145] G.S.H. Lock, The Growth and Decay of Ice, Cambridge University Press: Cambridge, 1990.

[146] P. V. Hobbs, Ice Physics, Oxford university press, London, 1974.

[147] Y. Gou, Z. Liu, J. Wang, S. Cheng, Frost formation on a bionic super-hydrophobic surface under natural convection conditions, Heat Transfer. 37 (2008) 412–420.

[148] ASME/ANSI, Performance Test Code 19.1 Test Uncertainty: Instruments and Apparatus, 1998.

[149] ASME B46.1, Surface Texture, Surface Roughness, Waviness and Lay, 2009.

[150] L. Cai, R. Wang, P. Hou, X. Zhang, Study on restraining frost growth at initial stage by hydrophobic coating and hygroscopic coating, Journal of Energy and Buildings. 43 (2011) 1159–1163.

[151] M.R. Conde, Properties of aqueous solutions of lithium and calcium chlorides: Formulations for use in air conditioning equipment design, International Journal of Thermal Sciences. 43 (2004) 367–382.

[152] K.F. Eid, M. Panth, A.D. Sommers, The physics of water droplets on surfaces: Exploring the effects of roughness and surface chemistry, European Journal of Physics. 39 (2018) 1–21.

[153] M.D. Larson, Around heat and moisture exchanger, M.Sc Thesis, University of Saskatchewan, 2006.

[154] http://nilex.com/sites/default/files/Nilex-CGSB-Vapor-Barrier-Product-Specifications-10-15mil.pdf, (n.d.).

[155] V. Krishnamurty, N.V.S. Rao, Heat transfer in non-circular conduits: part IV laminar forced convection in rectangular channels, Indian Journal of Technology. 5 (1966) 331–333.

[156] National Institute of Health, ImageJ: Image Processing and Analysis in Java, n.d. https://imagej.nih.gov/ij/.

[157] R.J. Cheng, Water Drop Freezing: Ejection of microdroplets, Science. 170 (1970) 1359–1396.

[158] S. Jung, M.K. Tiwari, D. Poulikakos, Frost halos from supercooled water droplets, Proceedings of the National Academy of Sciences. 109 (2012) 16073–16078.

[159] K.D. Esmeryan, C.E. Castano, R. Mohammadi, Y. Lazarov, E.I. Radeva, Delayed condensation and frost formation on superhydrophobic carbon soot coatings by controlling the presence of hydrophilic active sites, Journal of Physics D: Applied Physics. 51 (2018) 1–11.

[160] M. Fauchoux, Design and performance testing of a novel ceiling panel for simultaneous heat and moisture transfer to moderate indoor temperature and relative humidity, PhD Thesis, University of Saskatchewan, 2012.

[161] T.L. Bergman, A.S. Lavine, F.P. Incropera, D.P. DeWitt, Fundamentals of heat and mass transfer, 7th editio, John Wiley & Son, New York, 2002.

APPENDIX A

FROST SURFACE TEMPERATURE CALCULATIONS

Frost forms on a cold plate because of the driving potential between the air and the frost layer, which is the difference between the humidity ratio of the ambient air and the air at the interface between the air and the frost ($W_{air} - W_{f,surf}$). If the air at the frost surface is assumed to be saturated to simplify the analysis presented here, which is a good approximation for most cases, $W_{f,surf}$ would be a function of frost surface temperature. The frost surface temperature increases with time because the frost thermal resistance increases. It can be concluded from the literature that the frost surface temperatures approach approximately the same value as time progresses regardless of the plate temperature at relatively high air humidity ratios [82][58]. However, at lower plate temperatures (less than approximately -15°C), that frost density is very low specially at the early stage of frost formation [14], the frost surface temperature increases faster than a frost layer at relatively higher plate temperature. For the two plate temperature tested in this paper, the difference between the frost densities at two conditions, results in less frost mass at the lower plate temperature.

To justify the results presented here, frost surface temperature is calculated based on a simplified thermal resistance analysis. Without the frost, there will be convective heat transfer from the air to the plate. With the addition of the frost layer, there will be convective heat transfer from the air to the frost surface and conductive heat transfer through the frost layer. As frost grows on the plate, frost surface temperature, $T_{f,surf}$ will increase due to the increased insulation between the plate and the air. With the assumption of negligible phase change energy, an equivalent thermal resistance circuit for the heat transfer between the air and the plate, with a layer of frost on the plate is shown in Figure A.1. Using correlations for h and k_f, along with the measured δ_f, T_p and T_{air}, the temperature at the interface can be calculated.

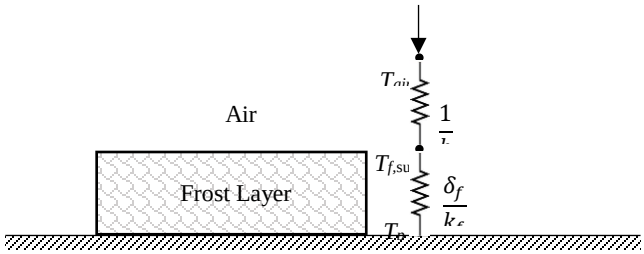

Figure A.1. Thermal resistance circuit for a frost layer on a plate (neglecting the heat of phase change).

The combination of the heat transfer coefficient for natural convection and radiation heat transfer on a horizontal plate, h, was calculated from the following equations[161];

$$Nu = 0.52\, Ra_{air}^{0.2} \tag{A.1}$$

$$h_{conv} = \frac{k_{air}\, Nu}{L} \tag{A.2}$$

$$h_{rad} = (5.67 * 10^{-8})\varepsilon(T_{air} + T_{f,surf})({T_{air}}^2 + {T_{f,surf}}^2) \tag{A.3}$$

$$h = h_{conv} + h_{rad} \tag{A.4}$$

The thermal conductivity of the frost layer is more difficult to calculate, as it is dependent on the properties of the frost, which are changing with time. To calculate the frost thermal conductivity, two limiting cases were considered, based on a model for heat transfer in a porous material given by [87] . The minimum and maximum limits assumed that the frost layer consists of layers of ice and air, which are connected in series and parallel arrangements, respectively. The following equations express the relationships for $k_{f,min}$ and $k_{f,max}$ as a function of frost density:

$$k_{f,min} = [\frac{\rho_f}{\rho_{ice}}\frac{1}{k_{ice}} + (1 - \frac{\rho_f}{\rho_{ice}})\frac{1}{k_{air}}]^{-1} \tag{A.5}$$

$$k_{f,max} = \frac{\rho_f}{\rho_{ice}}\, k_{ice} + (1 - \frac{\rho_f}{\rho_{ice}})k_{air} \tag{A.6}$$

The true frost thermal conductivity will be a value between $k_{f,min}$ and $k_{f,max}$. Using these equations, and the measured frost density and thickness, $T_{f,s}$ can be calculated from Eq.(A.7).

$$q'' = \frac{T_{air} - T_p}{\frac{1}{h} + \frac{\delta_f}{k_f}} = \frac{T_{air} - T_{f,surf}}{\frac{1}{h}} \tag{A.7}$$

The minimum and maximum values of $T_{f,surf}$ at each time step are shown in Figure A.2, for the two plate temperatures, T_p = -21°C and T_p = -10°C. Using the thermal circuit described in Figure A.1, it is assumed that the heat transfer through the frost layer is a constant value. Therefore, if the thermal conductivity of the frost is high, the temperature difference across the frost layer will be small. Conversely, if the thermal conductivity is low, the temperature difference will be high. The actual value of $T_{f,surf}$ will be somewhere between these two bounds for each test. However, based on the photography, at T_p = -21°C, frost layer shape is more close to series arrangement ($k_{f,min}$), and at T_p = -10°C frost layer shape is more close to parallel arrangement ($k_{f,max}$). The discussion given and Figure A.2, shows that it is possible that frost surface temperature at T_p = -21°C gets higher than the frost temperature at T_p = -10°C, which justify the higher mass accumulation at T_p = -10°C than at T_p = -21°C. However, a more detail study on the heat and mass transfer process near the frost surface is needed.

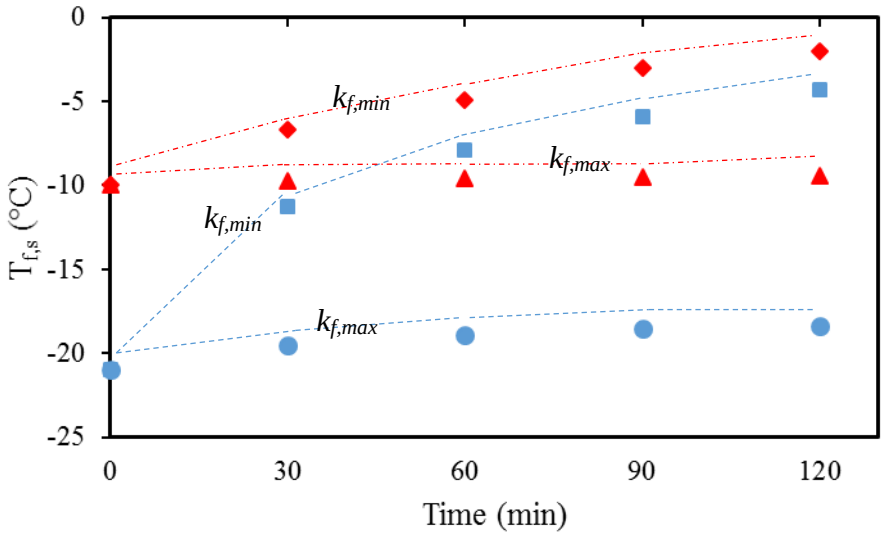

Figure A.2. Temperature at the interface between the air and frost layer ($T_{f,surf}$) as a function of time at two different plate temperatures.

APPENDIX B

COPYRIGHT PERMISSIONS

B.1 Permission for Manuscripts Used in Chapters 2

The manuscript used in Chapter 2 is published in ASME Journal of Thermal Science and Engineering Application.

It is our pleasure to grant you permission to use ***all or any part of the*** *ASME paper "*Experimental characterization of frost growth on a horizontal plate under natural convection*," by Shirin Niroomand, Melanie Fauchoux and Carey J. Simonson*

J. Thermal Sci. Eng. Appl., Accepted Manuscript, 2018, cited in your letter for inclusion in a PhD thesis entitled characterization of frost growth on a membrane to be published by University of Saskatchewan.

Permission is granted for the specific use as stated herein and does not permit further use of the materials without proper authorization. Proper attribution must be made to the author(s) of the materials. ***Please note****: if any or all of the figures and/or Tables are of another source, permission should be granted from that outside source or include the reference of the original source. ASME does not grant permission for outside source material that may be referenced in the ASME works. As is customary, we request that you ensure full acknowledgment of this material, the author(s), source and ASME as original publisher. Acknowledgment must be retained on all pages printed and distributed.*

Sincerely,

Beth Darchi
Publishing Administrator
ASME
2 Park Avenue, 6th Floor
New York, NY 10016-5990
Tel 1.212.591.7700
darchib@asme.org"

B.2 Permission for Manuscripts Used in Chapters 3

The manuscript used in Chapter 3 is published in ASME Journal of Heat Transfer. The following is a written permission to include the published manuscript in this Ph.D. thesis.

It is our pleasure to grant you permission to use ***all or any part of the*** *ASME paper "Effect of moisture transfer through a semipermeable membrane on condensation/frosting limit," by Shirin Niroomand, Melanie Fauchoux and Carey J. Simonson*
Journal of Heat Transfer, 2018, cited in your letter for inclusion in a PhD thesis entitled characterization of frost growth on a membrane to be published by University of Saskatchewan.
Permission is granted for the specific use as stated herein and does not permit further use of the materials without proper authorization. Proper attribution must be made to the author(s) of the materials. ***Please note****: if any or all of the figures and/or Tables are of another source, permission should be granted from that outside source or include the reference of the original source. ASME does not grant permission for outside source material that may be referenced in the ASME works. As is customary, we request that you ensure full acknowledgment of this material, the author(s), source and ASME as original publisher. Acknowledgment must be retained on all pages where figure is printed and distributed. ASME cannot grant permission to use any or all of the works of your paper HT-18-1133 until after publication with ASME. As of now this paper is in the stage of proofs. Once the paper has been published on line in the website, you can then send a request for permission to use this paper. PLEASE NOTE, that we do not keep these requests on file. Once publication is completed then send the request for permission.*
Many thanks for your interest in ASME publications.
Sincerely,

Beth Darchi
Publishing Administrator
ASME
2 Park Avenue, 6th Floor
New York, NY 10016-5990
Tel 1.212.591.7700
darchib@asme.org"

B.3 Permission for Manuscripts Used in Chapters 4

According to the College of Graduate Studies and Research at the University of Saskatchewan, a written permission is required from each of the co-authors for unpublished papers. The paper used in Chapter 4 is unpublished, therefore, copyright permissions are obtained from the co-authors as follows.

Copyright Permission Request Form

I am preparing the publication of a paper titled "*The mechanism of frost formation on a semipermeable membrane"* to be published as the fourth chapter of my Ph.D. thesis, and to be submitted to the Department of Mechanical Engineering at the University of Saskatchewan. The authors contributing in the completion of this manuscript are

S. Niroomand, M. Fauchoux, C. J. Simonson

I am requesting permission to use the materials described in the aforementioned manuscript in my Ph.D. thesis and all subsequent editions that may be prepared at the University of Saskatchewan. Please indicate agreeemnt by signing below:

Permission granted by: Carey Simonson

Signature:

Date:

Copyright Permission Request Form

I am preparing the publication of a paper titled "*The mechanism of frost formation on a semipermeable membrane"* to be published as the fourth chapter of my Ph.D. thesis, and to be submitted to the Department of Mechanical Engineering at the University of Saskatchewan. The authors contributing in the completion of this manuscript are

S. Niroomand, M. Fauchoux, C. J. Simonson

I am requesting permission to use the materials described in the aforementioned manuscript in my Ph.D. thesis and all subsequent editions that may be prepared at the University of Saskatchewan. Please indicate agreeemnt by signing below:

Permission granted by: Melanie Fauchoux

Signature:

Date:

B.4 Permission for Manuscripts Used in Chapters 5

According to the College of Graduate Studies and Research at the University of Saskatchewan, a written permission is required from each of the co-authors for unpublished manuscripts. The manuscript used in Chapter 5 is unpublished, therefore, copyright permissions are obtained from the co-authors as follows.

Copyright Permission Request Form

I am preparing the publication of a manuscript titled "*Evaluation of the frost properties on a membrane"* to be published as the fifth chapter of my Ph.D. thesis, and to be submitted to the Department of Mechanical Engineering at the University of Saskatchewan. The authors contributing in the completion of this manuscript are

S. Niroomand, M. Fauchoux, C. J. Simonson

I am requesting permission to use the materials described in the aforementioned manuscript in my Ph.D. thesis and all subsequent editions that may be prepared at the University of Saskatchewan. Please indicate agreeemnt by signing below:

Permission granted by: Carey Simonson

Signature:

Date:

Copyright Permission Request Form

I am preparing the publication of a manuscript titled "*Evaluation of the frost properties on a membrane"* to be published as the fifth chapter of my Ph.D. thesis, and to be submitted to the Department of Mechanical Engineering at the University of Saskatchewan. The authors contributing in the completion of this manuscript are

S. Niroomand, M. Fauchoux, C. J. Simonson

I am requesting permission to use the materials described in the aforementioned manuscript in my Ph.D. thesis and all subsequent editions that may be prepared at the University of Saskatchewan. Please indicate agreeemnt by signing below:

Permission granted by: Melanie Fauchoux

Signature:

Date: